12-2007

Advanced Microscopy Techniques for the Molecular Scale Analysis and Physical Characterization of *Escherichia coli* Spheroplasts

Claretta Jackson Sullivan
University of Tennessee - Knoxville

To the Graduate Council:

I am submitting herewith a dissertation written by Claretta Jackson Sullivan entitled "Advanced Microscopy Techniques for the Molecular Scale Analysis and Physical Characterization of *Escherichia coli* Spheroplasts." I have examined the final electronic copy of this dissertation for form and content and recommend that it be accepted in partial fulfillment of the requirements for the degree of Doctor of Philosophy, with a major in Life Sciences.

Mitchel J. Doktycz, Major Professor

We have read this dissertation and recommend its acceptance:

David P. Allison, Barry D. Bruce, David C. Joy, Engin H. Serpersu

Accepted for the Council:
Carolyn R. Hodges

Vice Provost and Dean of the Graduate School

(Original signatures are on file with official student records.)

To the Graduate Council:

I am submitting herewith a dissertation written by Claretta Jackson Sullivan entitled “Advanced Microscopy Techniques for the Molecular Scale Analysis and Physical Characterization of *Escherichia Coli* Spheroplasts.” I have examined the final electronic copy of this dissertation for form and content and recommend that it be accepted in partial fulfillment of the requirements for the degree of Doctor of Philosophy, with a major in Life Sciences.

Mitchel J. Doktycz, Major Professor

We have read this dissertation and
recommend its acceptance:

David P. Allison

Barry D. Bruce

David C. Joy

Engin H. Serpersu

Acceptance for the Council:

Carolyn R. Hodges
Vice Provost and Dean of the
Graduate School

(Original signatures are on file with official student records.)

Advanced Microscopy Techniques for the Molecular Scale Analysis and Physical Characterization of *Escherichia coli* Spheroplasts

A Dissertation Presented for the Doctor of Philosophy Degree
The University of Tennessee, Knoxville

Claretta Jackson Sullivan
December 2007

Dedication

This dissertation is dedicated to my parents Queen Esther Mace Jackson and the late Clyde Cullen Jackson who were my first teachers. Collectively, I have named the enduring love, hope, expectation and care they gave me “Esther pepper and C. C. Salt” because it flavors my life daily. I hope I can sprinkle the same on my children. Also sharing this dedication is my husband, Walter Wade Sullivan III. His support and kindness throughout this arduous journey have been unwavering. For that, I am so grateful.

Acknowledgements

I want to thank my advisor, Dr. Mitchel Doktycz for his guidance throughout this project. He has been very generous in sharing his time and knowledge. His training in thinking and patient coaching in writing manuscripts are most appreciated. I aspire to develop his ability to assemble and direct a cooperative, productive and creative interdisciplinary research team. To have been a graduate student in his lab was definitely my privilege.

I am also indebted to Dr. David Allison for welcoming me into AFM lab and for introducing me to the many nuances of AFM imaging. He too has freely shared his time and insights with me. I am inspired by his choice to continue to do science when he could easily choose otherwise. It has been my joy to work with him.

I want to also thank my thesis committee for their service. In addition to Drs. Doktycz and Allison, the committee includes Dr. Barry Bruce, Dr. David Joy and Dr. Engin Serpersu. The committee kindly provided important critical reviews throughout my dissertation work.

I am grateful to everyone associated with the Doktycz and Allison labs for being such a kindhearted and helpful group of people. Special thanks go to Dr. Jenny Morrell-Falvey for introducing me to confocal microscopy and for sharing her molecular biology expertise. I appreciate all the helpful discussions with Dr. Scott Retterer. His engineering background was invaluable in tailoring my perception of the AFM. Many thanks to Mr. Sankar Venkataraman and Dr. Jason Fowlkes for taking time away from their work to write Matlab code for mine.

Funding support from the DOE Office of Biological and Environmental Research
for this thesis work is also gratefully acknowledged.

To my family and friends who supported me throughout this work, I owe so much. The encouraging words, phone calls and notes pulled me through the most difficult times. In particular, I want to thank my husband, Walter W. Sullivan III, and my children, W. Geoffrey Sullivan and Sarah B. Sullivan. They have been the most affected by my return to graduate school. They willingly sacrificed many things to allow me to pursue this work and remained my motivation to its completion.

My mother, Mrs. Queen E. Jackson, my twin, Dr. Loretta E. Jackson-Williams, my other sister, Mrs. Mavis Y. Anderson and my brother, Rev. Dr. Alvin O. Jackson have been completely supportive. In addition, my father-in-law, Dr. Walter W. Sullivan, Jr., his wife, Mrs. Marilyn B. Sullivan, my brother-in-law, Mr. James E. Williams and my sisters-in-law, Mrs. Earnestine E. Jackson, Dr. Karen E. Sullivan and Mrs. Cheri W. Sullivan have made countless offers of support. They have said and done so many helpful things along the way. My dearest friends Mrs. Christene Franklin and her husband Mr. Vaughn Franklin have been so helpful. Many meals at their house gave me more time to study and work. After my family moved ahead to Virginia, they kindly welcomed me into their home. For these things and their enduring friendship, I am thankful. I also appreciate the coffee times with Dr. Linda Cain and Dr. Ruth Ann Manning. In many ways they made me believe that graduate school was a viable option for me. I am also grateful to Dr. Dabney Johnson who allowed me to work in her lab as I prepared for the graduate program. Also thanks to Dr. Madhu Dhar, a postdoc in the Johnson lab at the time, who patiently introduced me to general laboratory techniques. Finally, I acknowledge the encouragement from all other friends and family. For them, I am also grateful.

Abstract

Atomic force microscopy (AFM) holds a unique position in microbiology because of its potential for nanometer (nm) scale imaging and piconewton (pN) force detection. These features can be exploited to characterize bacteria from the cellular down to the molecular level. In order to pursue such characterization studies, reliable sample preparation techniques must be developed. Spheroplasts are bacteria which have been treated with enzymes to remove cell wall components. Because the cytoplasmic membrane is exposed in spheroplasts, they are suitable for localizing transporters and other membrane proteins using AFM techniques. Constituents on the surface of intact bacteria are responsible for their adhesion to various substrates *in vivo*. The absence of these constituents in spheroplasts necessitates specialized immobilization strategies. This study presents a technique in which spheroplasts are immobilized by cross linking them with glutaraldehyde to mica surfaces pretreated with aminopropyltriethoxysilane. As suggested by the AFM images, this approach facilitates stable imaging in appropriate buffers. Because the sample preparation strategies presented are compatible with optical and atomic force microscopies, investigations in which molecular system components are monitored can be targeted.

Evidence that the cells retain membrane integrity, continue glucose uptake, increase in diameter and initiate protein synthesis after immobilization is also presented. Based on this data, it is concluded that metabolic processes continue in immobilized spheroplasts. As a result of this finding, spheroplasts are proposed to be a platform for various imaging-based investigations.

Elasticity and indentation measurements on intact bacteria and spheroplasts revealed significant differences between the two forms. They also provided the justification for using glutaraldehyde fixed spheroplasts for molecular recognition experiments designed to locate the glucose transporter on the surface of spheroplasts. An avidin-biotin system was used in which biotin was tethered to the AFM tip using a polyethylene glycol linker, When this functionalized tip probed spheroplast surfaces previously immunolabeled with a biotinylated antibody and avidin, molecular recognition was demonstrated. The fact that the biotin functionalized tips can be used in multiple applications is an attractive feature of this strategy. That results from AFM experiments can be validated with optical microscopy techniques is also an advantage.

Table of Contents

List of Tables

List of Figures

Chapter 1

Background

"The STM's "Years of Apprenticeship" have come to an end, the foundations have been laid, and the "Years of Travel" begin. We should not like to speculate where it will finally lead, but we sincerely trust that the beauty of atomic structures might be an inducement to apply the technique to those problems where it will be of greatest service solely to the benefit of mankind." (Binnig, G., and Rohrer, H. (1987) Reviews of Modern Physics **59**(3), 615-625*)*

1.0 Introduction

The scanning probe microscopes use various detection schemes to sense the surface of a sample as it raster scans it with a sharp probe. The first of these microscopes, the scanning tunneling microscope (STM) was designed by Gerd Binnig and Heinrich Rohrer in 1982 to study the electrical properties of thin insulating layers (2). In the STM a small bias voltage is applied between the tip and the sample. When separation between the tip and sample is reduced to about 1nm, a tunneling current is generated and flows between them. This current is only a few nanoamps but is easily detected using a low noise amplifier. The tunneling current decays exponentially with increasing distance between the tip and sample. Consequently, only the atom at the apex of the tip significantly participates in the tunneling, a condition that is ideal for detecting small features on a surface. Because the STM is so sensitive, it can easily resolve atomic lattices. The STM requires a conducting surface and material scientists were also interested in developing an instrument with similar capabilities for non-conducting surfaces. This effort resulted in the atomic force microscope (AFM) by Binnig *et al* in 1986 (3).

The AFM tip traversing the surface of a sample is much like blind people using their sense of touch to probe surfaces to compensate for the loss of sight. The topography of the surface is determined as their fingers encounter areas of relative height or depth. As a result of this interaction, a mental picture of the object can be created. Using their fingers, they can also determine whether a surface is springy or hard; smooth or rough. These distinctions are made subconsciously based on how responsive the surface is to

pressure. Detecting temperature differences allows one to determine whether the surface is hot or cold. Through the use of special materials and sophisticated electronics, the AFM is capable of going through these same processes on the micro- and nanoscales.

As with other scanning probe microscopes, piezo electric devices are used in the AFM to precisely move the tip relative to the sample in the x, y (i.e. raster scan) and z directions. In the AFM, the probe is a sharp tip supported by a cantilever. The most common detection system employs a laser that is reflected on the back of the cantilever. As the tip moves across and encounters forces associated with the surface, the cantilever is deflected which in turn causes the reflection of the laser beam to change positions on the photodiode. These changes are relayed to a computer processor which converts this information into an image. The forces sufficient to cause detectable movement of the tip are in the pN range. This ability to detect such small forces accounts for the resolution of the instrument.

The proximity of the tip to the surface of the sample and the imaging conditions (air or liquid, pH etc.) determine which particular forces are measured. The fact that these forces are distinguishable by sample-tip separation distances is the basis of the various imaging modes in AFM. Contact mode imaging is based on the cantilever having intimate contact with the surface where short range repulsive forces are maximal. The feedback loop in contact mode is set such that a constant deflection is maintained. In contrast, intermolecular van der Waals forces predominate within tens of angstroms of the surface up to hundreds of nanometers (4-7). Electrostatic and magnetic forces dominate farther above the surface as van der Waals interactions decay exponentially with distance. Capillary, adhesive, electrostatic, hydrodynamic and other forces may also exist between the tip and sample unless measures are taken to minimize them. For example, the thin water layer typically present on surfaces in ambient air is often the source of capillary forces and can be eliminated by imaging in liquid. Varying the pH of the imaging buffer can address problems with electrostatic interactions (8,9). Each of these forces can be sufficient to cause the cantilever to deflect. Long range forces, although not used directly for imaging, can also affect cantilever behavior. In doing so, they provide the basis for the non-contact imaging modes like MacMode® where the

cantilever is oscillated with a nearby solenoid at its resonant frequency(10). The amplitude of the oscillation decreases with proximity to the sample and the feedback loop in MacMode® maintains an amplitude setpoint by adjusting the distance between the tip and the sample(11). (Figure 1) Note that figures and tables are included in Appendix A.

1.1 Applications of AFM

The capabilities of the AFM have been shrewdly extended beyond imaging by changing the way the tip is used. Published reports have demonstrated that the tip can be used as a micro pH probe, a micro thermometer, and a microanalyzer (12-14). Tips modified with biomolecules have been used to probe immobilized proteins or cells for their complementary molecules (15). As indicated in the following short review, AFM is especially compatible with biological investigations for several reasons. First, fixatives that might impair biological activity are not required. In fact, samples can be examined in biologically relevant conditions such as buffers and media, making live cell imaging of microbes a realistic objective. Secondly, AFM is capable of detecting forces in the pN range and precise control of the force applied to the cantilever can be maintained. This combination facilitates the evaluation of physical parameters of biological samples. Thirdly, rather than yielding the composite, statistical average of sample data, as is the case with many biochemical assays, the behavior of one unit (cell, subcellular structure, or molecule) can be monitored. This feature can be very important in determining mechanisms at the molecular level. As a way of illustrating the versatility of AFM, presented here are examples of how the technique has been used to address questions in biology on three levels – the molecular, subcellular and cellular.

As an imaging technique, AFM can provide structural information not accessible by other techniques as demonstrated by a report published by Lushnikov and colleagues. They used AFM to distinguish between two possible orientations of DNA within the SfiI restriction enzyme-DNA complex(16). SfiI is a type II restriction endonuclease which simultaneously binds and cuts two recognition sites. These sites can be located on the same DNA molecule (cis) or on two separate molecules (trans). It was known prior to their study that looped DNA structures are formed when the recognition sites are

presented on the same DNA molecule. It was also known that if Ca^{2+} is included in the reaction buffer instead of Mg^{2+}, the enzyme binds the DNA but does not cleave it. The authors designed DNA fragments of various lengths and cleverly located the restriction sites such that binding to the enzyme would result in a short arm and long arm of DNA that could be used to distinguish the conformations in high resolution AFM images. In particular, they wanted to know whether the DNA was crossed within the enzyme-DNA complex or merely bent. Ultimately, they concluded that there was no preferential orientation of the DNA within the complex.

In another example, a structure in the plasma membrane of live cells was revealed for the first time by AFM and suggested to participate in exocytosis, the process by which neurotransmitters, enzymes and hormones are released (17). These pit-like structures called fusion pores, contained smaller structures. Docking and fusion of membrane-bound secretory vesicles was known to occur in the final stages of exocytosis although the mechanism for this activity and the specific role of the plasma membrane were unclear. Because the authors were able to image live cells, they were able to visualize the dynamic changes of the fusion pores during exocytosis. Later experiments confirmed the presence of fusion pores and demonstrated the release of vesicular contents at the site of the pores (18). The fixation step required of electron microscopy (EM) is believed to have altered the structure of the pore so significantly that they were not identifiable in previous EM images. That the AFM can probe unaltered cells in dynamic environments was essential to the findings in this study.

The previous examples used “bare” tips. Alternatively, the tip can be functionalized by tethering reactive molecules, thus making it a chemical probe. Puntheeranurak *et al* employed this technique to investigate the Na^{+}-D-glucose co-transporter (SGLT1), a protein which couples translocation of glucose and sodium ions in mammalian epithelial cells (19). In their experiments, tips modified with an epitope-specific antibody or 1-thio-glucose were used to probe the topology and ligand-induced conformational changes of the protein. Their experiments were conducted in living Chinese hamster ovary cells transfected with a functional SGLT1 from rabbit (rbSGLT1). The tip was repeatedly cycled toward the cell surface followed by retraction away from the surface after contact. During the approach, the tethered molecule has an opportunity to bind its complement

on the cell surface. Upon retraction, if binding has occurred, the unbinding force is recorded as a sudden change in force just as the tethered molecule disengages and the cantilever returns to its baseline position. This unbinding force can be distinguished from nonspecific binding (20,21). By using cells with or without rbSGLT1 and by varying the buffer conditions (with or without antibody, Na^+, inhibitors, competitor etc.) the authors were able to compare the probability of having a binding event and the distribution of the unbinding force. Ultimately, they concluded that specific recognition events were occurring between the modified tips and SGLT1. These events decreased in the presence of a specific inhibitor, an observation which they attributed to conformational changes of the protein.

Biochemical activity inside cells is often initiated by physical dynamics at the cell surface. From mammalian biology comes the following example of how the AFM tip can provide the physical stimulus and the cell's response can be monitored using optical techniques (e.g. confocal, epifluorescence, etc). Osteoblasts are known to quickly increase intracellular calcium levels as a result of mechanical stimulation (22,23). Strain can be applied to the cells experimentally using a variety of methods including: poking with a micropipette, movement of magnetic microbeads in a magnetic field, optical tweezers, stretching of the substrate, fluid flow or hydrostatic pressure. However, none of these techniques enable both a precise control of the force applied and measurement of the mechanical properties at the point of application. Charras *et al* demonstrated that AFM techniques could meet both requirements when they used the cantilever to apply a strain on the surface of osteoblasts (24).

Their strategy was to glue a glass bead to the cantilever. (They had previously demonstrated that this arrangement yielded a more suitable interaction with the cell than did the sharpened tip of a standard cantilever.) The cells were treated in a medium containing a cell permeant, calcium-sensitive dye so that calcium levels could be assessed throughout the experiment. The cantilever was positioned above a cell and pushed into the surface. After a period of time, force data was recorded and the cantilever was retracted. Subsequent investigations based on this technique led the authors to estimate cellular strain thresholds; describe two pathways for detecting the stimuli in osteoblasts; and propose a mechanically coherent model for detection of whole

bone strain at the cellular level and its transduction to generate whole bone level changes. This report demonstrates the benefit of having physical access to cell surfaces.

Another example is based on the cochlea of the mammalian inner ear. It transduces sound into an electrical signal, a process required for hearing. Hair cells, an essential part of the cochlea's organ of Corti, have bundled, receptive organelles called stereocilia which move as a result of sound waves. Located on top of the hair cells, stereocilia are particularly important for sound transduction (25,26). These organelles differ in length but have a characteristic and geometric organization. Adjacent stereocilia are connected to each other with fine filaments called links. Mechanosensory transduction channels in the hair cells are directly opened or closed (to allow flow of cations) depending on mechanical stimulation of these links by sound waves. Therefore, understanding the behavior of stereocilia and links has great implications for understanding the process and problems of hearing. Langer and colleagues used the AFM tip to displace stereocilia in a way that simulates sound. They used AFM to determine the micromechanical properties of individual stereocilia of living hair cells (27,28). These reports laid the foundation for subsequent experiments which combined AFM probe techniques with patch clamp to simultaneously examine the electrical response of the cells (29).

A recent example from virology illustrates the benefit of using AFM for simulating the dynamic environment encountered by biological systems *in vivo*. Kienberger *et al* used MacMode® to watch the release of RNA from a type of human rhinovirus (HRV2)(30). High resolution images of the immobilized viruses yielded height measurements around 30nm which correlated well with those previously reported in literature. It was known before their study, that RNA is released from the HRV2 capsid in low pH conditions *in vivo*. The authors were able to simulate this condition by reducing the pH of the imaging buffer. After a period of time in the low pH buffer, RNA molecules could be seen as they were being extruded from the viruses. The presence of RNA was confirmed by comparing these images to those taken in buffer supplemented with RNase A. In the latter case, the fibers believed to be RNA were not present. Based on the presence of forklike structures at the end of fully released RNA, the authors were able to speculate

about the initial orientation of the RNA during extrusion. The ability to alter buffer conditions during imaging permits visualization of dynamic processes and is an important advantage of AFM.

Few areas of biological research have gained more from AFM than microbiology. The dimensional scale of microbes restricts the application of light microscopy techniques and the requirement for fixation in traditional electron microscopy techniques prevents live cell imaging. AFM is uniquely positioned to overcome these limitations. For example, high resolution AFM images have been essential in understanding the organization of the light harvesting complex in native membranes of photosynthetic bacteria (31). The importance of the technique for probing the physical properties and interaction forces of microbial surfaces has also been demonstrated as well as the advantage of integrating AFM with other techniques (32,33). In an effort to illustrate the applicability of AFM to questions in microbiology, the following examples are given.

As the “worker molecules” in the cellular environment, proteins interact with other cellular constituents (e.g. DNA, cofactors, proteins, lipids etc.) to perform all the activities required to sustain the cell. Understanding their structure and localization lends insight into their function. Soluble proteins are amenable to crystallographic structural techniques whereas membrane-bound proteins are less so because of their tendency to aggregate and to form a number of transmembrane helices. Therefore structural techniques which allow for the examination of these proteins in the membrane are important. In addition to relying on membrane lipids for structure, membrane proteins have transmembrane helices that interact specifically with each other to maintain their stability in the membrane. Understanding the forces required to disrupt this stability provides important structural information and is a very active area of research today.

Bacteriorhodopsin (BR) is a light-driven proton pumping protein from *Halobacterium salinarum* having 248 amino acids and 7 transmembrane helices. It is organized into trimers which are packed into 2-dimensional hexagonal lattices. In the membrane of the organism, these lattices form purple patches which can be isolated for study. BR orients predictably with the same, charged end facing up when membranes are adsorbed to freshly cleaved mica. Oesterhelt *et al* exploited this tendency in their AFM

study of BR(34). After imaging the membrane, they reduced the scan size and selected a monomer of interest. The tip was pushed into the protein to allow the protein to adsorb to the tip. As the tip was retracted at a fixed speed, the forces between the tip and sample were monitored. Their interpretation of the resulting force data allowed them to conclude that the first six helices were extracted in pairs due to specific interactions between the helices. Emphasized in this example of an AFM investigation on the molecular scale is the ability of the technique to provide single molecule data. At this resolution, AFM can be instrumental in understanding molecular mechanisms.

Subcellular structures of microbes can also be investigated by AFM as demonstrated by Touhami and colleagues. They generated high resolution AFM images to characterize the pili of a laboratory strain of *Pseudomonas aeruginosa* (PA01) (35). In addition, the authors immobilized PA01 to the cantilever and approached the mica substrate, giving pili on the bacteria the opportunity to adhere to the mica. This setup permitted the authors to calculate the forces required to either dissociate the pili from the mica or to break the pili. Although the two scenarios could not be distinguished in their experiments, the sensitivity of the AFM for force measurements is nevertheless highlighted.

The applicability of AFM in microbiology is also demonstrated in a report on *Bdellovibrio bacteriovorus*(36). This organism is a gram negative predator of other gram-negative bacteria. The authors contend that predation behavior at interfaces (air-solid or liquid-solid) may differ from those in solution. They simulated the air-solid interface by growing the bacteria on sterilized, small-pore filters placed on agar plates. In some experiments, *Bdellovibrio* were mixed with prey before placement onto the filters. Using this approach, the life cycle of *Bdellovibrio* was imaged by AFM periodically for several days. Key to this study was the ability of AFM to provide high resolution images without fixation. It was previously demonstrated that *Bdellovibrio* invaded following a violent collision with their prey; resides between the membranes of the prey; and utilizes the prey's macromolecules for growth. During this period the combined organism is called a bdelloplast. Following nutrient consumption, the *Bdellovibrio* divides into progeny cells and lyse the remains of the prey to swim away and repeat the process.

From EM studies, unaffected prey could be distinguished from bdelloplasts based on changes in their 2-dimensional shape, but this study provided evidence that there were also 3 dimensional changes. Specifically, bdelloplasts were shown to be “rounded up” and smoother than uninvaded cells. The enlargement at the site of attachment had been previously seen in EM images but researchers were unable to eliminate the possibility that this feature was an artifact of preparation. Again, the ability to image these cells without modification was important to the findings in this study. The authors subsequently demonstrate that predation occurs in biofilms of *E. coli* (37). This finding may have application in the treatment of illnesses associated with biofilms given that *Bdellovibrio* are harmless to eukaryotic cells. A broader discussion of the role of AFM in biofilm research has been given (38).

Despite being a versatile technique with broad applicability in the life sciences, AFM does have noteworthy limitations. As a surface technique, AFM cannot provide information about intracellular constituents and their activity. Also, the maximum scan range of the piezo scanner in the AFM is around 100μm making larger cells difficult or impossible to study with the technique. AFM imaging of rough surfaces requires slow scan speeds (< 1 line per second) to maintain the stability of the tip and to minimize image artifacts. Optical techniques, based on immunofluorescence labeling and fluorescent protein expression, are well-established and complement these shortfalls (39,40). The fact that the two imaging modes can be combined is particularly relevant to whole cell studies.

1.2 Thesis Overview

In the 17th century using simple microscopes, Robert Hooke and Antoni van Leeuwenhoek were the first to see living microorganisms(41). To this date, microscopy, albeit more sophisticated, remains essential for understanding the little creatures and their role in human life. Genome sequencing efforts have helped tremendously in understanding the genetic components of microbes but assigning function to gene products is dependent on localization, trafficking, and structural studies. Modern day microscopy techniques are compatible with these kinds of studies because spatial and temporal changes can be monitored in living cells. Of course, biochemical techniques

have also contributed, but they generally produce composite data which may not reflect the physiological state of every cell. Because they are essentially a “snapshot in time” cellular dynamics are not fully represented. Moreover, experimental conditions of these techniques may alter the behavior of the biological component under study. For example, proteins *in vivo* have a much different environment than proteins *in vitro*. (proteins, cofactors, different concentrations).

The intent of this review is to convey the utility of AFM for a variety of research applications in biology, particularly microbiology. Until the emergence of AFM, techniques for investigating processes in single microbes were limited as were techniques for imaging subcellular and molecular structures in microbes. While the imaging capabilities are impressive, the ability to simultaneously generate physicochemical data is unrivaled by other techniques. The fact that AFM can be used in buffers or media cannot be over emphasized. It is arguably, the most appealing feature of AFM because this provides a favorable environment for live cell imaging. The benefit of optical microscopy in biology is also highlighted. The available options for specifically labeling proteins of interest have been important in understanding cellular dynamics. Because samples for optical microscopy can also be maintained in liquid, it is suitable for complementing and validating AFM results.

This thesis work was undertaken in an effort to extend the utility of AFM for monitoring molecular changes in bacteria. The model organism is a modified form of the bacteria: the spheroplast. Spheroplasts are formed when the outer wall of bacteria is enzymatically removed. Several groups have employed AFM to investigate the outer surfaces of various bacteria but none have extensively studied the spheroplast (42-46). Because active transport in bacteria occurs primarily in the cytoplasmic membrane, spheroplasts are an appropriate model organism for localizing membrane proteins and studying their mechanisms *in vivo*. The fact that the constituents of the outer and cytoplasmic membranes differ significantly requires consideration in AFM studies. With the exception of the brief discussion regarding immobilizing intact bacteria, the focus of this study is the spheroplast, beginning with the problem of their immobilization. Because spheroplast preparation requires the bacteria to be without nutrients for a period of time, the issue of whether the cells remain metabolically active is confronted.

Also, properties of the spheroplasts which impact their use in AFM-based investigations are discovered. Finally, protein recognition on the surface of spheroplasts is demonstrated. Together, these experiments establish a role for AFM in single cell studies of spheroplasts of bacteria.

1.3 Intact bacteria immobilized using gelatin-coated mica

In order to image biological samples using AFM, cells and proteins must be anchored to the substrate to prevent displacement by the scanning tip. Because the surfaces of these samples can differ dramatically, so must the strategies for immobilization. Immobilization procedures are established for intact bacteria and have facilitated investigations on elasticity, adhesion, surface structure and swarming behavior (42,47-49). Drying the bacteria to the substrate is one way of immobilizing them although cells are apparently dehydrated during the process as indicated by their flattened or collapsed appearance in AFM images (50). Moreover, cells immobilized this way are often not stable when imaged in liquid. A simple and effective immobilization strategy for both gram-negative and gram-positive bacteria is to briefly incubate a bacterial suspension on a gelatin-coated mica surface (51,52). This technique results in isolated bacteria distributed throughout the sample which reduces the amount of time required to find a region of interest. The cells can be stably imaged in air or liquid, using contact or noncontact imaging modes.

Bacterial adhesion to substrates is believed to occur in two stages: the initial, reversible attachment and the more durable, irreversible attachment which follows (53,54). Rinsing has been shown to displace bacteria in the earlier stages of adhesion and irreversible attachment occurs within minutes (55). Considering that bacteria immobilized on gelatin-coated mica can be rinsed under a stream of water without removing the bacteria and that the bacteria are permitted to contact the surface for several minutes before rinsing, it is speculated that bacteria in the sample prepared for AFM imaging are irreversibly attached. Intact bacteria mounted by this method were imaged in water using AFM or confocal fluorescence microscopy. (Figure 2) No apparent morphological abnormalities are observed in these cells except that some *E. coli* cells constitutively expressing cytoplasmic GFP (CC-GFP) are slightly elongated, compared to cells without

the plasmid. (Note that bacterial strains used in this report and their relevant characteristics are listed in Table 1.) In these images, bacterial cells appear to be hydrated and measure within the expected height and length ranges. Over 350 bacteria are seen in the 75 μm x 75 μm scan area of the AFM image. Several bacterial species, including *E. coli*, bind collagen and gelatin (denatured collagen) via specific binding sites on the intact bacterial surface (56,57). It is likely that these binding sites, along with electrostatic and hydrophobic interactions, contribute to retaining bacteria on gelatin-coated substrates. Given its effectiveness, gelatin-coated mica is the substrate used for immobilizing the intact bacteria in this thesis.

Chapter 2

Mounting *E. coli* Spheroplasts for AFM imaging

This chapter is a combination of two papers published in the journal *Ultramicroscopy* which address the issue of immobilizing bacteria for imaging by AFM. The first paper entitled "Mounting *E. coli* Spheroplasts for AFM imaging" was authored by Claretta Sullivan, Jennifer Morrell, David Allison and Mitchel Doktycz (58). The second paper entitled "Comparison of the Indentation and Elasticity of *E. coli* and its Spheroplasts by AFM" was authored by Claretta Sullivan, Sankar -, Scott Retterer, David Allison, and Mitchel Doktycz (59).

Data, images, and text relevant to immobilizing bacteria have been included from both papers. Images are presented in color where they were published in black and white. Text has been edited in such a way to prevent redundancy and to provide continuity. In both papers, co-authors graciously provided direction, reviewed the data and manuscripts, responded with feedback and offered editorial comments. Under their guidance, I selected the topic, performed the experiments, analyzed the data, conducted the necessary literature review and drafted the manuscripts.

2.0 Introduction and Significance

Ongoing genomics and post-genomics-based studies are providing complete inventories of the molecular components that constitute biological systems. Deducing function, however, is more complex and requires complementary techniques that identify and characterize these systems at the molecular and cellular level. One significant challenge is characterizing the large fraction of the proteome (on the order of 25–30%) that is at or near the cell membrane. Biochemical techniques and prediction programs are used routinely for predicting the topology of transmembrane proteins. For 3-dimensional (3-D) structural analysis, crystallography remains the premier, high resolution technique. Unfortunately, hydrophobic stretches of amino acids, typically found in membrane proteins, impair their ability to form 3D crystals. Furthermore, the relatively large quantities of protein required for crystallography can be difficult to generate with membrane proteins. The problem lies in the fact that lipids provide a necessary framework for the structure and function of membrane proteins but they must be removed for crystal formation. Other techniques in membrane protein dynamics allow lipids to be present but require isolation of the proteins from cellular membranes and subsequent reconstitution into model lipid bilayers. After this potentially long and tedious process, the structure and function of the reconstituted protein can differ from that of the

native one. Alternative techniques which can improve the efficiency with which membrane proteins can be studied are of great interest to membrane biologists. Published work has already shown the potential of AFM to be a valuable tool in this regard (60). In addition, the technique has been used for investigating adherent eukaryotic cells (14,61-63) and immobilized microbes (43,64-67).

The small size of bacterial cells presents unique problems in imaging when compared to eukaryotic cells. AFM overcomes limitations in spatial resolution associated with optical microscopy and is therefore emerging as an important research tool in microbiology (68). Although high-resolution imaging of bacteria is possible with electron microscopy (EM), cells traditionally must be fixed with cross-linking agents and imaged under vacuum, conditions that prevent imaging of live cells. In contrast, live cells can be imaged under physiological conditions with nanometer resolution using AFM. In addition to recording cell morphologies, surfaces can be probed by the AFM stylus to reveal structural and physicochemical properties not accessible via other microscopy techniques. Such data have yielded important insights concerning turgor pressure in magnetotactic bacteria and surface proteins in lactic acid bacteria. (66,67).

Another impediment in working with gram-negative bacteria is that they contain a cell wall that restricts access to the cytoplasmic membrane (69). As the selective barrier for the cell, the cytoplasmic membrane is the location of transporters, channels and other proteins whose function is to judiciously exchange materials between the cell and its environment (70). Understanding the structure, function, and organization of these proteins has implications for rational drug design, bioengineering and biotechnology (71-74). Given the difficulty of working with membrane proteins, and the capabilities of AFM, experiments to examine the cytoplasmic membrane of gram negative bacteria were targeted. Before such experiments could be conducted however, consideration was given to the surfaces of the bacteria involved.

Like other gram negative bacteria, the cell wall of *E. coli* includes an outer membrane (with appendages such as fimbriae, pili, and flagella), peptidoglycan and periplasmic space. (Figure 3) Lipids of the outer membrane are asymmetrically arranged in such a way that lipopolysaccharides (LPS) are primarily in the outer leaflet and phospholipids

make up the inner leaflet (75-77). Each LPS molecule is made of lipid A, a core polysaccharide, and an O-antigen. The lipid A region of each molecule contributes six or seven saturated fatty acid chains to the hydrophobic core of the bilayer. This saturation significantly reduces the fluidity of outer leaflet. The core polysaccharide region has been shown to be anionic and requires divalent cations to remain in the bilayer. Molecular dynamics simulations demonstrate that the integrity of the outer membrane is dependent on these cations mediating the significant repulsive forces between neighboring LPS molecules (78). The terminating and hydrophilic O-antigen is the most variable portion of the LPS. Its polysaccharide repeats vary in composition, order and structure. It is also characteristic for a given strain of bacteria. This complexity in the outer membrane maximizes its ability to serve as a protective barrier for the bacteria against hydrophobic antibiotics, bile salts, detergents and other detrimental substances. (Figure 4)

The periplasmic space is the gel-like portion of the cell wall which is between the outer leaflet of the cytoplasmic membrane and the inner leaflet of the outer membrane (79). It contains the peptidoglycan, the rigid structure which confers the shape of the bacteria. The peptidoglycan also mediates osmotic stress as the bacteria navigate environs with differing osmolarities. The repeating unit of the peptidoglycan is generally made of a disaccharide of N-acetylglucosamine and N-acetylmuramic acid and a peptide containing L-alanine, D-glutamic acid, meso-diaminopimelic acid and D-alanine (80,81). The sugars alternate to form the backbone of the polymer and are connected via a 1→4 glycosidic bonds. The peptide is attached to the muramic acid and extends away from the glycan chain. (Figure 5) Although considerable debate surrounds the orientation of the glycan chains in the bacteria, the molecular constituents are not disputed (1,82,83).

Gram-negative bacterial cell walls can be removed enzymatically by treatment with lysozyme and ethylenediaminetetraacetate (EDTA) to allow access to the cytoplasmic membrane (84). Lysozyme cleaves glycan polymers at the glycosidic bond of N-acetylmuramic acid residues and quantitatively produces disaccharides (85). On the other hand, EDTA chelates the divalent ions between LPS molecules in the outer cell membrane (86-88). The combination of lysozyme and EDTA therefore leads to the degradation of the cell wall structure. The resulting spheroplasts are osmotically

sensitive but believed to be viable (84,89-91). They can be maintained in sucrose containing buffers which maintain osmotic balance and can be grown in broth where they retain a uniformly spherical shape. This uniformity is lost when the spheroplasts are grown on soft agar, a characteristic attributed to differences in local stresses provided by the agar (92,93). Nevertheless, specialized growth conditions have been formulated for their long term propagation in vitro (94-96). Spheroplasts of various bacteria have proven to be useful research models to study mechanosensitive ion channels, lipopolysaccharide translocation, solute uptake, and the effects of antimicrobial agents (97-101).

From a biomedical perspective, clinical and histological studies revealed that bacteria without cell walls, known as cell wall deficient (CWD) forms, are present in human diseases including Lyme disease, Crohn's disease, endocarditis, acute coronary syndromes, sarcoidosis, osteomyelitis, arthritis, inflammatory bowel syndrome, and meningitis (102-104). Complications in bone marrow transplants and disease treatment as a result of antibiotic resistance have also been associated with CWD bacteria (103). In plant biology, cell wall deficient bacteria have been used as plant biocontrol agents as they can form symbiotic relationships with plants (94). Conventional genetic techniques can not distinguish between CWD or spheroplasts and their intact counterparts because they are genetically identical. In this case, alternative imaging techniques may provide the best opportunity for characterizing the organisms. Electron microscopy has played a significant role in characterizing these organisms as spherical with a single, cytoplasmic membrane (84,96,103-106). Although high resolution imaging is possible with EM, the requirements for fixation and staining of samples for image contrast severely limits the study of living organisms. AFM would be an attractive technique for studying these organisms because they could be maintained and imaged in biocompatible conditions. Moreover, AFM is capable of simultaneously achieving nanometer spatial resolution and piconewton force detection allowing for detailed studies of cell surface morphology and monitoring of cell-tip interactions. This capability has been used to measure cell elastic and structural properties, identify specific molecules in the membrane of living cells, and to measure binding affinities at the single molecule level (107-114). It is expected that the approaches described in this thesis for imaging

spheroplasts by AFM would also be relevant to investigations of other cell types including CWD forms.

Immobilization of spheroplasts is a prerequisite for AFM-based imaging studies intended to characterize membrane transporters and other cytoplasmic membrane constituents (e.g. phospholipids, lipid rafts, membrane-associated proteins). Otherwise, forces generated by the tip during scanning could displace the cells. Further, physical access to the cytoplasmic membrane of immobilized spheroplasts facilitates experiments that can determine protein location, charge contributions and interactions with proteins or other molecules tethered to the AFM probe (12,110,111,115-117). Adhesion molecules, present on the exposed surfaces of intact bacteria, likely account for their immobilization on the gelatin-treated substrate (118,119). The absence of these molecules necessitates alternative strategies for immobilizing the spheroplasts for AFM imaging. Despite their relevance as model organisms in biomedical research, spheroplasts and CWD forms have yet to become the subject of extensive AFM investigations. While procedures for making spheroplasts have been established for decades, immobilizing them for microscopy studies has only recently become a requirement. Described in this chapter, are immobilization techniques for spheroplasts in appropriate buffer conditions which allow stable AFM imaging of the cells. A comparable effectiveness for immobilizing CWD is also generally proposed.

2.1 Spheroplast Immobilization using warm gelatin

The major transport proteins in bacteria localize to the cytoplasmic membrane, a surface normally not exposed due to the presence of the outer cell wall. Therefore, characterization of proteins in this membrane by AFM requires removal of the outer wall using a spheroplasting procedure that renders the cells osmotically sensitive (84). When these spheroplasts were immobilized using the protocol designed for intact bacteria, stable imaging was not possible (Figure 6). Instead, the spheroplasts appeared to move from their original position and change morphology after multiple scans due to force interactions with the cantilever tip. These findings are similar to behavior described for *Deinococcus geothermalis* in which a firm but slippery attachment was found to exist when these microbes were attached to stainless steel and imaged in water (120). The

observation that spheroplasts are not securely immobilized using this method is likely due to different, less stable interactions between gelatin-coated mica and the cytoplasmic membrane which lacks the surface proteins, lipopolysaccharides and pili thought to contribute to immobilization of intact bacteria. For this reason, it was necessary to find an alternative method for immobilizing spheroplasts for AFM studies.

Techniques for immobilizing spherical yeast cells have been published which involve stabilizing the cells in agarose or trapping them in the pores of a filter membrane before imaging (121,122). (Notably, the filters are effective for spherical cells but not for rod-shaped cells(32).) Although yeast cells and bacterial spheroplasts are both round, yeast cells are significantly larger, have a rigid cell wall, and are less fragile than spheroplasts. Attempts to trap the spheroplasts in the pores of membranes were unsuccessful, possibly because the flexible cell membrane allows many spheroplasts to compress and pass through the filter. This idea is supported by the finding that CWD forms are able to penetrate filters having only 220nm pores (104). Confocal microscopy images show that some spheroplasts are retained in membrane (Figure 7a,b). However, these cells could not be seen in AFM experiments (Figure 7c,d). This is probably because the height of the filter (7-22μm according to the manufacturer) causes many of the spheroplasts to be buried within the membrane. There were areas on the surface of the membrane suggested, by the contrast in the image, to be different (arrows). These may be spheroplasts but the rough topography of the filter surface prevents a clear determination. This approach was not pursued further in this study.

Instead, a method was developed in which a small volume of warm gelatin is applied to a freshly cleaved mica surface followed immediately by addition of the spheroplast suspension. After a brief period of incubation, the spheroplast sample can be stably imaged for several hours in a 0.25M sucrose solution which prevents rupture of the osmotically sensitive spheroplasts. Unlike the rod-shaped intact *E. coli* cells, the more than 125 spheroplasts in the 75 μm_75 μm scan area are clearly round and measure 1–3 μm in diameter (Figure 8a), consistent with published measurements (84,90). To address whether this method resulted in stable immobilized cells, multiple sample preparations were scanned repeatedly without any apparent movement of spheroplasts. The outcome of such an experiment is given in Figure 8b –e. Repeated scans of two

spheroplasts, made over a period of 3 hours, result in no detectable changes in spheroplast morphology or height measurement, indicating the usefulness of this technique for stabilizing spheroplasts for AFM imaging. Height measurements varied considerably between individual spheroplasts, ranging from 10 to 250nm (Figure 8d, e and data not shown). These differences could be explained by either dehydration or by entrapment of spheroplasts at different depths in the gelatin layer. To confirm that the spheroplasts are not lysed in the gelatin, z-series optical sections were collected from cells expressing GFP using confocal fluorescence microscopy (Figure 9a). This experiment confirms that the spheroplasts are indeed spherical and are arranged at varying heights within the gelatin layer (Figure 9b). Thus, apparently only a portion of the spheroplast surface is accessible for characterization using AFM (Figure 10). A model describing the process by which gelatin associates from individual single stranded coils into a fibrous network and its dependence on concentration and thermal history has been published (123). Further, AFM-based investigations produced images of intermediate steps throughout this gelation process (124). Although the time scale in which these experiments were performed precludes visualization of a fibrous gelatin network, it is likely that an underdeveloped network is involved in the immobilization of spheroplasts via an entrapment mechanism.

Although spheroplasts having the expected morphology could be seen in samples prepared as described, occasionally spheroplasts with irregular boundaries and “lumpy” surfaces could also be seen. (Figure 11) This observation raises questions about the affect the gelatin temperature might have on the cell. It is possible that some cells were damaged in spite of appearing to be normal in the AFM images. Did membrane lipids undergo a change due to the temperature of the gelatin? Might folding of the membrane proteins and their function also be affected by the elevated temperature? Additionally, the possibility that a thin layer of gelatin remains on the surface of the spheroplasts cannot be eliminated. In view of these observations, alternate strategies which do not involve the use of warm gelatin were developed for immobilizing spheroplasts.

2.2 Immobilization using mica pretreated with APTES/glut

It was demonstrated through confocal microscopy that using warm gelatin to immobilize spheroplasts results in some of the spheroplasts becoming embedded in the gelatin to various depths. It is possible that gelatin masks the surface of the spheroplasts preventing direct contact between the tip and the cell. Furthermore, the temperature of the gelatin may affect the characteristics and integrity of the membrane and its proteins. Therefore an alternative immobilization technique that allows for rapid, facile mounting of cells and increased accessibility to the cantilever was pursued.

Glutaraldehyde is one of several cross-linking agents used in light, electron and atomic force microscopy. It is a small molecule able to crosslink the free nitrogens of the amino acids of proteins with the aldehyde groups on both ends of the glutaraldehyde molecule (125). Wang *et al* reported that mica pretreated with aminopropyltriethoxysilane and glutaraldehyde (APTES/Glut) was an effective substrate for immobilizing and imaging chromatin using AFM (126). The immobilization of chromatin was believed to result from interactions between proteins on the chromatin and the treated substrate. Adapting this procedure, an aliquot of a spheroplast suspension was applied to APTES/Glut treated mica. Figure 12 is a schematic of what is believed to occur. Amino groups on the surface of the substrate (resulting from APTES deposition) are crosslinked by glutaraldehyde to the amino groups of various proteins on the bottom of the spheroplasts. Conceivably, only the surface of the spheroplast in contact with the mica surface is affected by the crosslinking, leaving the exposed surface both in its native state and accessible to the tip.

The images shown in Figure 13 indeed show that spheroplasts can be immobilized on APTES/glut substrate and imaged in buffer. As with the previous method, the cells are distributed throughout the surface. Although the cells are clearly anchored to the substrate, the topograph image shows that their shape tends to follow the direction of the scan. (Figure 13a arrows). Distinct features of the cell surface cannot be resolved even after reducing the scan size to approximately 1μm. (Figure 13b,c). This suggests that the surface complies substantially during imaging due to the absence of the mechanical support provided by either the gelatin matrix or the peptidoglycan. The

condition of the cell gradually declines over time, perhaps because membrane constituents are accumulating on the tip. Altogether, these observations indicate that more tip-sample interactions occur during scanning when spheroplasts are mounted on APTES/glut substrates, further substantiating the argument that access of the tip to the sample is umimpeded. The irregularly shaped cells with the lumpy surfaces (seen with the warm gelatin immobilization) do not occur with the APTES/glut substrate. This is attributed to the fact that the temperature of the sample was never elevated beyond ambient air temperature. Finally, CC-GFP *E. coli* were mounted on APTES/glut surfaces and imaged by confocal microscopy to demonstrate that this mounting procedure is compatible with light microscopy techniques. (Figure 14a). With this finding, validation experiments can be conducted across microscopy techniques using the same sample preparation.

That the interaction between the glutaraldehyde and the surface proteins is nonspecific suggests that the APTES/glut surface could also be used to secure spheroplasts of other bacteria. To test this possibility, spheroplasts were generated using *Pseudomonas aeruginosa.* Note, the spheroplasting procedure was the same as the one used for *E. coli* except that a higher concentration of lysozyme was required. As can be seen in Figure 14b, the spheroplasts of *P. aeruginosa* are immobilized as well as those of *E. coli*. Repeated attempts to apply the strategy to intact *E. coli* were unsuccessful. It may be that the motility of the bacteria interferes with the ability of glutaraldehyde to crosslink the cells.

In summary, adhesion proteins associated with the outer surface and pili of *E. coli* are likely contributors to the immobilization of the intact bacteria on gelatin-coated mica. In order to study bacterial cytoplasmic membrane proteins by AFM, access to the cytoplasmic membrane can be achieved by removing the outer cell wall from the bacteria. However, simple adhesion of spheroplasts to a gelatin surface does not occur as it does for intact bacteria. Entrapment of spheroplasts by applying a warm layer of gelatin is shown to be one immobilization strategy. Upon cooling, gelatin molecules reassociate in an effort to reform collagen fibers, and these gelation intermediates are believed to entrap the spheroplasts, stabilizing them for AFM imaging. The degree of entrapment varies for the spheroplasts, and some are buried below the gelatin matrix.

Local probe techniques such as AFM rely on the tip having access to the surfaces being examined. For cellular imaging, this requires that sample preparation include a way to secure the cells to the substrate and simultaneously retains the tip's access to the surface. While the warm gelatin immobilization meets the first condition, the strategy could not satisfy the second. A preferred approach is to modify the substrate with amino groups then crosslink the cells to the surface using glutaraldehyde. In this way the cells are securely fastened to the substrate. Additionally, the cytoplasmic membrane surface closest to the tip is unaffected by the fixation that influences the membrane contacting the substrate. This is a robust method of immobilization as the cells are not displaced during repeated scanning. The inability to discern membrane features however, implies that the cytoplasmic surface is very pliable and may present challenges for generating high resolution images.

Chapter 3

Assessing Metabolic Activity in Immobilized Spheroplasts

"By the means of Telescopes, there is nothing so far distant but may be represented to our view; and by the help of Microscopes, there is nothing so small as to escape our inquiry; hence there is a new visible World discovered to the understanding." Robert Hooke, 1665. Quoted by Gest, H. (2004) Notes and Records of the Royal Society 58(2), 187-210.

3.0 Introduction

Cells are sustained by a variety of metabolic pathways which transport nutrient molecules into the cell and waste products out of the cell. In bacteria, these processes are controlled by feedback mechanisms which convey the environment's suitability for providing the nutrients needed by the bacteria for survival (127,128). The cell responds to this input in ways that optimize transport of substrates in or out of the cell as appropriate. Responses may include chemotaxis, increased synthesis of transport molecules, allosteric changes in binding proteins and repression of proteins that inhibit transport. The ability to routinely follow these responses in living cells, in real time, on the molecular scale would be a significant advancement in microbiology. Optical and atomic force microscopies have been important techniques for protein localization and investigating the surface properties of bacteria (109,129-131). Combining the techniques has the potential to facilitate molecular systems level questions. These techniques are particularly attractive because they allow cells to be imaged in buffers and media (i.e. without harsh fixatives which eliminate the possibility of viewing live cells).

Whether metabolic processes continue to function during imaging-based investigations is fundamentally important yet many AFM-based studies of bacteria do not address this question directly. Reasonably, viability can be assumed when logarithmic phase cells are imaged shortly after being taken out of growth media. The generation of the spheroplasts and the mounting procedure are executed in buffers (not media) and can take several hours. This lengthy sample preparation protocol raises questions about the

condition of the organism during imaging. The goal of this chapter is to demonstrate that metabolic pathways are active in the immobilized spheroplasts, making them suitable organisms for live cell imaging-based investigations of dynamic processes. To begin, the condition of the spheroplasts after immobilization is determined by evaluating membrane integrity, metabolic activity, the potential for increasing cell mass and protein synthesis. These measures aid in assessing cell condition and molecular system function after mounting.

3.1 Cell Condition

Live cell imaging makes it possible to monitor dynamic processes in real time. While mounting intact bacteria for imaging can be accomplished in a short time, several hours are required to complete the sample preparation protocol for spheroplasts. This can be significantly longer than the generation time of the cells. The lengthy sample preparation and the fact that stationary phase bacteria were used, raises questions about the condition of the spheroplasts during imaging. It is believed that attachment to surfaces in biofilms benefits intact bacteria because nutrients are concentrated at the membrane (132,133). Constituents of the *E. coli* cytoplasmic membrane are primarily phospholipids and proteins, making the surface of the spheroplasts markedly different from the intact bacteria surface which presents lipolysaccharides in addition to proteins and macromolecular structures specifically used for adhesion (134-136). Do these differences in membrane components affect how nutrients are concentrated on the spheroplasts surface? Does direct contact of the cytoplasmic membrane with the substrate have an unexpected affect on the metabolism of the organism? In the absence of shaking in the incubator, is the diffusion of carbon sources to the bacteria and waste products away from the bacteria sufficient to sustain growth? While these questions are not answered directly in the current study, they do justify questioning the metabolic condition of the immobilized spheroplasts.

Unlike higher order mammals where heart rate and brain activity might be used to determine whether animals are living, viability in microorganisms is less clear and sometimes controversial (137,138). Viability studies of intact bacteria have been reviewed and are based on a variety of strategies (137,139,140) Researchers

commonly use the ability of laboratory strains of bacteria to form colonies on agar plates as criteria for viability (141,142). This test however can lead to false negatives due to the limited number of culture conditions typically used. That is to say, some cells require special conditions (e.g. nutrients, temperature, longer time etc.) to grow colonies. Varying these conditions can be time and labor intensive. Furthermore, depending on the application, it may be important to distinguish between colonies originating from damaged cells and healthy cells (138). Some researchers have used membrane integrity as criteria for viability (143-147). A limitation of this approach is the false positives which occur when membrane integrity persists in the absence of metabolic activity. In addition to viability studies for intact bacteria, there are studies that correlate the viability of spheroplasts suspended in media containing penicillin with an increased cell mass, RNA, DNA and β-galactosidase synthesis (91,93,148,149). The current paper presents evidence of spheroplast metabolic activity after the mounting procedure described above.

Live/Dead® BacLight™ is a commercially available viability assay which is based on two nucleic acid stains, SYTO9 and propidium iodide. SYTO9 is able to freely cross the cell membrane and has a moderate binding affinity for DNA. The quantum yield of SYTO9 increases dramatically upon binding to DNA (147,150). On the other hand, propidium iodide (PI), which can only cross porous membranes, has a higher affinity for DNA. Whether PI displaces SYTO9 upon binding or an energy transfer occurs between the two fluorophores is controversial but researchers agree that red fluorescence indicates that membrane integrity has been compromised resulting in PI having access to intracellular DNA (150) . On the other hand, green fluorescence indicates that PI has been excluded by a functioning, intact membrane.

The Live/Dead® BacLight™ assay was applied to I108 and EH strains of *E. coli*. These strains were selected in anticipation of later experiments to study the glucose transporter. In *E. coli*, the uptake of glucose is mediated specifically by enzymes EII^{Glc} and EII^{Man} of the phosphotransferase system (151,152). The I108 strain expresses endogenous *ptsG*, the gene that codes for EII^{Glc}, as well as a second copy of *ptsG* from a plasmid. The EH strain only expresses the endogenous *ptsG* gene. Both intact and spheroplasts forms of the bacteria were immobilized and tested. Additionally, a mutant

strain, ZSC112ΔG (ΔGluc), defective in glucose uptake has been previously described and was also tested (151). The results are shown in Figure 15 where both SYTO9 (green) and PI (red) labeled cells are present in the samples. The majority of the cells are only stained with SYTO9, suggesting that most of the cells have retained membrane integrity. The intact cells were harvested from logarithmic phase cells, and as expected, dividing cells can be seen within the sample. (Figure 15a,c,e) When this same assay was applied to spheroplasts of *E. coli*, again the majority of the cells were only labeled with the SYTO9. (Figure 15b,d,f) The varying shades of green supports the conclusion that both dyes can be present within a single cell.

3.2 Determination of Metabolic Activity

To determine whether the cells were metabolically active, additional experiments that examined metabolic uptake were conducted. A commercially available, fluorescently labeled glucose molecule, 2NBDG, has been used to demonstrate metabolic activity based on specific uptake in viable *E. coli* and the lack of uptake in ethanol killed cells (153). The approach for the current study was to test for 2NBDG uptake in I108, EH and ΔGluc strains of *E. coli*. As before, both intact and spheroplasts forms of the bacteria were tested. The results are shown in Figure 16 and Figure 17. Both the intact *E. coli* and the spheroplasts of the I108 and EH strains are able to take up the fluorescent analog. As predicted, neither the intact bacteria nor the spheroplasts of the ΔGluc show the fluorescent staining that would indicate glucose uptake. Although the transmission image shows that the cells are present, the absence of fluorescence confirms the cells' inability to take up the labeled glucose. (Figure 16e,f and Figure 17e,f)

A concern with this assay is the possibility of glucose entering a compromised cell nonspecifically, resulting in false positives. This is a particular concern for spheroplasts because the only barrier to the glucose is the cytoplasmic membrane. In order to address this issue a combination of fluorescently labeled glucose and propidium iodide was used. In principle, the cells which retain specific glucose transport capability will be green as a result of 2NBDG uptake. As before, those cells with compromised membranes will be red because of propidium iodide binding intracellular DNA. As seen in Figure 18a-d, the expected results were observed. In both the intact cells, there are

clearly two populations of cells – green and red. The green indicates that the glucose was able to enter the cells through the glucose uptake pathway and the red represents those cells which have sustained membrane damage.

As a general rule, microbes carrying genetic mutations are not distinguishable in the commercial Live/Dead® BacLight™ assay. As a result, researchers have resorted to using cells either killed thermally, chemically or with UV radiation as controls (145,147,154). Ethanol killed *E. coli* have also been used as the control in 2NBDG assays (155). Such controls introduce another variable into the experiment which may adversely affect the outcome. In contrast, the combination of using propidium iodide, 2NBDG, and ΔGluc cells avoids this problem because all cells are treated identically. The inability of the ΔGluc cells to take up 2NBDG means that they only become fluorescent when the propidium iodide breaches the cell membrane. (Figure 18e,f) This is especially valuable for the spheroplasts studies for which lysis, the primary method used for disruption of function, is undesirable. One disadvantage of using 2NBDG with PI is that the fluorescence of the 2NBDG does not persist as long as the SYTO9 stain. This observation may be due to bleaching effects or because the glucose is metabolized in such a way that it loses fluorescence (156).

Images from Live/Dead® BacLight™ and the glucose propidium iodide assays were further compared. Cells from 7 distinct fields were counted and scored as either green or red. The results are shown in Table 2. Additionally, AFM images were generated on fixed samples of the spheroplasts imaged in air and in contact mode. (Figure 19) Presumably cells with stable membranes would retain their spherical shape (i.e. increased height) upon fixation whereas lysed cells would appear significantly flattened in the AFM image. Indeed the images support this idea because two populations of cells are found in the image. The pyramidal appearance of some cells is an imaging artifact that occurs due to cell height and tip geometry (157). Eleven fields from AFM images of fixed spheroplasts were evaluated for spherical and flat cells. (Table 2) Strikingly, the three assays yield very similar proportions of live and dead cells.

A spheroplasted cell's ability to increase its overall mass is another indication of continued metabolic activity. To test whether the spheroplasts retained this capacity

after mounting, spheroplasts were incubated overnight in media doped with penicillin G. Previous reports demonstrated that the bacteriocidal effect of penicillin stems from its ability to make the cells vulnerable to lysis due to impaired cell wall synthesis (149,158,159). Literature reports further demonstrate that cells survive as long as an osmoprotectant environment is provided (160). Using a strain of *E. coli* which constitutively expresses cytoplasmic GFP (CC-GFP), it was noted that the diameters of the spheroplasts at time 0 and time = 3.5hr did not differ from the normal range of 1-2μm (Figure 20a,b). In contrast, diameters of 6 of 23 CC-GFP cells in the field examined after overnight incubation in LB/penicillin media were increased to as much as 5μm, supporting the hypothesis that spheroplasts are metabolically active after mounting (Figure 20c). The fraction of cells with the larger diameter was consistently less than the fraction of cells indicated to be metabolically active in Table 2. Cells immobilized at various stages of cell division may account for this discrepancy. The media from the overnight sample is always turbid and intact bacteria can be isolated from the media. This indicates that a population of cells undergoes normal division. Whether the rare intact cells within the spheroplasts suspension are dividing or whether spheroplasts less susceptible to the effects of penicillin have produced reverted progeny was not determined. In some cases, the smaller spherical cells appear to be associated with the larger ones. (Figure 21) This association may result from the cell's incomplete separation from the parental cell. Gram negative bacteria are known to produce outer membrane vesicles (75,161). It is possible that the larger diameters are associated with CC-GFP cells whereas the smaller diameters belong to membrane vesicles that have been immobilized on the surface. Further experiments are required to determine definitively the nature of these two populations. The overnight samples were fixed in 0.5% glutaraldehyde and imaged with AFM to confirm the changes in diameter (Figure 22).

Another demonstration of metabolic activity is protein synthesis. Additional experiments were conducted on a strain of *E. coli* expressing cytoplasmic GFP under arabinose inducible conditions (AI-GFP). A plasmid containing the gene was transformed into *E. coli*. Spheroplasts of the cells were generated which were subsequently mounted on the APTES/glut surface as previously described. The cells were then incubated for two hours in a recovery broth (0.25M sucrose, 0.01M $MgSO_4$, 500units/ml penicillin G in LB,

selective antibiotic). Components of the broth prevent lysis, provide nutrients and inhibit the renewal of the peptidoglycan. At time = 0, these AI-GFP spheroplasts were only detectable on the transmission channel. (Figure 23 a,b) The broth was subsequently replaced with fresh recovery broth supplemented with 0.2% arabinose and incubated for an additional 2 hours. The addition of arabinose in the media prompted synthesis of cytoplasmic GFP as seen in Figure 23c,d. Similarly treated cells which were incubated in only fresh recovery broth did not fluoresce (data not shown).

Optical and atomic force microscopies allow imaging of microbes in buffers and media preserving the dynamic state of the organisms. The sample preparation required for imaging varies in severity and length depending on the technique to be used and whether intact or spheroplasts of the bacteria are to be investigated. While sample preparation for intact bacteria can be completed in less than an hour, preparing a sample of spheroplasts requires several hours. In the case of intact bacteria, when cells are clearly dividing (as indicated by septum formation), viability is generally assumed. On the other hand, spheroplasts of bacteria do not have the telling septum and viability after the extensive sample preparation procedure is a legitimate concern. The aim of the experiments in the current chapter was to determine whether spheroplasts of *E. coli* retain indicators of viability after the mounting procedure for AFM. A variety of complementary imaging-based assays provide evidence of metabolic activity, membrane integrity, increasing cell mass and protein synthesis. Together these results make a compelling case for the cell's ability to maintain metabolic systems under stress and give confidence and significance to findings based on the sample preparation described herein. Further, the data also demonstrates the importance of robust sample preparation techniques in facilitating single live cell imaging studies.

Chapter 4

Comparing the Elasticity of Intact *E. coli* and its Spheroplasts

Hooke's description of blue Mould: "The whole substance of these pretty bodies was of a very tender constitution, much like the substance of the softer kind of common white Mushroms, for by touching them with a Pin, I found them to be brused and torn" Robert Hooke, 1665. Quoted by Gest, H. (2004) Notes and Records of the Royal Society 58(2), 187-210.

This chapter is a portion of a manuscript published in the journal *Ultramicroscopy* which compared the elasticity of bacteria with the elasticity of its spheroplasts. The paper entitled “Comparison of the Indentation and Elasticity of *E. coli* and its Spheroplasts by AFM” was authored by Claretta Sullivan, Sankar Venkataraman, Scott Retterer, David Allison, and Mitchel Doktycz (59).

Data, images and relevant text have been included. Images are presented in color where they were published in black and white. Introductory statements have been added and text has been edited in such a way to prevent redundancy and to provide continuity. My co-authors graciously provided direction, reviewed the data, responded with feedback and offered editorial comments. Under their guidance, I selected the topic, performed the experiments, analyzed the data, conducted the necessary literature review and drafted the manuscript.

4.0 Introduction

Previously, sample preparation protocols were established which allowed routine mounting of spheroplasts of bacteria for AFM imaging. An important next step is to begin to understand the surface of spheroplasts as researchers report that mechanical properties of biological samples influence the resolution of the technique (162-169). Indeed, the images produced are a convolution of the mechanical properties of the sample, tip geometry, and interactions between the sample and tip. Spheroplasts have neither the mechanical support provided by the LPS and peptidoglycan of intact bacteria nor the cholesterols and actin networks which contribute to cellular tone in eukaryotic cells. Constituents of the *E. coli* cytoplasmic membrane are primarily phospholipids and proteins, making the surface of the spheroplasts markedly different from the intact bacterial cell (134-136). The peptidoglycan together with the tightly associated LPS

molecules (which limit the fluidity of the outer membrane) are predicted to result in the outer cell surface having a different response from those that have been spheroplasted.

In addition to being a high resolution imaging technique, AFM can be used to assess the nanomechanical property of biological samples (170-172) . This is accomplished through the use of force distance curves which record vertical cantilever deflection as the vertical piezo moves the AFM tip toward the surface, makes contact with the surface, and is retracted from the surface. (Figure 24) These curves can be used to measure surface indentation and elasticity. As the AFM tip is moved into and out of proximity of a surface, the cantilever deflects in proportion to the forces that result from interactions with the surface. The deflection of the cantilever is recorded as output voltage by measuring the change in the position of a reflected laser spot on a photodiode. After contact on a relatively hard surface such as mica, cantilever deflection (voltage) is equal to piezo movement (distance). Consequently, this voltage to distance relationship can be used to convert voltage to tip displacement in nanometers. To make the conversion, the slope of the force distance curve in the region after contact is determined; voltage values along the curve are multiplied by the inverse of this slope; and the curve is plotted again using the original x values and the converted y values. In the resulting curves, vertical movement of the tip approaching, contacting and retracting from the surface is recorded on the X axis in nanometers while deflection of the cantilever is plotted in nanometers on the Y axis.

AFM force-distance curves have been used to determine the elasticity of mammalian cells in the context of understanding associated physiological changes and motility (62,169,173,174). Other researchers investigated cellular elasticity as it relates to microbial adhesion and physiology (67,108,175). Posed here, however, is the question of how the spheroplasts respond mechanically to AFM imaging compared to intact bacteria as this can have important consequences on imaging resolution. To address this question, indentation and elasticity were measured on intact *E. coli*, glutaraldehyde fixed spheroplasts and untreated spheroplasts of *E. coli*.

4.1 Considerations for Successful Imaging of Spheroplasts

Given the effective immobilization techniques for spheroplasts described previously, this section addresses aspects of imaging that are impacted by the cantilever. Although “tip” and “cantilever” are often used interchangeably, their distinction is useful in the context of this discussion. The sharp tip, which contacts the sample during imaging, is mounted on a flexible cantilever. The laser beam, used to monitor deflection, is reflected from the back of the cantilever to the photodiode. The choice of cantilever is an important one and requires consideration because they vary in material, size and shape. Tip geometry is also a variable. These features together determine the mechanical forces imposed on the sample during imaging. Commercially available silicon cantilevers are stiffer than their silicon nitride counterparts. High aspect ratio tips which have a smaller radius of curvature are better for imaging rigid samples with tall features but they are costlier and more fragile than low aspect ratio tips. On the other hand, the blunter silicon nitride tips may avoid puncturing fragile, tall samples such as cells. To illustrate the importance of cantilever selection, intact *E. coli* were imaged using a type Ic silicon Maclever. According to the manufacturer, this cantilever has an estimated spring constant of 0.6 nN/nm but the spring constant is known to vary from 0.15nN/nm to 1.5nN/nm. The cantilever tip radius of curvature is said to be less than 10nm. As shown in Figure 25a and b, MacMode imaging with the type Ic Maclever provides acceptable images of intact *E. coli*. However, when the cantilever was moved to a location on the bacteria and repeatedly brought into contact and retracted from that location (movement in the z plane only), and subsequently imaged, damage apparently occurred. (Figure 25c). When a second location on the bacteria was similarly treated, the same kind of damage was detected. (Figure 25d). This is only one example of how cantilever selection may impact experimental results. The other possibility is selecting cantilevers too soft for the condition of the experiment. For example, imaging intact bacteria with the softer silicon nitride cantilever is progressively more difficult with the smaller spring constants. This is probably because these softer cantilevers are more vulnerable to forces of adhesion (capillary forces) always present when imaging in air. Careful attention should be given to the selection of cantilevers.

Anticipating that the spheroplasts would be more delicate than the intact bacteria, a softer, silicon nitride cantilever having a nominal spring constant of 0.1 nN/nm was used in MacMode for their imaging. (Figure 26a) Although somewhat user dependent, as a general rule, successful imaging of spheroplasts required lower servo gains and scanning speeds than those used for imaging intact bacteria. Measurements taken from individual spheroplasts under these conditions reveal that the lateral diameters of the cells are approximately 1μm, similar to measurements determined from EM images of thin sections (84). Height measurements of approximately 100nm, however, are considerably less than the diameter. (Figure 26b,c) Despite using MAC Mode®, an intermittent contact mode designed to minimize the vertical force applied during imaging, it is likely that the apparent compression of the spheroplast is caused by forces exerted by the tip.

Earlier reports concluded that fixation of mammalian cells with glutaraldehyde increased the cellular elastic modulus significantly (176,177). Since the exposed cytoplasmic membrane of spheroplasts primarily contains phospholipids and proteins, we conducted experiments to determine whether increased rigidity (resulting from fixation of spheroplasts), would affect the cell height. Spheroplasts were treated with 0.5% glutaraldehyde after they had been immobilized on APTES/glut treated mica. When these fixed spheroplasts were imaged by AFM in MAC Mode® with a silicon nitride cantilever having a spring constant of 0.1 nN/nm, the diameters of the fixed spheroplasts were similar to the untreated spheroplasts. (Figure 27) However, the height measurements were increased from 100nm to around 250nm. Nevertheless, the increased height measurements of these fixed spheroplasts were also considerably less than the diameters. This finding raised the possibility that even the glutaraldehyde-fixed spheroplasts were being compressed by the AFM tip, albeit to a lesser degree than unfixed spheroplasts.

To determine whether the reduced height was a consequence of the tip used for imaging or inherent to the spheroplasts, the experiment was repeated on untreated spheroplasts with the softer silicon nitride cantilever having a nominal spring constant of 0.01nN/nm. (Figure 28a). The resonant frequency of the first harmonic of this cantilever was very low and found to be unstable in liquid therefore the 2^{nd} harmonic was used instead.

Following this change to the softer cantilever (0.01nN/nm), the height increased to 300-400 nm, as opposed to the 100nm height found when imaging with the stiffer cantilever. (Figure 28b) These results further supported the notion that compression of the spheroplast occurred during imaging and was caused by excessive cantilever force. Untreated spheroplasts were also imaged in contact mode using the softer (0.01nN/nm) cantilever. (Figure 28c) As seen in the image, the spheroplasts conformed to the shape of the tip and resulted in an image of the tip. It is important to note that intermittent contact imaging, which applies a lower force, was required to prevent these tip artifacts. The ATPES/glut substrate stably immobilized the cells as repeated contact mode imaging did not remove the cells. However, the spheroplasts were severely deformed and often punctured by the tip. Contact mode imaging of normal intact bacteria does not result in similar distortions nor were differences in height measurements noted between those taken with either of the cantilevers.

4.2 Spring Constant Determination

Quantitation of the physical properties of a sample requires knowledge of the physical properties of the cantilever. While the manufacturer can provide estimates of this information, the experimentalist needs to appreciate the variance in cantilever dimensions due to manufacturing tolerance(162). One way to minimize miscalculations in spectroscopy data due to differences in cantilever dimensions is to determine the cantilever spring constant directly. To do so, force distance curves are generated on a hard surface. In addition to calculating the spring constant of the cantilever, these curves can be used to measure surface indentation and elasticity. As the AFM tip is moved into and out of proximity of a surface, the cantilever deflects in proportion to the forces that result from interactions with the surface. The deflection of the cantilever tip is recorded by measuring the change in the position of a reflected laser spot on a photodiode. The output voltage of the photodiode is recorded as a function of the vertical position of the piezo during approach and retraction of the cantilever. After contact between the tip and a relatively hard surface such as mica, deflection is equal to piezo movement. Consequently, the voltage to distance relationship extracted from a force distance curve recorded on a hard surface can be used to determine the calibration coefficient used to convert voltage to tip displacement in nanometers. The spring

constant of the cantilever can be determined by the thermal method if this calibration coefficient is supplied (178-180). Additionally, the calibration coefficient allows plotting of force distance curves where vertical movement of the cantilever approaching, contacting and retracting from the surface is recorded on the X axis in nanometers while deflection of the cantilever when contact is made can be plotted in nanometers on the Y axis.

Determining the best way to generate control force distance curves

Three methods of determining the spring constants of type IVc MacLevers were evaluated. The goal of these experiments was to determine the source of variation when the spring constant of the same cantilever is measured. In each case, force distance curves were generated in an environmental chamber filled with dry nitrogen in order to minimize the capillary adhesion typically present in ambient air. The recorded force distance curves were preceded by several curves to stabilize the piezo. Each method can be considered as having three parts: (1) the approach of the tip to the surface; (2) the generation of the force distance curve, and (3) the calculation of the spring constant by the Thermal K software. All approaches began 50 μm away from the surface. Generally, force distance curves were generated, the slope in the contact region of the curve recorded, the cantilever was retracted from the surface and the conversion coefficient was used as input into the Thermal K program. The methods differed principally in where repetition occurred within the experiment. In the first case, (FDC Method 1) for each force distance curve (i.e. conversion coefficient), Thermal K was prompted to calculate the spring constant ten times. In the second case (FDC Method 2), upon contact with the surface, twenty force distance curves were generated and the conversion coefficient recorded. After retracting the tip each of these conversion coefficients was entered into the Thermal K program and a spring constant calculated. Finally, in the third case (FDC Method 3), for every approach, the conversion coefficient was determined and the spring constant was calculated. (Table 3. Spring Constant Determination - Type IVc)

Ultimately, FDC Method 3 was preferred for collecting force distance curves on the following basis. The small standard deviations in the conversion coefficients of FDC Method 1 and 2 suggest that once the tip is in contact with the surface, little variation

occurs. Similarly, the Thermal K calculations are stable. In contrast, when a new approach is initiated for each spring constant measurement as is the case when using FDC Method 3), the standard deviation increases. (Table 4) Considering that approach and retraction may occur multiple times during an experiment, it was determined that FDC Method 3 more realistically reflects experimental conditions. Limitations in controlling the thickness of cantilevers during the manufacturing process causes significant deviations from their estimated spring constants, providing the impetus to determining the spring constant of the cantilever directly (162).

Calculating the spring constant of the bacteria

When measuring the spring constant of a bacterium, two springs are present in series (the bacterium and the cantilever). In this case, the cantilever deflection occurs over a greater distance as soft samples generally exhibit an initially gradual change in deflection. The spring constant of the bacterium (kb) can be calculated using the equation $k_b = k_c s/(1-s)$ where k_c is the spring constant of the cantilever and s is the slope from a force distance curve taken on the bacterium (66). The nominal spring constant, given by the manufacturer, of the softer cantilever is 0.01nN/nm. However, in order to improve the accuracy of the spring constant calculations for bacteria and spheroplasts, FDC method 3 (described above) was used to generate the force distance curves needed in order calculate the spring constants (k_c) of the cantilevers used.

The spring constants of the cantilevers used on the intact bacteria, fixed spheroplasts and untreated spheroplasts were determined to be 0.0343 nN/nm, 0.0349nN/nm and 0.0519 nN/nm respectively. The magnetic coating, which is added after the cantilever is manufactured, likely contributes to the difference in the spring constants over the nominal value reported by the manufacturer. Approach force distance curves were collected and averaged from selected locations on the surface of intact bacteria, fixed spheroplasts and untreated spheroplasts. Approach force distance curves were also collected and averaged from nearby regions of the substrate surface for comparison. A subsequent image was generated to assess the condition and location of the measured cell. (Figure 29) For each data set, approximately 20 force distance curves were generated within the perimeter of the cell of interest. At least 6 force distance curves were generated at a location outside the cell on the substrate. The control force

distance curves on the gelatin-treated mica were comparable to controls on APTES/Glut treated mica suggesting that any difference between the substrates is negligible for this analysis.

4.3 Indentation

To extract information about indentation from the force distance curves, a computer algorithm was developed to automatically divide the curves into regions. Similar analyses have been described by Li and Logan (175). Relevant to this chapter are the regions before sample contact and during constant compliance. (Figure 30) Upon approach, the tip is too far away from the sample to be deflected, therefore the slope of the force distance curve before contact is zero. This region provides a base line and is set to zero cantilever deflection. Upon hard sample contact, the tip deflects. However with soft samples, such as the cells measured here, the tip begins to indent the sample upon contact. This indentation causes the slope of the force distance curve to change continuously until the slope becomes constant in the constant compliance region.

In order to estimate indentation, control (hard surface) and experimental (cell surface) curves were plotted together. Indentation is defined as the difference between the two curves at the start of the constant compliance region. (Figure 31 and Table 5) The indentation for the intact bacterium is 50nm, similar to values reported previously (66,175). The least amount of indentation, 20nm, occurred on the fixed spheroplast due to the stiffening of the membrane caused by the glutaraldehyde cross-linking. The 160nm indentation of the untreated spheroplast is noteworthy because it represents a significant fraction of the total height of the spheroplast. Curvilinear regions exist in the force distance curves as a result of interactions between the tip and the bacterial surface. The curve is protracted in the case of the untreated spheroplasts because of its tendency to deform. Reaching the quasiequlibrium represented by the linear region of the curve is thus delayed. While qualitative observations can be made, quantitative assertions about this region are complicated by the uncertain point of contact. Therefore the degree of indentation is difficult to determine precisely. Moreover, it is impossible to know whether deflection occurs at the instant of contact or after significant indentation has occurred. If the latter is true, then the indentation for the untreated spheroplast is

underestimated. This possibility is less of a concern in the intact bacteria because indentation is limited by the rigid peptidoglycan.

From the force distance curves generated with the softer cantilevers, slopes for intact *E. coli*, fixed and untreated spheroplasts were recorded. (Table 5) These slopes were substituted in the formula given above for calculating $k_{b.}$ It was determined that the spring constants of the intact bacteria and the fixed spheroplast were 0.194 nN/nm and 0.571 nN/nm respectively. Previously reported spring constants of untreated, intact bacteria range from 0.020 N/m to 0.26 N/m (66,181,182). The measurements provided in this report are within this range, albeit near the higher end. Variations may be attributed to differences in turgor pressure, protocols for force distance curve acquisition and physiology of the bacteria. In the case of the fixed spheroplast, the relative rigidity suggested by the spring constant may be due to the effects of the glutaraldehyde as it has been shown to dramatically increase the elastic moduli of mammalian cells (176,177). On the other hand, when considering the margin of error, the slope measurements on the fixed spheroplasts are only slightly different from the control slope measurements. For the measurement system used here, namely two springs in series, sensible measurements will be obtained when the two springs have similar spring constants. The similarity of the slopes of the fixed spheroplast to that of the control curve indicates that the surface may be much softer than the value obtained. Therefore further experiments are required to interpret the data related to the fixed spheroplast. For the untreated spheroplast, the slope is essentially identical to the slope on the control curve. In this case, the spheroplast is much softer than the cantilever and the cantilever does not deflect until after the spheroplast has been indented.

We have chosen to compare the spring constants of the bacteria rather than employ Hertzian models to calculate Young's moduli for comparison as assumptions regarding homogeneous contact surfaces, defined indenter shape, small deformations, infinite sample thickness and the axisymmetric contact can not be confirmed in AFM measurements on cells. (172,183,184). The spring constant is a direct measurement and provides a quantitative basis for comparison within the experimental system and the parameters described in this chapter.

Experiments to determine the relative indentation and elasticity of intact bacteria, glutaraldehyde fixed spheroplasts and untreated spheroplasts revealed that indentation was a significant fraction of the height of the cell. Considering the indentation and the spring constant measurements together, it appears that even the softer silicon nitride cantilevers (0.01nN/nm) are too stiff to accurately measure the elasticity of the untreated spheroplasts. Due to their morphological similarities, these findings are expected to be applicable to cell wall deficient forms of bacteria.

4.4 Conclusion

The strategy of chemically cross-linking the spheroplasts to an APTES/glut substrate was confirmed to be an effective immobilization strategy as it permits reliable imaging of spheroplasts in liquid. Imaging spheroplasts with stiffer silicon nitride cantilevers (0.1nN/nm) is possible, however the softer silicon nitride cantilevers (0.01nN/nm) resulted in improved height measurements during imaging. The apparent dependence of the height of the spheroplasts on the spring constant of the cantilevers used for imaging raises concerns about the effect that cellular elasticity might have on subsequent AFM-based experiments. At issue is whether compression of the spheroplasts during imaging can be circumvented for AFM-based localization experiments (e.g. immunogold labeling and molecular recognition). While conceivably the unaltered cell surface is the most desirable platform for such experiments, the data presented here demonstrate that mechanical properties of biological samples cannot be ignored.

Chapter 5

Localizing the Glucose Transporter in Spheroplasts of Bacteria Using Microscopy Techniques

"...future improvements of glasses may yet further enlighten our understanding, and ocular inspection may demonstrate that which as yet we may think too extravagant either to feign or suppose." Robert Hooke, 1665. Quoted by Gest, H. (2004) Notes and Records of the Royal Society 58(2), 187-210.

5.0 Introduction

The development of new molecular labeling strategies in optical microscopy, particularly the family of GFP proteins, has been the basis of important insights into bacterial physiology and morphology (185-187). Despite these advances, direct imaging of molecular scale objects is not possible with optical microscopy which remains limited in resolution by the wavelength of visible light. In contrast, the high resolution of AFM, made possible by its ability to detect forces in the piconewton range, is an attractive complement to optical microscopy techniques (65,68,131). The usefulness of AFM in capturing physicochemical and morphological data has been demonstrated in several microbiological applications including: studies on the light harvesting complexes of photosynthetic bacteria, microbial adhesion, motility, biofilms, ultrastructure, morphological development and membrane protein structure (31-33,37,38,188). Other reports clarify the conditions required for high resolution imaging of bacteria and thus enable molecular system investigations in single cells (50,51,59,67,121). The advantage of being able to conduct imaging experiments in buffers and media cannot be overstated. Even when fixed cells are being investigated, to be able to maintain biological reagents (e.g. antibodies, proteins, peptide-conjugated ligands etc.) in buffers is advantageous. In this setting, complex interactions between substrates, transporters and genetic elements could be observed. As an incremental step toward reaching this goal, experiments to identify molecular system components on fixed spheroplasts were undertaken.

The potential of AFM to image membrane proteins in whole cells was recognized very early in the development of the technique. Striking images of native membranes and

proteins reconstituted in lipid bilayers reinforced the expectation that AFM would play an important role in the identification of individual proteins on the surface of cells (31). In spite of the progress made in the field, this prospect has been slow to materialize because the compliant surface of the cell reduces the resolution of AFM images (162,165-169,189). Researchers have circumvented this problem by tethering molecules to the probe, such as antibodies and ligands, which interact specifically with membrane proteins (21,110,116,190). As the tethered molecule on modified tip encounters its complement, a binding event occurs which is detected by deflection of the tip. Indeed this strategy has been used to identify membrane proteins in living eukaryotic cells (113,191,192). This progress is important in membrane biology, given the limited techniques for studying membrane proteins in whole cells. Functional studies of membrane proteins often require purification of the protein and subsequent reconstitution into artificial membrane systems or the use of isolated membranes or membrane patches(193). Although necessary because membrane proteins depend on the presence of lipids for structure and function, many of the cellular dynamics are lost with these approaches. Evaluating membrane proteins in whole cells would provide the best understanding of their *in vivo* function and integration into molecular systems.

Like eukaryotic cells, transport proteins in bacteria are located in the cytoplasmic membrane. Bacteria differ in that a cell wall covers this membrane. In gram negative bacteria, this composite structure includes pili, fimbriae, flagella, the outer membrane, a periplasmic space and the peptidoglycan. AFM-based localization studies of transport proteins in bacteria therefore require direct access to the cytoplasmic membrane where those proteins are located. Having established protocols for immobilizing spheroplasts of bacteria, the benefits of microscopy for their study, and the utility of imaging techniques in studying membrane proteins, the focus turns to the molecular scale characterization of spheroplasts of bacteria. For this purpose, the glucose transporter of *E. coli* was chosen because it is well-characterized and reagents necessary for its investigation are generally available. The glucose transporter is part of the phosphotransferase system in bacteria which catalyzes the phosphorylation of various sugars as well as the translocation of those sugars from the periplasm across the cytoplasmic membrane(194-196) This modular system is comprised of general proteins, Enzyme I and Histidine Protein, which sequentially pass phosphoryl groups from

cytoplasmic phosphoenolpyruvate to sugar-specific Enzyme II (EII) protein complexes which ultimately pass the phosphoryl group to the sugar. To varying degrees, EII complexes differ in amino acid sequence, structure and substrate selectivity (196). The three functional parts of EII complexes (IIA^{sugar}, IIB^{sugar}, IIC^{sugar}) may be a single polypeptide with multiple functional domains (e.g. $IIBCA^{Bgl\ (\beta\text{-glycosides})}$) or a combination of multiple subunits (e.g. $IIA^{Glc\ (glucose)}$ + $IICB^{Glc}$), depending on the organism and the transporter (194). Cytoplasmic IIA and IIB sequentially transfer the phosphoryl group to the membrane-bound IIC domain which contains the sugar recognition site and translocation activity(196).

The glucose transporter of *E. coli*, encoded by the *crr* and *ptsG* genes, has two subunits, IIA^{Glc} and $IICB^{Glc}$, respectively (197,198). The topology of the membrane-bound subunit, $IICB^{Glc}$, has been determined and predicts eight transmembrane helices (199). (Figure 32) The IIC^{Glc} domain (residues 1-386) is located at the NH_2-terminal whereas the hydrophilic IIB^{Glc} (residues 391-476) is located at the COOH terminal. Both termini face the cytoplasm and a linker separates the two domains (151,199). The topology of $IICB^{Glc}$ was determined by fusing a hydrophilic segment of a membrane protein with a reporter enzyme, such as bacterial alkaline phosphatase (PhoA) or β-galactosidase, whose activity is determined by its subcellular location (200,201). From the topology study, *E. coli* strains without endogenous PhoA but expressing glucose transporter/PhoA fusion proteins from a plasmid were described(199). A particular mutant (I108) in which the fusion site is isoleucine 108, was shown to have PhoA activity, suggesting proper folding of the enzyme in the periplasm. Although the PhoA in the topology study served as a reporter enzyme, the experiments described in this chapter use the PhoA as a chemical tag for localizing the glucose protein in the membrane of spheroplasts.

5.1 Immunolabeling Intact *E. coli* and Spheroplasts for Confocal Microscopy

In order to visually confirm that the tagged glucose transporter localizes to the cytoplasmic membrane and to demonstrate specificity of antibodies for PhoA, fluorescence immunolabeling experiments were conducted using the I108 strain of *E. coli*. Although I108 cells express both the endogenous and PhoA-tagged glucose

transporters, the latter is expressed from a plasmid and is immunolabeled with antibodies against PhoA. For the control, the EH strain of *E. coli* was used. These cells express neither the glucose/PhoA fusion protein nor the endogenous PhoA however, they do express the endogenous glucose transporter (i.e. without the PhoA tag). Consequently, no immunolabeling is expected using PhoA antibodies. It is also important to note that both I108 and EH bacteria were assayed using the fluorescent glucose uptake assay in Chapter 3. Both strains were found to take up the glucose but the assay does not determine which version of the transporter is responsible for uptake.

In the first immunolabeling experiments, intact I108 and EH were labeled with a rabbit purified, polyclonal antibody against bacterial alkaline phosphatase (YNNE124PAb, Accurate Chemical Corporation, Westbury, NY). A goat anti-rabbit antibody conjugated to Alexa 488 (A-11008, Invitrogen, Carlsbad, California) was used for fluorescent secondary labeling. With the cell wall preventing access of the antibody to the fused protein, only when cells appeared to be damaged, did labeling occur with the mutant strain I108. (Figure 33a,b) Neither were the intact cells of the control strain (EH) labeled. (Figure 33c,d)

Spheroplasts of I108 and EH were separately immunolabeled with two different primary antibodies and three different secondary labels as appropriate. The results are shown in Figure 34. Spheroplasts of I108 are clearly fluorescent when treated with the YNNE124PAb antibody followed by the Alexa 488- or Alexa 568-conjugated secondary. (Figure 34a,b,c). A similar labeling pattern was observed when a biotinylated rabbit primary antibody to alkaline phosphatase (200-4634, Rockland Chemicals, Gilbertsville, PA) was used in combination with streptavidin-conjugated quantum dots (Qdot® 525 streptavidin conjugate, Invitrogen, Carlsbad, California). (Figure 34d). Whenever I108 cells were labeled with antibodies to PhoA, the fluorescence was localized to the membrane. In contrast, immunolabeling the control EH spheroplasts did not result in fluorescence. (Figure 34e, f, data not shown) Together, these results indicate that the alkaline phosphatase part of the fusion protein is indeed anchored on the periplasmic side of the cytoplasmic membrane in cells where it is expressed. Furthermore, the specificity of the antibodies for the alkaline phosphatase is also demonstrated.

5.2 Molecular Recognition Using AFM

Molecular recognition is the basis of antibody/antigen, receptor/ligand and transporter/substrate interactions in biological systems. AFM can provide unique information about these systems because of its ability to detect forces on the order of those generated in bimolecular interactions (110). The foundation for AFM-based molecular recognition was established in experiments where the tip was transformed into a chemical probe by direct attachment of ligands and proteins (202-206). The altered tips were then used in approach/retraction cycles (i.e. tip movement restricted to the z direction) on soluble proteins which had been immobilized on a hard substrate. Researchers attributed large adhesion peaks on the retraction curves, near the original point of contact, to specific interactions between the opposing molecules. Since those initial reports, experience has shown that nonspecific interactions contribute to these large adhesion peaks. Measures taken to distinguish between specific and nonspecific interactions in more recent studies have demonstrated the benefit of having the tip associated molecule attached via a flexible linker because stretching of the linker generates a distinct feature in the retraction curve and it separates tip adhesion from the interaction (116,207). (Figure 35) Molecular recognition is often based on a set of noncovalent interactions whose orientation and spatial arrangement confer specificity. Importantly, a favorable encounter between the tethered molecule and its complement on the probed surface is encouraged by the free orientation facilitated by the linker (208,209). Furthermore, having only covalent bonds between the tethered molecule and the tip ensures that the energy to break the bond under study will be less than the energy required to break the bonds used for tethering. In addition to investigating isolated, immobilized proteins, researchers recently used tips modified with antibodies and ligands to probe cell surfaces (19,113,210).

The high affinity and specificity with which the avidin tetramer binds biotin has been exploited in molecular recognition assays where one binding partner is used as a molecular tag and the other is conjugated to a reporter molecule (211). The persistence of the reporter is dependant on the presence of the tagged molecule. In the context of localizing the glucose transporter in AFM molecular recognition experiments, an avidin/biotin system was applied. Notably, previous reports demonstrated the ability of

AFM to identify specific interactions between tethered biotin and immobilized avidin (21). This approach has several advantages over the strategy of tethering antibodies. Importantly, PEG linkers with biotin attached on one end are commercially available. This means that tip functionalization only involves attachment of the linker to the activated tip. Because antibodies are not typically available as PEG conjugates, in addition to attaching the linker to the activated tip, a subsequent step would be required to attach the antibody to the linker. Also, using the well characterized avidin/biotin system means that the biotin tips are somewhat generic in that they are compatible with any sample displaying (strept)avidin molecules (e.g. avidin-conjugated, biotin-DNA treated with avidin, streptavidin-gold colloid, (strept)avidin quantum dots etc.). Relative to an avidin-biotin system, tips functionalized with an antibody are restricted in their application. Colloid gold is routinely used to generate contrast in electron microscopy images of cells. It is used much less in AFM because the size of the colloid is on the order of proteins and the two cannot be distinguished unequivocally in AFM images, a problem that is avoided in the tethered biotin/avidin system.

In the current study, a biotinylated antibody against PhoA was applied to fixed I108 spheroplasts. Fixed cells were used because results from elasticity and indentation measurements indicated that their surfaces were more mechanically stable (Chapter 4). The I108 strain of *E. coli* expresses a PhoA-tagged glucose transporter as demonstrated in the confocal experiments above. The EH strain of *E. coli*, similarly treated, was used as the control because neither the tagged glucose transporter nor PhoA is expressed. The treatment of the labeled spheroplasts with avidin was expected to provide a complementary surface for the tip-tethered biotin. A schematic of the labeling strategy is given in Figure 36.

A complete description of the tethering procedure is given in *Chapter 6, Materials and Methods.* Briefly, cleaned silicon nitride tips were treated with aminopropyltriethoxysilane and N,N-diisopropylethylamine in the gas phase to generate activated amino groups on the tip surface. The tips were soaked in a solution of chloroform and NHS-dPEG™$_{12}$-biotin (Quanta Biodesign, Powell, OH) so that amide bond formation occurred between the NH_2 groups on the tips and the NHS-ester of the heterobifunctional PEG linker. At

the conclusion of this treatment, the biotin molecules were attached to the tip via the polyethylene glycol linker which is estimated by the manufacturer to be 5.8 nm long.

The sample was imaged and a single cell was centered within a small (< 3μm) scan area. A location was chosen in the center of the spheroplasts where force-distance curves were generated using the biotin-tethered tip. (Figure 37a) For each bacteria, a set of 550 force distance curves were generated after which the cell was imaged again to ensure that it was not damaged and remained in the same location. (Figure 37b) Retraction curves in each set were analyzed according to guidelines given previously for distinguishing nonspecific adhesion from specific (20,21). Namely, retraction curves displaying a continuous slope beyond the point of contact were considered to represent nonspecific interactions. In contrast, curves with evidence of nonlinear stretching of the linker were counted as representing binding events between the tethered biotin and surface bound avidin. Actual retraction curves representing no interaction, nonspecific interactions, and a binding event are given in Figure 38. The data in Table 6 and Table 7 and in the corresponding Figure 39 were generated using three sample preparations and three cantilevers, each of which is represented at least once for each strain. The maximum number of binding events (21.82%) occurred on one of the I108 cells. The minimal number of binding events (2.18%) is associated with one of the control cells. Two I108 cells (Table 6, cells 2 and 4) as well as two EH cells (Table 7, cells 2 and 5) have binding activity near 10%. These data are outliers given that the overall binding activity in the I108 cells (15.39%) was statistically higher ($p<0.0080$) than in EH cells (5.96%). Because binding events clearly occurred more often on the I108 cells than on the EH cells, molecular recognition is asserted. The findings in these AFM experiments are consistent with the notion that surface avidin is available to the tethered biotin on the I108 cells because of the presence of the glucose transporter labeled with the biotinylated primary antibody. Furthermore, these AFM data are substantiated because results from confocal experiments confirm the presence of the transporter and the specificity of the antibody for it.

5.3 Conclusion

Fluorescence immunolabeling was used to demonstrate that the PhoA-tagged glucose transporter in the I108 strain of *E. coli* localizes to the cytoplasmic membrane. Confocal images only show labeling when I108 cells are converted into spheroplasts suggesting that the antibody is unable to penetrate the cell wall in order to access the PhoA tag which is in the periplasm of the intact bacteria. Several combinations of primary and secondary labeling of the tagged transporter were used to confirm the presence of the transporter in the cytoplasmic membrane of spheroplasts. Control cells (EH) failed to show this specific labeling. AFM experiments were conducted on fixed samples of the same types of cells. Immunolabeling was achieved using a biotinylated antibody and avidin treatment. Cells were subsequently probed with a tip to which biotin had been tethered. Results from these AFM experiments support the findings from the fluorescence immunolabeling experiments in that more binding events occurred when the functionalized tip was used on the labeled cells displaying the tagged transporter.

Chapter 6

Materials and Methods

This chapter is a compilation of the methods sections from all the papers published during and submitted for publication during this thesis project. In some cases, methods evolved to improve efficiency and effectiveness resulting in slight differences from those published previously. Text has been edited in such a way to prevent redundancy and to provide continuity. In the writing of each paper, co-authors graciously provided direction, reviewed the data and manuscripts, responded with feedback and offered editorial comments. Under their guidance, I selected the topic, performed the experiments, analyzed the data, conducted the necessary literature review and drafted the manuscripts.

6.0 Bacterial Strains

E. coli Expressing Arabinose Inducible GFP (AI-GFP)

The sequence encoding Green Fluorescent Protein (GFP) was amplified from pFA6-GFP (212) using primers that introduced 5' *Pst*I and 3' *Hind*III restriction sites. The resulting PCR product was digested with *Pst*I and *Hind*III and cloned into pBAD24 (213) that was also digested with *Pst*I and *Hind*III. The ligation mix was transformed into *E. coli* strain BL21 (DE3) (Invitrogen) and grown overnight at 37˚C on LB agar plates supplemented with 50µg/ml ampicillin. Cells containing the desired construct were identified by screening for GFP expression after 2 hours growth in LB medium containing 0.2% arabinose using a Leica TCS SP2 scanning confocal microscope. The GFP expression vector was subsequently purified from *E. coli* cells using standard methods. Clone 3mC was used in the current experiments. For selection 50µg/ml ampicillin is required.

E. coli Expressing Constitutive Cytoplasmic GFP (CC-GFP)

CC-GFP was a generous gift from Dr. Dale Pelletier, U.S.A., Oak Ridge National Laboratory, Oak Ridge, TN. This BL21-AI *E. coli* (Invitrogen, Carlsbad, CA) carries a pBBR1MCS-5 plasmid (214) which was modified for Gateway insertional cloning (Invitrogen, Carlsbad, CA) and contains the gene sequence for constitutively expressed GFP. For selection, 5 mg/ml gentamicin was added to the media.

The remaining mutants of *E. coli* (I108, EH and ΔGluc) were generous gifts from Dr. Bernhard Erni, Department of Chemistry & Biochemistry, University of Berne, Berne Switzerland. CC118 is a mutant of *E. coli* in which the alkaline phosphatase gene was deleted(215). Buhr *et al* transformed this mutant with vectors which code for glucose transporter (EII^{Glc}) fused with alkaline phosphatase (PhoA) (199). A particular one of these transformants, I108, was used in this thesis work in experiments requiring a tagged glucose transporter. CC118 cells carrying an "empty" plasmid (EH) were used as a control. Selection was accomplished by adding 100μg/ml ampicillin to cultures of EH and I108. Finally, the mutant strain, ZSC112ΔG (ΔGluc) is defective in glucose uptake and was previously described (151). Chloramphenicol was added to a final concentration of 15μg/ml for selection of ΔGluc.

The *Pseudomonas aeruginosa* strain PAO1 was obtained from Dr. Soeren Molin of The Technical University of Denmark.

6.1 Cell Cultures

Unless otherwise noted, cultures were grown overnight at 37°C in a shaking incubator in Luria Broth (LB) supplemented with the appropriate antibiotic for selection. When logarithmic phase cells were required, a fresh culture was inoculated from the overnight culture on the morning of experimentation and returned to the incubator shaker for 5 hours to insure that the cultures were in logarithmic phase when harvested.

6.2 Spheroplasting

The spheroplasting procedure used is an adaptation of the one published by Birdsell and Cota-Robles (84). Briefly, 1ml of stationary phase *E. coli* bacteria from an overnight culture was collected by centrifugation at 4.5 rcf (relative centrifugal force) and washed in 1ml 0.01M Tris-HCL buffer, pH 8.0 (TB). The cells were pelleted by centrifugation and resuspended in 500μl of 0.5M sucrose / 0.01M Tris-HCL buffer (TBS1) to induce plasmolysis. After 20 minutes in a 37°C incubator shaker, lysozyme (Sigma, St. Louis, MO) was added to the cell suspension at a final concentration of 50μg/ml. Note that a 500μg/ml concentration of lysozyme was required to make spheroplasts of

Pseudomonas aeruginosa (PA01). The suspension was returned to the incubator shaker for an additional 20 minutes before it was diluted 1:1 with TB. Ethylenediaminetetraacetic acid (EDTA) was added to a final concentration of 10 mM and the sample returned to the incubator shaker for 20-30 minutes. Light microscopy was used to confirm that >90% of the rod shaped bacteria were spherical.

Cells were pelleted at 0.5 rcf for 25 minutes. (The pellet was often a loose pellet or a thin layer of cells lining the bottom of the tube.) The supernatant was carefully removed with a pipet and quickly replaced with 1ml of 0.25M sucrose / 0.01M Tris-HCL / 10mM $MgSO_4$ buffer (TBS2) using a large bore pipet (to prevent excessive lysis). Again the cells were pelleted at 0.5 rcf for 20 minutes and resuspended in 200-300μl TBS2.

6.3 Mica Preparation

Gelatin-coated mica

Mica was cut with scissors to the size necessary to fit the microscope (approx. 22 x 30 mm rectangle). It was cleaved on both sides until both the desired thickness was achieved and only unbroken layers remained. A gelatin solution was prepared by dissolving 0.5g gelatin (Sigma #G6144) in 100 ml of nanopure distilled water at 60°C. The temperature of the solution was maintained for 10 minutes by heating in a microwave for short periods as necessary. The mica was quickly submerged and removed from the solution and supported on edge on a paper towel to dry in ambient air overnight. (47,51). In some cases rhodamine 6G (Aldrich Chemical, Milwaukee, WI) was added to the gelatin solution at a final concentration of 3 ng/ml. This was done to aid in localizing the spheroplasts within the gelatin layer using confocal microscopy.

APTES/Glut mica

The APTES/Glut mica was prepared according to a published procedure (126). Briefly, the tops of two 1.5ml tubes were cut and placed (open end up) in the bottom of a dessicator. The dessicator was purged with argon for 2 minutes. Freshly cleaved rectangles (22 x 30mm) of cut mica were placed into the dessicator. To one top, 30μl of APTES (99% Sigma-Aldrich, St. Louis, MO) was added and 10μl N,N-diisopropylethylamine (Sigma Aldrich) was added to the other top. The dessicator was

purged for 2 minutes then sealed for at least 2.5 hours. After this time, the two tops were removed and the dessicator purged for 2 minutes. The mica was removed and stored for later use in a sealed dessicator. Prior to use, 200μl of 2.5% glutaraldehyde was added for 20 minutes, rinsed vigorously in a stream of nanopure deionized water, dried under a stream of dry nitrogen and placed in a covered dish until used.

6.4 Immobilization

Intact bacteria

For imaging stationary phase *E. coli* bacteria, 1ml of an overnight culture was pelleted at 4.5 rcf and washed in the same volume of nanopure deionized water. The cells were collected again by centrifugation and promptly resuspended in 500μl of nanopure deionized water. This cell suspension (100μl) was applied to the gelatin-coated mica and allowed to rest for 10 minutes before it was rinsed with a stream of water. Throughout the procedure, care was taken to ensure that the sample was never allowed to dry.

Spheroplasts – (Using Membrane Filters)

This immobilization strategy is an adaptation of one reported previously by Kasas et al (121). Polycarbonate Isopore™ membrane filters (pore sizes 0.8μm, 0.6μm, and 0.4μm, Millipore Corporation, Billerica, MA) were cut using a single paper hole punch. It was then placed atop the filter in a 1000μl filtered pipet tip. This pipet tip was placed in a 1.5ml tube after the bottom of the pipet tip was trimmed to prevent contact with the bottom of the tube. An O-ring matching the inner diameter of the pipet tip was placed on the membrane before 400μl of the spheroplasts suspension was added. The spheroplasts were centrifuged at 0.5 rcf in 30 second increments until most of the suspension passed through the filter. Using forceps, the filter was removed, rinsed and placed in the AFM liquid chamber for imaging. Throughout the procedure, care was taken to ensure that the sample was never allowed to dry.

Spheroplasts – (Using Warm Gelatin)

The gelatin solution (~500μl) was warmed in a water bath or heating block set to between 50 and 55°C. A 4μl aliquot of this warm gelatin was applied onto the freshly

cleaved mica and spread with the pipette tip. Approximately 20 µl of the spheroplast suspension was then immediately added using a large bore pipette tip (i.e. 1ml pipette tip) to avoid lysing the fragile spheroplasts. After allowing the sample to stand for 30 minutes in a humidity chamber, the sample was rinsed copiously with TBS2 to remove loosely bound cells. The sample was never allowed to dry.

Spheroplasts – (Using APTES/glut Mica)

The spheroplast suspension (200µl) was added to the APTES/Glut prepared mica surface. After 1 hour in a humidity chamber, the sample was thoroughly rinsed in a stream of TBS2, placed in the AFM and imaged in the same buffer. Care was taken to ensure that the sample was never allowed to dry. Fixed spheroplasts were prepared likewise except after the immobilization on APTES/Glut mica, 200µl of 0.5% or 2.5% glutaraldehyde was added to the immobilized spheroplasts for 20 minutes. The sample was then rinsed in TBS2 prior to imaging in liquid. A rinse with water was used for samples to be imaged in air.

6.5 Activity Assays

Commercial Live/Dead® BacLight™ Assay

Bacteria were immobilized as described above. Samples were treated using the concentration recommended by the manufacturer of the Live/Dead® Baclight™ Viability kit (# L7012, Molecular Probes, Eugene, OR). To stain the cells, 0.75µl of SYTO9 and 0.75µl of propidium iodide were added to 500µl of water or TBS2 (for intact bacteria or spheroplasts, respectively) and vortexed. To the appropriate sample, 100µl of the Live/Dead® Baclight™ solution was added for 15 minutes. The sample was covered to minimize exposure to light. After this treatment, the majority of the liquid was removed, a coverslip was placed on the sample which was imaged using confocal microscopy.

Fluorescent Glucose Assay

Bacteria were immobilized as described above. Fluorescent glucose (2-NBDG, #N13195 Molecular Probes, Eugene, OR) was diluted with water or TBS2 to a 100µM final concentration. After vortexing the solution, intact bacteria were treated with the water-based dilution and spheroplasts were treated with the TBS2-based solution of the

glucose analog. In either case, 100μl of the appropriate solution was applied to the sample. The sample was kept for 5 minutes under a light blocking cover to minimize exposure to light. After this treatment, the sample was rinsed (intact bacteria in water, spheroplasts in TBS2) and the excess liquid removed. A coverslip was placed on the sample which was imaged using confocal microscopy.

Propidium Iodide and Fluorescent glucose Assay

Bacteria were immobilized as described above. Fluorescent glucose (2-NBDG, #N13195 Molecular Probes, Eugene, OR) was diluted with 500μl of water or TBS2 to make a 100μM solution. To this solution 0.75μl of the propidium iodide from the Live/Dead® Baclight™ Viability kit (# L7012, Molecular Probes, Eugene, OR) was added. After vortexing, intact bacteria were treated with the water-based dilution and spheroplasts were treated with the TBS2-based solution. In either case, 100μl of the appropriate solution was applied to the sample. The sample was kept for 10 minutes under a light blocking cover to minimize exposure to light. After this treatment, the sample was rinsed (intact bacteria in water, spheroplasts in TBS2) and the excess liquid removed. A coverslip was placed on the sample which was imaged using confocal microscopy.

Spheroplast Overnight Growth Assay

CC-GFP cells were immobilized on APTES/glut as described above. Following immobilization, the mica was placed between a slide and coverslip and the cells were imaged immediately. Alternatively, some cells were incubated at 37ºC in a recovery broth (0.25M sucrose / LB / 500 units per ml penicillin G and selective antibiotic) for 2 hours, rinsed in TBS2 and imaged periodically thereafter. Cells to be kept overnight were treated with fresh recovery broth after the initial 2 hour treatment and returned to 37ºC. The following morning, these cells were rinsed in TBS2 and imaged.

Inducible Expression Assay

AI-GFP cells were used to generate spheroplasts which were immobilized on APTES/glut mica as described. Cells were imaged before induction. To induce expression, samples were placed in recovery broth at 37ºC for 2 hours and imaged.

Cells were subsequently incubated at 37ºC in fresh recovery broth which included 0.2% arabinose for an additional 2 hours and imaged.

6.6 Fluorescence Microscopy

A Leica TCS SP2 confocal laser scanning microscope system (Leica Microsystems Inc., Exton, PA) was used for fluorescence imaging. A 63x oil immersion objective was used for viewing the cells. *E. coli* and spheroplasts of *E. coli* were immobilized on mica as described above. An aliquot of the appropriate buffer was added before the mica was sandwiched between a slide and coverslip. Cells treated with streptavidin quantum dots, Alexa 488, SytO9, or glucose analog 2-NBDG were observed using Ar/Ar-Kr laser for 488nm excitation and emission was detected between 520nm and 550nm. In samples containing propidium iodide or Alexa 568, the He-Ne laser was used for excitation at 543nm whereas emission was detected between 560nm and 605nm. In samples where multiple fluorophores were used, fluorescence was detected sequentially rather than simultaneously. Images were processed using Leica confocal software version 2.5.

6.7 Atomic Force Microscopy

Fixed spheroplasts

Samples of fixed spheroplasted cells were loaded into a Pico Plus atomic force microscope (Agilent Technologies (formerly Molecular Imaging Inc., Tempe, AZ)) and imaged using a 100µm scanning head. The instrument was operated in air or liquid and in MacMode or contact mode at 256 or 512 pixels per line scan at speeds ranging from 0.6 to 2 Hz. Type IVe Silicon nitride cantilevers (Maclevers, Agilent Technnologies) with a nominal spring constant of 0.1 N/m and a resonant frequency in air of 38 kHz were used. All of the images presented are first-order flattened.

Live spheroplasts

Samples of spheroplasted cells were loaded in the liquid cell of the AFM and imaged using a 100 µm scanning head. The instrument was operated in MAC Mode® or contact mode at 256 or 512 pixels per line scan at speeds ranging from 0.6 to 2 Hz. Spheroplasts were imaged in TBS2 using Type IVe or Type IVc silicon nitride cantilevers

(Maclevers, Agilent Technnologies) having nominal spring constants 0.1 N/m and 0.01N/M respectively. The approximate resonant frequency in air of the former is 38kHz and 7kHz for the latter. Because the first harmonic of the type IVc cantilever in liquid was unreliable, the second harmonic, having a resonant frequency of approximately 6.5 kHz in liquid, was used. All of the images presented are first-order flattened.

Live intact bacteria

Samples of intact bacteria were loaded in the liquid cell of the AFM and imaged using a 100 μm scanning head. The instrument was operated in MACMode at 256 or 512 pixels per line scan at speeds ranging from 0.6 to 2 Hz. Bacteria were imaged in water using Type Ic silicon cantilever or Type IVc silicon nitride cantilevers (Maclevers, Agilent Technnologies) having nominal spring constants 0.6 N/m and 0.01N/M respectively. The approximate resonant frequency in air of the former is 35kHz and 7kHz for the latter. Because the first harmonic of the type IVc cantilever in liquid was unreliable, the second harmonic, having a resonant frequency of approximately 6.5 kHz in liquid, was used. All of the images presented are first-order flattened.

6.8 Cantilever Spring Constant Determination

Before force distance curves were collected on the bacteria, six control force distance curves were collected on a mica surface using the procedure described in section 6.9. For each approach, the inverse of the slope was entered as the conversion coefficient into ‘Thermal K,’ a program that interfaces with the imaging software to calculate the spring constant of a cantilever by the thermal method (178-180). The mean of these six spring constants was called S1. After imaging a sample, six additional approaches to the surface in air were made. Force distance curves were generated for each approach and spring constants were again determined as described above. The mean of these spring constants was called S2. The average of S1 and S2 was used in the calculations as the spring constant of the cantilever.

6.9 Force Distance Curve Acquisition

Approach Curve Data Acquisition on Substrate (used in cantilever spring constant calculation, based on FDC Method 3)

Freshly cleaved mica was loaded into the AFM and allowed to equilibrate in dry nitrogen for 30 minutes to minimize humidity in the chamber. After this time, the nitrogen stream was reduced to a minimal flow and the surface was scanned in contact mode to ensure that a clean surface was being used. Force distance curves were generated in contact mode from six 50 μm approaches to mica in air. The sweep duration of the force distance curves was 0.5 seconds. After each approach, the slope in the contact region from the 5^{th} curve was recorded and used in determining the spring constant of the cantilever.

Approach Curve Data Acquisition on Bacteria (used in bacteria spring constant calculation, based on FDC Method 3)

From a low-resolution MAC Mode® scan of a surface containing either intact bacteria or spheroplasts, an area of interest containing isolated cells was identified. This area was scanned at higher resolution and a single isolated bacterium of interest was identified within the scanned area. After recording this scan, the cursor was placed in the center of the identified bacteria and force distance curves were generated using a sweep duration of 0.2 seconds. After placing the cursor over the sample and allowing 5 force distance curves to be taken to stabilize the instrument, approximately 20 measurements were recorded. The cursor was then relocated to a region outside the perimeter of the cell on the substrate where at least 6 control force distance curves were similarly obtained. A subsequent image was generated to confirm that the condition and location of the cell of interest had not been changed by the force distance curve measurements.

Retraction Curve Data Acquisition on Bacteria

From a low-resolution MAC Mode® scan of a surface containing immobilized and immunolabeled spheroplasts, an area of interest containing isolated cells was identified. This area was scanned at higher resolution and an isolated spheroplast of interest was identified within the scanned area. After recording this scan, the cursor was placed in the center of the identified bacteria. The z-range of the vertical piezo was limited to

approximately 1000nm and the sweep duration was set to one second. A total of 550 force distance curves were collected per bacteria containing 2000 datapoints each. A subsequent image was generated to confirm that the condition and location of the cell of interest had not been changed by the force distance curves.

6.10 Force Distance Curve Analysis

Approach Curve Analysis

A Matlab-based automatic algorithm was developed to analyze force distance curves in order to: identify the approach region, obtain the slope in the region of constant compliance; identify the boundaries between regions; and to calculate the indentation values. An average of 20 force distance curves collected from each sample was plotted and the instantaneous slopes at each data point were calculated. The mean value of the last 20 points in the approach curve was calculated to be the slope over the constant compliance region. A line was drawn by using this slope and the median point over the sample space was used for determining the slope. Another line to mark the base of the curve was drawn by using a slope of zero and the first data point in the approach curve. In order to identify the end of the nonindentation region and the beginning of the constant compliance region, the data points from the shifted curve were fit to the two lines (base and slope respectively) and a threshold (0.05) was set on the values obtained. Ideally, when the points fit the line, the value should be equal to zero and when it is greater than 0.05, we identified the point to be on the boundary. This threshold was user-defined and could be changed to suit the requirements. These two regions were then defined as well as the value of slope in the constant compliance region. In order to find the indentation, a reference control curve was obtained on the sample substrate. This curve was plotted with the force distance curves from the specimen.

Retraction Force Distance Curve Analysis

Retraction force distance curves were evaluated offline to determine if a binding event occurred. The retraction curve retraces the approach curve unless a characteristic adhesion peak develops after the point of contact (170). (Figure 35) To distinguish between nonspecific adhesion and a binding event, the beginning of the adhesive peak is examined more closely. If the slope of the adhesion peak is constant until liftoff, then

nonspecific adhesion is indicated. On the other hand, if the adhesion peak develops away from the surface (i.e. after the point corresponding to contact on the approach curve) then a binding event may be indicated. Additional considerations include the length (along the x-axis) of the nonlinear region. The tether used in these experiments is 5.8 nm. Retraction curves suggesting that the linker was stretched beyond 12 nm were not considered binding events. Also, datasets dominated by large nonspecific adhesion peaks were discarded. A binary scoring system was used and curves were scored as representing a binding event or not. In order to calculate the percentage of binding event for each location, the number of binding events was divided by the total number of retraction curves collected at that site. The percentage of retraction curves without binding events was similarly determined. The percentages were compared using the Student's t-Test.

6.11 Tip Functionalization

Preparing the tips for functionalization

Using a glass, serological pipette, chloroform (enough to cover the cantilevers) was transferred into three glass Petri dishes. Five to seven tips were soaked together in the chloroform. After five minutes, the cantilevers transferred to the second dish for five minutes. They were transferred again to the third dish of chloroform for five minutes. The tips were removed and the chloroform was given time to evaporate (approximately 1 minute). The cleaning process was continued by placing the cantilevers in a UV cleaner. The cleaner was sealed and the UV lamp was turned on for fifteen minutes. After that time, the UV lamp was turned off and the cantilevers removed.

Adding NH_2 groups to the tips

The tops of two 1.5ml tubes were cut and placed (open end up) in the bottom of a dessicator. The dessicator was purged with argon for 2 minutes. The cantilevers were placed into the dessicator. To one top, 30μl of APTES (99% Sigma-Aldrich, St. Louis, MO) was added and 10μl N,N-diisopropylethylamine (Sigma Aldrich) was added to the other top. The dessicator was purged for 2 minutes then sealed for at least 2.5 hours. After this time, the two tops were removed and the dessicator purged for 2 minutes. The

cantilevers were removed and treated further or stored for later use in a sealed dessicator.

Adding the poly(ethylene glycol) (PEG) linker to the NH_2-modified tips

The containers and forceps which contact the cantilevers from this point on were cleaned with ethanol followed by chloroform. The cantilevers were soaked in chloroform for five minutes. To a 1ml microbeaker (Electron Microscopy Sciences, Hatfield, PA) was added 1ml of a 1mg/ml solution of the NHS-dPEG™$_{12}$-biotin (Quanta Biodesign, Powell, OH) in chloroform. To this solution, 10µl of triethylamine was added using a glass capillary pipet. The NH_2-modified cantilevers were immersed in this solution and covered for 2-3 hours. Following this treatment, tips were washed in chloroform and allowed to dry for 1 minute before use or storage in a dessicator.

6.12 Immunolabeling

Spheroplasts were treated with 5mg/ml BSA in TBS2 for 1 hour. The sample was rinsed in TBS2 and incubated 1 hour in the primary antibody diluted 1:100 in TBS2 containing 5mg/ml BSA. Either purified anti-alkaline phosphatase (*E. coli*) from Accurate Chemical Corporation, Westbury, NY (YNNE124PAb –Rabbit) or biotinylated anti-alkaline phosphatase (*E. coli*) from Rockland Chemicals, Gilbertsville, PA, (200-4634 - Rabbit) was the primary antibody. The sample was then rinsed copiously in TBS2. Alexa Fluor 488 goat anti-rabbit IgG from Invitrogen, Carlsbad, California (A-11008) was diluted 1:1000 in TBS2 or a 0.5mg/ml solution of avidin from Sigma-Aldrich, St. Louis, MO (A9275) was used for secondary labeling. The sample was incubated for 30 minutes. All of the preceding incubations were conducted in a humidity chamber. The sample was thoroughly washed in TBS2, placed between a slide and coverslip and imaged using confocal microscopy. Regardless of whether immobilized spheroplasts or a spheroplasts suspension was used, the reaction volume was 200µl. Washing the spheroplast suspension was accomplished by pelleting the cells at 0.5 rcf for 20 minutes between each incubation. Similarly, intact cells were labeled as suspensions in TB and pelleted for washing at 4.5 rcf.

Chapter 7

Conclusion

"...we have not yet overcome one World when there are so many others to be discovered, every considerable improvement of Telescopes or Microscopes producing new Worlds and Terra-Incognita to our view." Robert Hooke, 1665. Quoted by Gest, H. (2004) Notes and Records of the Royal Society 58(2), 187-210.

7.0 Summary

This work establishes a platform, based on spheroplasts of bacteria, to which molecular systems level inquiries can be made. Sample preparation techniques are developed which prepare the spheroplasts for imaging and a strategy for AFM-based single molecule recognition on bacteria is presented. A prerequisite for this study is immobilization of the cells. Because spheroplasts lack the surface molecules that are exploited to immobilize intact bacteria for imaging studies, alternative immobilization strategies are developed. For this purpose, crosslinking the spheroplasts to the substrate is proven to be effective. Immobilization results in cells being captured in one location on the substrate and therefore available for continuous observation. Importantly, these immobilization techniques are also compatible with optical microscopy techniques. This feature facilitates tracking intracellular molecular components using optical techniques with fluorescent labels and probing surface molecules using AFM techniques. In both imaging modalities, the buffer can be augmented to provide whatever environment is necessary for the experiment (enhancers, substrates, ions, etc.). Furthermore, in characterizing immobilized spheroplasts, this study provides compelling evidence that metabolic activity is preserved through the sample preparation. Assays for glucose uptake, protein synthesis and increased cell mass helped to make this determination. The belief that this platform is suitable for evaluating molecular systems in the "live" cell is therefore confirmed.

Because the outer membrane and cell wall of the bacteria are removed, the cytoplasmic membrane, a surface not previously studied using AFM, can be examined. It is

determined that the cell enclosed by only the cytoplasmic membrane is too soft for measuring elasticity using the cantilevers currently available. This finding is supported by indentation measurements and implies that significant deformation of the cell surface occurs when live spheroplasts are imaged.

Intermolecular forces are very small and only a few techniques, such as AFM, micropipette aspiration and surface force apparatus have the sensitivity to measure them (202). Of these techniques, only AFM has the ability to detect forces within a single pair of interacting partners. A general procedure for sensing the presence of membrane proteins in spheroplasts of bacteria is reported. This molecular recognition capability of AFM is demonstrated by using tips functionalized with biotin to probe fixed cells labeled with a biotinylated antibody and avidin. Given the availability of biotin and avidin reagents, this strategy is applicable to many systems and as demonstrated, can be validated using confocal fluorescence imaging.

7.1 Future Directions

What kinds of questions can be answered using the experimental platform provided by this work? Further investigations of the molecular events involved in glucose transport can be readily envisioned. The Hinterdorfer group, which investigates glucose transport in mammalian cells, has demonstrated molecular recognition on live cells using tips functionalized either with an epitope-specific antibody or thio-glucose (112). Testing substrate recognition of the glucose transporter in live spheroplasts would be an important next step. This group also developed PicoTrec, a promising technique for generating AFM imaging and recognition data simultaneously (216). Specific interactions between the tip and immobilized protein are identified in the image as dark spots. To date, application of this technique has been limited to immobilized protein on hard surfaces as the technique is very sensitive to the deformation that occurs during imaging of live cells. Experiments to apply PicoTrec to spheroplasts should be pursued to evaluate the distribution of individual proteins across the cell surface.

Immunofluorescence and GFP fusion proteins were the basis of optical microscopy studies which localized proteins in bacteria that are similar to eukaryotic cytoskeleton

proteins. These proteins assemble into various macromolecular structures (filaments, rings and spirals) and influence the shape of the bacteria. Although researchers have shown that these structures are required for maintaining the shape of the bacteria, their exact roles remain undetermined. In addition, the proteins are required for cell division and participate in DNA segregation (129,217-219). How do these proteins perform their intracellular function and also contribute to the periplasmic peptidoglycan? Are their macromolecular structures located in the cytoplasm as generally assumed or are they assembled on the periplasmic side of the cytoplasmic membrane? Mammalian cytoskeleton proteins were previously imaged through the cell membrane (173,220). Given the softness of the spheroplasts, one might expect to see evidence of the bacterial cytoskeleton proteins during AFM imaging. Could their intracellular functions be performed by individual proteins in the cytoplasm and the structural role of the macromolecular assembly performed in the periplasm? Conceivably, using a microscope system with combined optical and atomic force capability, the proteins could be fluorescently labeled and tracked as they appeared on the surface of the spheroplasts. Optical techniques do not have the resolution to determine whether the ringed or spiral structures appear inside or outside of the cytoplasmic membrane. To answer this question, under growth conditions, spheroplasts could be examined for evidence of these structures.

As mentioned earlier in this thesis, the ability to study CWD forms of bacteria using AFM has implications for biomedical research. These bacteria are hearty and able to evade immune systems. Understanding the molecular properties unique to CWD bacteria could be very useful in combating the diseases caused by them. The applicability of this platform to CWD bacteria is generally assumed. Simple application of the strategies proposed here would determine whether this assumption is valid. If they are shown to be valid, experiments to understand their survival mechanisms can be pursued in earnest. These cells are known to hide in macrophages to evade the immune system. The AFM would allow simulation of this environment and conditions which lead to killing of the bacteria can be evaluated.

To facilitate these experiments however, techniques for simultaneously observing multiple properties of single cells must be assembled. Progress has already been made

in this regard as the potential for combining AFM with other techniques has been established (24,29,221-223). With the technical challenges of combining imaging modalities overcome, the focus turns to developing a versatile experimental platform for following molecular events as they occur in single bacterial cells. Such a platform includes sample preparation procedures that are portable between these complementary microscopy techniques. Portability allows researchers to have the option of tracking individual or multiple components of the system using either or both techniques without introducing sample preparation artifacts. This system is a unique platform on which entire molecular systems can be studied in the single cell.

List of References

1. Dmitriev, B., Toukach, F., and Ehlers, S. (2005) *Trends In Microbiology* **13**(12), 569-574
2. Binnig, G., Rohrer, H., Gerber, C., and Weibel, E. (1982) *Physical Review Letters* **49**(1), 57-61
3. Binnig, G., Quate, C. F., and Gerber, C. (1986) *Physical Review Letters* **56**(9), 930-933
4. Hutter, J. L., and Bechhoefer, J. (1993) *Journal of Applied Physics* **73**(9), 4123-4129
5. Hutter, J. L., and Bechhoefer, J. (1994) *Journal of Vacuum Science & Technology B* **12**(3), 2251-2253
6. Goodman, F. O., and Garcia, N. (1991) *Physical Review B* **43**(6), 4728-4731
7. Bonnell, D. (ed). (2001) *Scanning Probe Microscopy and Spectroscopy: theory, techniques and applications*, 2nd Ed., Wiley-VCH, New York
8. Arai, T., Aoki, D., Okabe, Y., and Fujihira, M. (1996) *Thin Solid Films* **273**(1-2), 322-326
9. Butt, H. J., Cappella, B., and Kappl, M. (2005) *Surface Science Reports* **59**(1-6), 1-152
10. Han, W. H., Lindsay, S. M., and Jing, T. W. (1996) *Applied Physics Letters* **69**(26), 4111-4113
11. Lantz, M., Liu, Y. Z., Cui, X. D., Tokumoto, H., and Lindsay, S. M. (1999) *Surface And Interface Analysis* **27**(5-6), 354-360
12. Ahimou, F., Denis, F. A., Touhami, A., and Dufrene, Y. F. (2002) *Langmuir* **18**(25), 9937-9941
13. Price, D. M., Reading, M., Hammiche, A., and Pollock, H. M. (1999) *International Journal of Pharmaceutics* **192**(1), 85-96
14. Domke, J., Parak, W. J., George, M., Gaub, H. E., and Radmacher, M. (1999) *European Biophysics Journal with Biophysics Letters* **28**(3), 179-186
15. Hinterdorfer, P., and Dufrene, Y. F. (2006) *Nature Methods* **3**(5), 347-355
16. Lushnikov, A. Y., Potaman, V. N., Oussatcheva, E. A., Sinden, R. R., and Lyubchenko, Y. L. (2006) *Biochemistry* **45**(1), 152-158
17. Schneider, S. W., Sritharan, K. C., Geibel, J. P., Oberleithner, H., and Jena, B. P. (1997) *Proceedings of the National Academy of Sciences of the United States of America* **94**(1), 316-321
18. Cho, S. J., Quinn, A. S., Stromer, M. H., Dash, S., Cho, J., Taatjes, D. J., and Jena, B. P. (2002) *Cell Biology International* **26**(1), 35-42
19. Puntheeranurak, T., Wildling, L., Gruber, H. J., Kinne, R. K. H., and Hinterdorfer, P. (2006) *Journal of Cell Science* **119**(14), 2960-2967
20. Willemsen, O. H., Snel, M. M. E., van der Werf, K. O., de Grooth, B. G., Greve, J., Hinterdorfer, P., Gruber, H. J., Schindler, H., van Kooyk, Y., and Figdor, C. G. (1998) *Biophysical Journal* **75**(5), 2220-2228
21. Riener, C. K., Stroh, C. M., Ebner, A., Klampfl, C., Gall, A. A., Romanin, C., Lyubchenko, Y. L., Hinterdorfer, P., and Gruber, H. J. (2003) *Analytica Chimica Acta* **479**(1), 59-75
22. Xia, S. L., and Ferrier, J. (1992) *Biochemical and Biophysical Research Communications* **186**(3), 1212-1219
23. Walker, L. M., Publicover, S. J., Preston, M. R., Ahmed, M., and El Haj, A. J. (2000) *Journal of Cellular Biochemistry* **79**(4), 648-661

24. Charras, G. T., Lehenkari, P. P., and Horton, M. A. (2001) *Ultramicroscopy* **86**(1-2), 85-95
25. Furness, D. N., and Hackney, C. M. (1985) *Hearing Research* **18**(2), 177-188
26. Furness, D. N., Richardson, G. P., and Russell, I. J. (1989) *Hearing Research* **38**(1-2), 95-109
27. Langer, M. G., Koitschev, A., Haase, H., Rexhausen, U., Horber, J. K. H., and Ruppersberg, J. P. (2000) *Ultramicroscopy* **82**(1-4), 269-278
28. Langer, M. G., Fink, S., Koitschev, A., Rexhausen, U., Horber, J. K. H., and Ruppersberg, J. P. (2001) *Biophysical Journal* **80**(6), 2608-2621
29. Langer, M. G., and Koitschev, A. (2002) The biophysics of sensory cells of the inner ear examined by atomic force microscopy and patch clamp. In. *Atomic Force Microscopy in Cell Biology*
30. Kienberger, F., Zhu, R., Moser, R., Blaas, D., and Hinterdorfer, P. (2004) *Journal of Virology* **78**(7), 3203-3209
31. Scheuring, S., Levy, D., and Rigaud, J. L. (2005) *Biochimica Et Biophysica Acta-Biomembranes* **1712**(2), 109-127
32. Gaboriaud, F., and Dufrene, Y. F. (2007) *Colloids and Surfaces B-Biointerfaces* **54**(1), 10-19
33. Ubbink, J., and Schar-Zammaretti, P. (2005) *Micron* **36**(4), 293-320
34. Oesterhelt, F., Oesterhelt, D., Pfeiffer, M., Engel, A., Gaub, H. E., and Muller, D. J. (2000) *Science* **288**(5463), 143-146
35. Touhami, A., Jericho, M. H., Boyd, J. M., and Beveridge, T. J. (2006) *Journal of Bacteriology* **188**(2), 370-377
36. Nunez, M., Martin, M. O., Duong, L. K., Ly, E., and Spain, E. M. (2003) *Biophysical Journal* **84**(5), 3379-3388
37. Nunez, M. E., Martin, M. O., Chan, P. H., and Spain, E. M. (2005) *Colloids and Surfaces B-Biointerfaces* **42**(3-4), 263-271
38. Beech, I. B., Smith, J. R., Steele, A. A., Penegar, I., and Campbell, S. A. (2002) *Colloids and Surfaces B: Biointerfaces* **23**(2-3), 231-247
39. Stephens, D. J., and Allan, V. J. (2003) *Science* **300**(5616), 82-86
40. Tsien, R. Y. (2003) *Nature Cell Biology*, SS16-SS21
41. Gest, H. (2004) *Notes and Records of the Royal Society of London* **58**(2), 187-201
42. Cross, S. E., Kreth, J., Zhu, L., Qi, F. X., Pelling, A. E., Shi, W. Y., and Gimzewski, J. K. (2006) *Nanotechnology* **17**(4), S1-S7
43. Touhami, A., Jericho, M. H., and Beveridge, T. J. (2004) *Journal Of Bacteriology* **186**(11), 3286-3295
44. Li, A., Lee, P. Y., Ho, B., Ding, J. L., and Lim, C. T. (2007) *Biochimica Et Biophysica Acta-Biomembranes* **1768**(3), 411-418
45. Yang, L., Wang, K. M., Tan, W. H., He, X. X., Jin, R., Li, J., and Li, H. M. (2006) *Analytical Chemistry* **78**(20), 7341-7345
46. Del Sol, R., Armstrong, I., Wright, C., and Dyson, P. (2007) *Journal Of Bacteriology* **189**(6), 2219-2225
47. Beckmann, M. A., Venkataraman, S., Doktycz, M. J., Nataro, J. P., Sullivan, C. J., Morrell-Falvey, J. L., and Allison, D. P. (2006) *Ultramicroscopy* **106**(8-9), 695-702
48. Liu, Y. T., Black, M. A., Caron, L., and Camesano, T. A. (2006) *Biotechnology and Bioengineering* **93**(2), 297-305

49. Pelling, A. E., Li, Y., Cross, S. E., Castaneda, S., Shi, W., and Gimzewski, J. K. (2006) *Cell Motility and the Cytoskeleton* **63**(3), 141-148
50. Bolshakova, A. V., Kiselyova, O. I., and Yaminsky, I. V. (2004) *Biotechnology Progress* **20**(6), 1615-1622
51. Doktycz, M. J., Sullivan, C. J., Hoyt, P. R., Pelletier, D. A., Wu, S., and Allison, D. P. (2003) *Ultramicroscopy* **97**(1-4), 209-216
52. Venkataraman, S., Allison, D. P., Qi, H., Morrell-Falvey, J. L., Kallewaard, N. L., Crowe, J. J. E., and Doktycz, M. J. (2006) *Ultramicroscopy* **106**(8-9), 829-837
53. Dunne, W. M. (2002) *Clinical Microbiology Reviews* **15**(2), 155-+
54. An, Y. H., and Friedman, R. J. (1998) *Journal Of Biomedical Materials Research* **43**(3), 338-348
55. Palmer, J., Flint, S., and Brooks, J. (2007) *Journal Of Industrial Microbiology & Biotechnology* **34**(9), 577-588
56. Visai, L., Speziale, P., and Bozzini, S. (1990) *Infection and Immunity* **58**(2), 449-455
57. Shen, W., and Ljungh, A. (1993) *Current Microbiology* **27**(6), 311-316
58. Sullivan, C. J., Morrell, J. L., Allison, D. P., and Doktycz, M. J. (2005) *Ultramicroscopy* **105**(1-4), 96-102
59. Sullivan, C. J., Venkataraman, S., Retterer, S. T., Allison, D. P., and Doktycz, M. J. (2007) *Ultramicroscopy* **107**(10-11), 934-942
60. Goncalves, R. P., and Scheuring, S. (2006) *Surface And Interface Analysis* **38**(11), 1413-1418
61. Mahaffy, R. E., Park, S., Gerde, E., Kas, J., and Shih, C. K. (2004) *Biophysical Journal* **86**(3), 1777-1793
62. Matzke, R., Jacobson, K., and Radmacher, M. (2001) *Nature Cell Biology* **3**(6), 607-610
63. Rotsch, C., Jacobson, K., and Radmacher, M. (1999) *Proceedings of the National Academy of Sciences of the United States of America* **96**(3), 921-926
64. Ahimou, F. O., Touhami, A., and Dufrene, Y. F. (2003) *Yeast* **20**(1), 25-30
65. Dufrene, Y. F., Boonaert, C. J. P., Gerin, P. A., Asther, M., and Rouxhet, P. G. (1999) *Journal Of Bacteriology* **181**(17), 5350-5354
66. Arnoldi, M., Fritz, M., Bauerlein, E., Radmacher, M., Sackmann, E., and Boulbitch, A. (2000) *Physical Review E* **62**(1), 1034-1044
67. Schaer-Zammaretti, P., and Ubbink, J. (2003) *Ultramicroscopy* **97**(1-4), 199-208
68. Dufrene, Y. F. (2002) *Journal Of Bacteriology* **184**(19), 5205-5213
69. White, D. (2000) *The Physiology and Biochemistry of Prokaryotes*, Second Edition Ed., Oxford University Press, Inc., New York
70. Costerton, J. W., Ingram, J. M., and Cheng, K. J. (1974) *Bacteriological Reviews* **38**(1), 87-110
71. Ponte-Sucre, A. (2007) *Applied Microbiology And Biotechnology* **76**(2), 279-286
72. Borges-Walmsley, M. I., and Walmsley, A. R. (2001) *Trends In Microbiology* **9**(2), 71-79
73. Matsunaga, T., Suzuki, T., Tanaka, M., and Arakaki, A. (2007) *Trends In Biotechnology* **25**(4), 182-188
74. Lang, C., Schuler, D., and Faivre, D. (2007) *Macromolecular Bioscience* **7**(2), 144-151
75. Beveridge, T. J. (1999) *Journal of Bacteriology* **181**(16), 4725-4733

76. Nikaido, H., and Vaara, M. (1987) Outer Membrane. In: Neidhardt, F. C. (ed). *Escherichia Coli and Salmonella Typhimurium Cellular and Molecular Biology*, American Society for Microbiology
77. Erridge, C., Bennett-Guerrero, E., and Poxton, I. R. (2002) *Microbes And Infection* **4**(8), 837-851
78. Kotra, L. P., Golemi, D., Amro, N. A., Liu, G. Y., and Mobashery, S. (1999) *Journal of the American Chemical Society* **121**(38), 8707-8711
79. Hobot, J. A., Carlemalm, E., Villiger, W., and Kellenberger, E. (1984) *Journal Of Bacteriology* **160**(1), 143-152
80. Pink, D., Moeller, J., Quinn, B., Jericho, M., and Beveridge, T. (2000) *Journal of Bacteriology* **182**(20), 5925-5930
81. Park, J. T. (1987) The Murein Sacculus. In: Neidhardt, F. C. (ed). *Escherichia Coli and Salmonella Typhimurium Cellular and Molecular Biology*, American Society for Microbiology
82. Koch, A. L. (1998) *Research In Microbiology* **149**(10), 689-701
83. Vollmer, W., and Holtje, J. V. (2004) *Journal of Bacteriology* **186**(18), 5978-5987
84. Birdsell, D. C., and Cota-Robles, E. H. (1967) *Journal of Bacteriology* **93**(1), 427-437
85. Chipman, D. M., and Sharon, N. (1969) *Science* **165**(3892), 454-&
86. Vaara, M. (1992) *Microbiological Reviews* **56**(3), 395-411
87. Pelletier, C., Bourlioux, P., and Vanheijenoort, J. (1994) *Fems Microbiology Letters* **117**(2), 203-206
88. Leive, L. (1965) *Biochemical And Biophysical Research Communications* **21**(4), 290-&
89. Amro, N. A., Kotra, L. P., Wadu-Mesthrige, K., Bulychev, A., Mobashery, S., and Liu, G. Y. (2000) *Langmuir* **16**(6), 2789-2796
90. Wild, P., Gabrieli, A., Schraner, E. M., Pellegrini, A., Thomas, U., Frederik, P. M., Stuart, M. C. A., and VonFellenberg, R. (1997) *Microscopy Research and Technique* **39**(3), 297-304
91. Lederberg, J. (1956) *Proceedings of The National Academy of Sciences of The United States of America* **42**, 574-577
92. Lederberg, J., and St. Clair, J. (1957) *Journal of Bacteriology* **75**, 143-150
93. Ehrenfeld, E., and Koch, A. L. (1968) *Biochimica Et Biophysica Acta* **169**(1), 44-57
94. Innes, C. M. J., and Allan, E. J. (2001) *Journal of Applied Microbiology* **90**, 301-308
95. Elvira-Recuenco, M., and van Vuurde, J. W. L. (2003) *Microbiological Research* **158**(4), 271-279
96. Bourgeois, L., and Beaman, B. L. (1976) *Journal of Bacteriology* **127**(1), 584-594
97. Stewart, Z., Martinac, B., and Dobson, J. (2000) *Electro- and Magnetobiology* **19**(1), 81-89
98. Cui, C., Smith, D. O., and Adler, J. (1995) *Journal of Membrane Biology* **144**(1), 31-42
99. Tefsen, B., Geurtsen, J., Beckers, F., Tommassen, J., and de Cock, H. (2005) *Journal of Biological Chemistry* **280**(6), 4504-4509
100. Llamas, M. A., Rodriguez-Herva, J. J., Hancock, R. E. W., Bitter, W., Tommassen, J., and Ramos, J. L. (2003) *Journal of Bacteriology* **185**(16), 4707-4716

101. Abriouel, H., Valdivia, E., Galvez, A., and Maqueda, M. (1998) *Applied and Environmental Microbiology* **64**(11), 4623-4626
102. Onwuamaegbu, M., Belcher, R., and Soare, C. (2005) *Journal of International Medical Research* **33**(1), 1-20
103. Domingue, G. J., and Woody, H. B. (1997) *Clinical Microbiology Reviews* **10**(2), 320-&
104. Beran, V., Havelkova, M., Kaustova, J., Dvorska, L., and Pavlik, I. (2006) *Veterinarni Medicina* **51**(7), 365-389
105. Schuhardt, V. T., Huber, T. W., and Pope, L. M. (1969) *Journal of Bacteriology* **97**(1), 396-401
106. Chiodini, R. J., Van Kruiningen, H. J., Thayer, W. R., and Coutu, J. A. (1986) *Journal of Clinical Microbiology* **24**(3), 357-363
107. Arnoldi, M., Kacher, C. M., Bauerlein, E., Radmacher, M., and Fritz, M. (1998) *Applied Physics a-Materials Science & Processing* **66**, S613-S617
108. Touhami, A., Nysten, B., and Dufrene, Y. F. (2003) *Langmuir* **19**(11), 4539-4543
109. Dufrene, Y. F. (2004) *Nature Reviews Microbiology* **2**(6), 451-460
110. Allison, D. P., Hinterdorfer, P., and Han, W. H. (2002) *Current Opinion In Biotechnology* **13**(1), 47-51
111. Gad, M., Itoh, A., and Ikai, A. (1997) *Cell Biology International* **21**(11), 697-706
112. Puntheeranurak, T., Wildling, L., Gruber, H., and Kinne, R. (2006) *Journal Of Cell Science* **119**, 2960-2967
113. Pfister, G., Stroh, C. M., Perschinka, H., Kind, M., Knoflach, M., Hinterdorfer, P., and Wick, G. (2005) *Journal Of Cell Science* **118**(8), 1587-1594
114. Dupres, V., Menozzi, F. D., Locht, C., Clare, B. H., Abbott, N. L., Cuenot, S., Bompard, C., Raze, D., and Dufrene, Y. F. (2005) *Nature Methods* **2**(7), 515-520
115. Hinterdorfer, P., Gruber, H. J., Kienberger, F., Kada, G., Riener, C., Borken, C., and Schindler, H. (2002) *Colloids And Surfaces B-Biointerfaces* **23**(2-3), 115-123
116. Hinterdorfer, P., Baumgartner, W., Gruber, H. J., Schilcher, K., and Schindler, H. (1996) *Proceedings Of The National Academy Of Sciences Of The United States Of America* **93**(8), 3477-3481
117. Touhami, A., Hoffmann, B., Vasella, A., Denis, F. A., and Dufrene, Y. F. (2003) *Microbiology-Sgm* **149**, 2873-2878
118. Van Houdt, R., and Michiels, C. W. (2005) *Research in Microbiology* **156**(5-6), 626-633
119. Pizarro-Cerda, J., and Cossart, P. (2006) *Cell* **124**(4), 715-727
120. Kolari, M., Schmidt, U., Kuismanen, E., and Salkinoja-Salonen, M. S. (2002) *Journal of Bacteriology* **184**(9), 2473-2480
121. Kasas, S., and Ikai, A. (1995) *Biophysical Journal* **68**(5), 1678-1680
122. Gad, M., and Ikai, A. (1995) *Biophysical Journal* **69**(6), 2226-2233
123. Harrington, W. F., and Rao, N. V. (1970) *Biochemistry* **9**(19), 3714-3724
124. Mackie, A. R., Gunning, A. P., Ridout, M. J., and Morris, V. J. (1998) *Biopolymers* **46**(4), 245-252
125. Kiernan, J. (2000) *Microscopy Today* **8**(00-1), 8-12
126. Wang, H. D., Bash, R., Yodh, J. G., Hager, G. L., Lohr, D., and Lindsay, S. M. (2002) *Biophysical Journal* **83**(6), 3619-3625
127. Bonner, P. J., and Shimkets, L. J. (2006) *Molecular Microbiology* **61**(5), 1101-1109
128. Boin, M. A., Austin, M. J., and Hase, C. C. (2004) *Fems Microbiology Letters* **239**(1), 1-8

129. Carballido-Lopez, R., and Errington, J. (2003) *Developmental Cell* **4**(1), 19-28
130. Moller-Jensen, J., and Lowe, J. (2005) *Current Opinion In Cell Biology* **17**(1), 75-81
131. Wright, C. J., and Armstrong, I. (2006) *Surface and Interface Analysis* **38**(11), 1419-1428
132. Beveridge, T. J. (1988) *Canadian Journal Of Microbiology* **34**(4), 363-372
133. Zobell, C. E. (1943) *Journal Of Bacteriology* **46**(1), 39-56
134. Martin, E. L., and Macleod, R. A. (1971) *Journal Of Bacteriology* **105**(3), 1160-&
135. Miura, T., and Mizushim.S. (1968) *Biochimica Et Biophysica Acta* **150**(1), 159-&
136. Joseleaupetit, D., and Kepes, A. (1975) *Biochimica Et Biophysica Acta* **406**(1), 36-49
137. Kell, D. B., Kaprelyants, A. S., Weichart, D. H., Harwood, C. R., and Barer, M. R. (1998) *Antonie Van Leeuwenhoek International Journal of General and Molecular Microbiology* **73**(2), 169-187
138. Bogosian, G., and Bourneuf, E. V. (2001) *Embo Reports* **2**(9), 770-774
139. Breeuwer, P., and Abee, T. (2000) *International Journal of Food Microbiology* **55**(1-3), 193-200
140. Keer, J. T., and Birch, L. (2003) *Journal of Microbiological Methods* **53**(2), 175-183
141. Ohtomo, R., and Saito, M. (2001) *Microbial Ecology* **42**(2), 208-214
142. Herigstad, B., Hamilton, M., and Heersink, J. (2001) *Journal of Microbiological Methods* **44**(2), 121-129
143. Mangoni, M. L., Papo, N., Barra, D., Simmaco, M., Bozzi, A., Di Giulio, A., and Rinaldi, A. (2004) *Biochemical Journal* **380**, 859-865
144. Anderson, M., Bollinger, D., Hagler, A., Hartwell, H., Rivers, B., Ward, K., and Steck, T. R. (2004) *Journal of Clinical Microbiology* **42**(2), 753-758
145. Zhang, T., and Fang, H. H. P. (2004) *Biotechnology Letters* **26**(12), 989-992
146. Bunthof, C. J., van Schalkwijk, S., Meijer, W., Abee, T., and Hugenholtz, J. (2001) *Applied and Environmental Microbiology* **67**(9), 4264-4271
147. Biggerstaff, J. P., Le Puil, M., Weidow, B. L., Prater, J., Glass, K., Radosevich, M., and White, D. C. (2006) *Molecular and Cellular Probes* **20**(2), 141-146
148. Kusaka, I. (1967) *Journal of Bacteriology* **94**(4), 884-&
149. Hurwitz, C., Reiner, J. M., and Landau, J. V. (1958) *Journal of Bacteriology* **76**(6), 612-617
150. Stocks, S. M. (2004) *Cytometry Part A* **61A**(2), 189-195
151. Buhr, A., Flukiger, K., and Erni, B. (1994) *Journal of Biological Chemistry* **269**(38), 23437-23443
152. Garcia-Alles, L. F., Zahn, A., and Erni, B. (2002) *Biochemistry* **41**(31), 10077-10086
153. Matsuoka, H., Oishi, K., Watanabe, M., Kozone, I., Saito, M., and Igimi, S. (2003) *Bioscience Biotechnology and Biochemistry* **67**(11), 2459-2462
154. Berney, M., Hammes, F., Bosshard, F., Weilenmann, H. U., and Egli, T. (2007) *Applied and Environmental Microbiology* **73**(10), 3283-3290
155. Yoshioka, K., Takahashi, H., Homma, T., Saito, M., Oh, K. B., Nemoto, Y., and Matsuoka, H. (1996) *Biochimica Et Biophysica Acta-General Subjects* **1289**(1), 5-9
156. Yoshioka, K., Saito, M., Oh, K. B., Nemoto, Y., Matsuoka, H., Natsume, M., and Abe, H. (1996) *Bioscience Biotechnology and Biochemistry* **60**(11), 1899-1901

157. Velegol, S. B., Pardi, S., Li, X., Velegol, D., and Logan, B. E. (2003) *Langmuir* **19**(3), 851-857
158. Park, J. T., and Strominger, J. L. (1957) *Science* **125**(3238), 99-101
159. Lederberg, J. (1957) *Journal of Bacteriology* **73**(1), 144-144
160. Hugo, W. B., and Russell, A. D. (1960) *Journal of Bacteriology* **80**(4), 436-440
161. Mashburn-Warren, L. M., and Whiteley, M. (2006) *Molecular Microbiology* **61**(4), 839-846
162. Hansma, H. G., and Hoh, J. H. (1994) Biomolecular Imaging with the Atomic Force Microscope. In.
163. You, H. X., and Yu, L. (1999) *Methods in Cell Science* **21**(1), 1-17
164. Firtel, M., and Beveridge, T. J. (1995) *Micron* **26**(4), 347-362
165. Reich, Z., Kapon, R., Nevo, R., Pilpel, Y., Zmora, S., and Scolnik, Y. (2001) *Biotechnology Advances* **19**(6), 451-485
166. Radmacher, M., Tillmann, R. W., Fritz, M., and Gaub, H. E. (1992) *Science* **257**(5078), 1900-1905
167. Haydon, P. G., Lartius, R., Parpura, V., and Marchese-Ragona, S. P. (1996) *Journal Of Microscopy-Oxford* **182**, 114-120
168. Hoh, J. H., and Schoenenberger, C. A. (1994) *Journal Of Cell Science* **107**, 1105-1114
169. Radmacher, M. (1997) *Ieee Engineering In Medicine And Biology Magazine* **16**(2), 47-57
170. Heinz, W. F., and Hoh, J. H. (1999) *Trends In Biotechnology* **17**(4), 143-150
171. Vinckier, A., and Semenza, G. (1998) *Febs Letters* **430**(1-2), 12-16
172. Alessandrini, A., and Facci, P. (2005) *Measurement Science and Technology* **16**, R65-R92
173. Rotsch, C., and Radmacher, M. (2000) *Biophysical Journal* **78**(1), 520-535
174. Ng, L., Hung, H. H., Sprunt, A., Chubinskaya, S., Ortiz, C., and Grodzinsky, A. (2007) *Journal Of Biomechanics* **40**(5), 1011-1023
175. Li, X., and Logan, B. E. (2004) *Langmuir* **20**(20), 8817-8822
176. Hutter, J. L., Chen, J., Wan, W. K., Uniyal, S., Leabu, M., and Chan, B. M. C. (2005) *Journal of Microscopy-Oxford* **219**, 61-68
177. Braet, F., Rotsch, C., Wisse, E., and Radmacher, M. (1998) *Applied Physics a-Materials Science & Processing* **66**, S575-S578
178. Hutter, J. L., and Bechhoefer, J. (1993) *Review of Scientific Instruments* **64**(7), 1868-1873
179. Butt, H. J., and Jaschke, M. (1995) *Nanotechnology* **6**(1), 1-7
180. Burnham, N. A., Chen, X., Hodges, C. S., Matei, G. A., Thoreson, E. J., Roberts, C. J., Davies, M. C., and Tendler, S. J. B. (2003) *Nanotechnology* **14**(1), 1-6
181. Velegol, S. B., and Logan, B. E. (2002) *Langmuir* **18**(13), 5256-5262
182. Yao, X., Walter, J., Burke, S., Stewart, S., Jericho, M. H., Pink, D., Hunter, R., and Beveridge, T. J. (2002) *Colloids and Surfaces B-Biointerfaces* **23**(2-3), 213-230
183. Costa, K. D., Sim, A. J., and Yin, F. C. P. (2006) *Journal of Biomechanical Engineering-Transactions of the Asme* **128**(2), 176-184
184. Unertl, W. N. (1999) *Journal of Vacuum Science & Technology A* **17**(4), 1779-1786
185. Meyer, P., and Dworkin, J. (2007) *Research In Microbiology* **158**(3), 187-194
186. Norman, C., Liu, Z. W., Rigby, P., Raso, A., Petrov, Y., and Martinac, B. (2005) *European Biophysics Journal With Biophysics Letters* **34**(5), 396-402

187. Carballido-Lopez, R., and Errington, J. (2003) *Trends In Cell Biology* **13**(11), 577-583
188. Muller, D. J., and Engel, A. (1999) *Journal Of Molecular Biology* **285**(4), 1347-1351
189. Horber, J. K. H., and Miles, M. J. (2003) Scanning Probe Evolution in Biology. In.
190. Riener, C. K., Kienberger, F., Hahn, C. D., Buchinger, G. M., Egwim, I. O. C., Haselgrubler, T., Ebner, A., Romanin, C., Klampfl, C., Lackner, B., Prinz, H., Blaas, D., Hinterdorfer, P., and Gruber, H. J. (2003) *Analytica Chimica Acta* **497**(1-2), 101-114
191. Kienberger, F., Moser, R., Riener, C., Gruber, H. J., Schindler, H., Blaas, D., and Hinterdorfer, P. (2001) *Biophysical Journal* **80**(1), 291A-292A
192. Kada, G., Blayney, L., Jeyakumar, L. H., Kienberger, F., Pastushenko, V. P., Fleischer, S., Schindler, H., Lai, F. A., and Hinterdorfer, P. (2001) *Ultramicroscopy* **86**(1-2), 129-137
193. Seddon, A. A., Curnow, P., and Booth, P. J. (2004) *Biochimica Et Biophysica Acta-Biomembranes* **1666**(1-2), 105-117
194. Siebold, C., Flukiger, K., Beutler, R., and Erni, B. (2001) *Febs Letters* **504**(3), 104-111
195. Postma, P. W., Lengeler, J. W., and Jacobson, G. R. (1993) *Microbiological Reviews* **57**(3), 543-594
196. Lengeler, J. W., Jahreis, K., and Wehmeier, U. F. (1994) *Biochimica Et Biophysica Acta-Bioenergetics* **1188**(1-2), 1-28
197. Erni, B., and Zanolari, B. (1986) *Journal Of Biological Chemistry* **261**(35), 6398-6403
198. Saffen, D. W., Presper, K. A., Doering, T. L., and Roseman, S. (1987) *Journal Of Biological Chemistry* **262**(33), 16241-16253
199. Buhr, A., and Erni, B. (1993) *Journal Of Biological Chemistry* **268**(16), 11599-11603
200. Manoil, C., Mekalanos, J. J., and Beckwith, J. (1990) *Journal Of Bacteriology* **172**(2), 515-518
201. Traxler, B., Boyd, D., and Beckwith, J. (1993) *Journal Of Membrane Biology* **132**(1), 1-11
202. Wong, J., Chilkoti, A., and Moy, V. T. (1999) *Biomolecular Engineering* **16**(1-4), 45-55
203. Micic, M., Chen, A., Leblanc, R. M., and Moy, V. T. (1999) *Scanning* **21**(6), 394-397
204. Moy, V. T., Florin, E. L., and Gaub, H. E. (1994) *Colloids And Surfaces A-Physicochemical And Engineering Aspects* **93**, 343-348
205. Lee, G. U., Kidwell, D. A., and Colton, R. J. (1994) *Langmuir* **10**(2), 354-357
206. Dammer, U., Hegner, M., Anselmetti, D., Wagner, P., Dreier, M., Huber, W., and Guntherodt, H. J. (1996) *Biophysical Journal* **70**(5), 2437-2441
207. Ebner, A., Madl, J., Kienberger, F., Chtcheglova, L. A., Puntheeranurak, T., Zhu, R., Tang, J. L., Gruber, H. J., Schutz, G. J., and Hinterdorfer, P. (2007) *Current Nanoscience* **3**(1), 49-56
208. Raab, A., Han, W. H., Badt, D., Smith-Gill, S. J., Lindsay, S. M., Schindler, H., and Hinterdorfer, P. (1999) *Nature Biotechnology* **17**(9), 902-905
209. Hinterdorfer, P., Kienberger, F., Raab, A., Gruber, H., Baumgartner, W., Kada, G., Riener, C., Wielert-Badt, S., Borken, C., and Schindler, H. (2000) *Single Molecules* **1**(2), 99-103

210. Puntheeranurak, T., Wimmer, B., Castaneda, F., Gruber, H. J., Hinterdorfer, P., and Kinne, R. K. H. (2007) *Biochemistry* **46**(10), 2797-2804
211. Wilchek, M., and Bayer, E. A. (1988) *Analytical Biochemistry* **171**(1), 1-32
212. Wach, A., Brachat, A., AlbertiSegui, C., Rebischung, C., and Philippsen, P. (1997) *Yeast* **13**(11), 1065-1075
213. Guzman, L. M., Belin, D., Carson, M. J., and Beckwith, J. (1995) *Journal of Bacteriology* **177**(14), 4121-4130
214. Kovach, M. E., Elzer, P. H., Hill, D. S., Robertson, G. T., Farris, M. A., Roop, R. M., and Peterson, K. M. (1995) *Gene* **166**(1), 175-176
215. Calamia, J., and Manoil, C. (1992) *Journal Of Molecular Biology* **224**(3), 539-543
216. Kienberger, F., Ebner, A., Gruber, H. J., and Hinterdorfer, P. (2006) *Accounts Of Chemical Research* **39**(1), 29-36
217. Ma, X. L., Ehrhardt, D. W., and Margolin, W. (1996) *Proceedings Of The National Academy Of Sciences Of The United States Of America* **93**(23), 12998-13003
218. Sun, Q., and Margolin, W. (1998) *Journal Of Bacteriology* **180**(8), 2050-2056
219. Jones, L. J. F., Carballido-Lopez, R., and Errington, J. (2001) *Cell* **104**(6), 913-922
220. Braet, F., Seynaeve, C., De Zanger, R., and Wisse, E. (1998) *Journal Of Microscopy-Oxford* **190**, 328-338
221. Madl, J., Rhode, S., Stangl, H., Stockinger, H., Hinterdorfer, P., Schutz, G. J., and Kada, G. (2006) *Ultramicroscopy* **106**(8-9), 645-651
222. Sharma, A., Anderson, K. I., and Muller, D. J. (2005) *FEBS Letters* **579**(9), 2001-2008
223. Rong, W. Z., Ding, W., Madler, L., Ruoff, R. S., and Friedlander, S. K. (2006) Mechanical Properties of Nanoparticle Chain Aggregates by Combined AFM and SEM: Isolated Aggregates and Networks. In.

Appendices

Appendix A – Figures and Tables

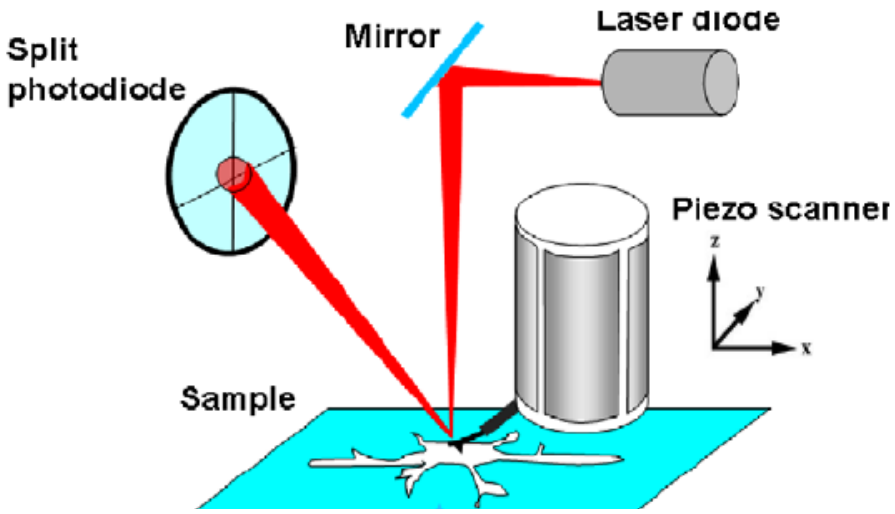

Figure 1. Schematic of an AFM. In the top-scanning AFM, the tip is mounted on the piezo scanner. A laser is reflected from the back of the cantilever to a photodiode. Changes in the position of the cantilever are monitored by corresponding changes in the position of the laser spot on the photodiode. Figure from Alessandrini, A and Facci, P. (2005) *Measurement Science and Technology* 16, R65-R92

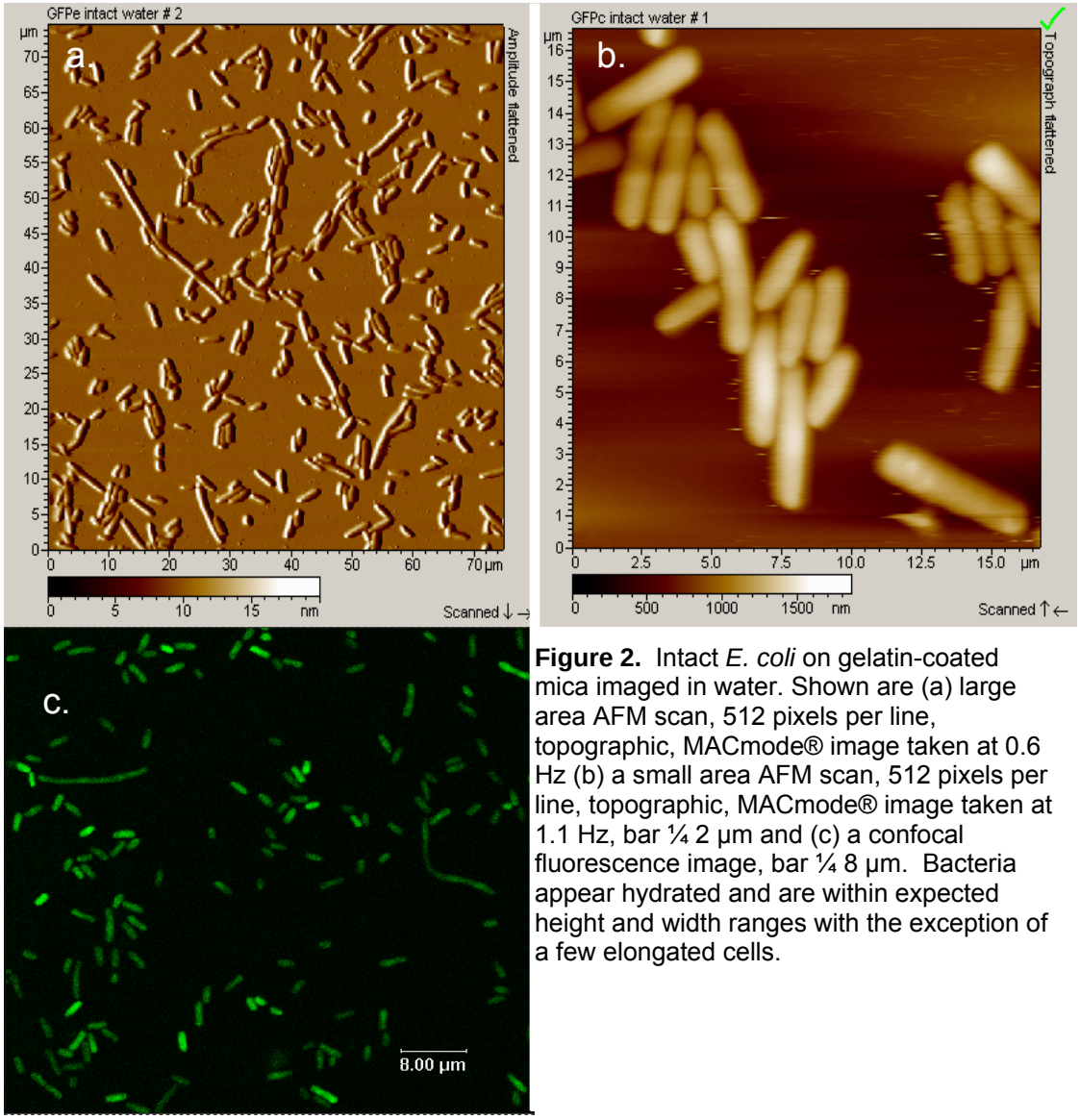

Figure 2. Intact *E. coli* on gelatin-coated mica imaged in water. Shown are (a) large area AFM scan, 512 pixels per line, topographic, MACmode® image taken at 0.6 Hz (b) a small area AFM scan, 512 pixels per line, topographic, MACmode® image taken at 1.1 Hz, bar ¼ 2 µm and (c) a confocal fluorescence image, bar ¼ 8 µm. Bacteria appear hydrated and are within expected height and width ranges with the exception of a few elongated cells.

Table 1. Bacterial Strains

Strain	Relevant Characteristics
EH	expresses only the endogenous copy of PtsG
I108	expresses the ptsG/PhoA fusion from a vector in addition to endogenous PtsG
ΔGluc	does not take up glucose
CC-GFP	constitutively expresses cytoplasmic GFP
AI-GFP	arabinose inducible cytoplasmic GFP expression

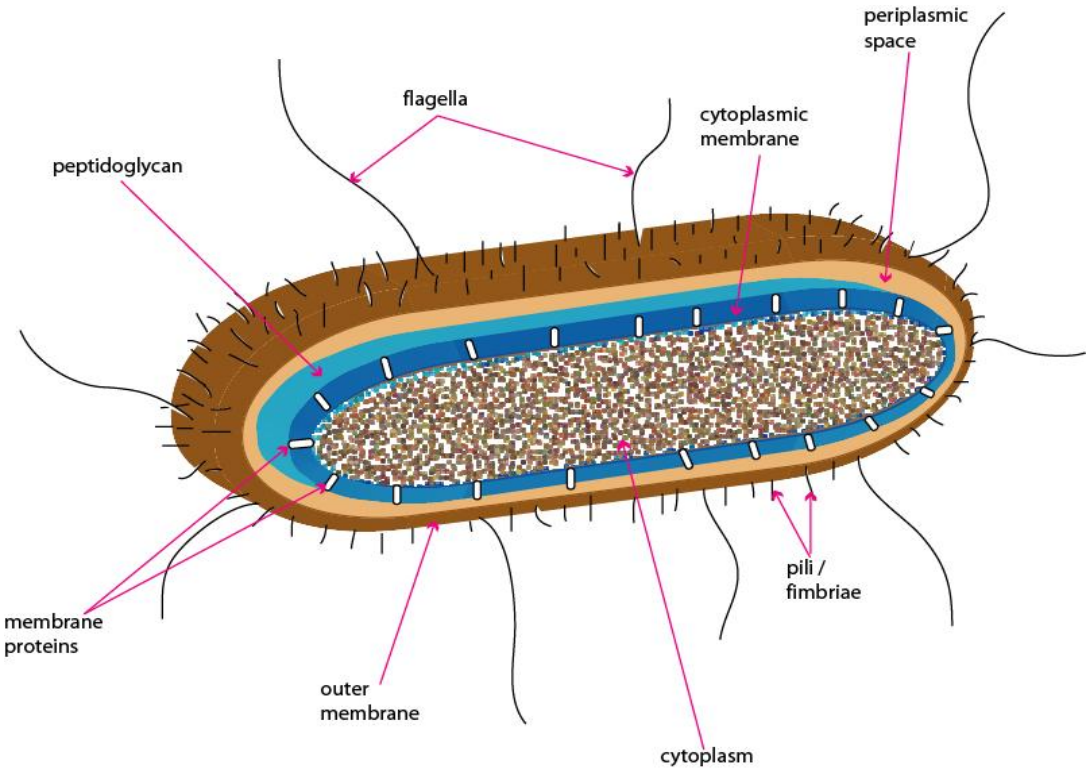

Figure 3. The cellular structure of *E. coli*. Removal of the cell wall results in osmotically sensitive spheroplasts.

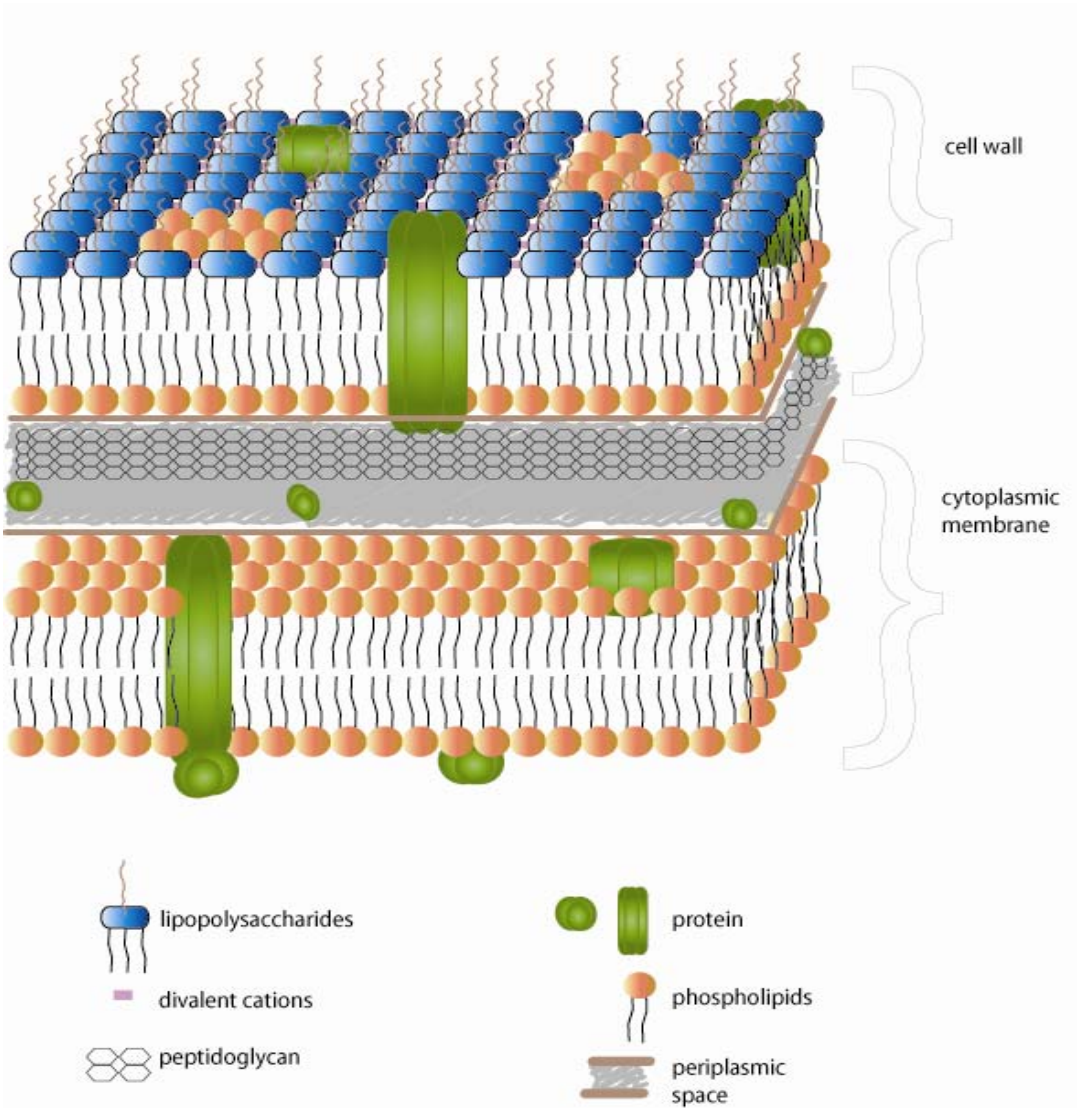

Figure 4. Cell envelope of gram-negative bacteria.

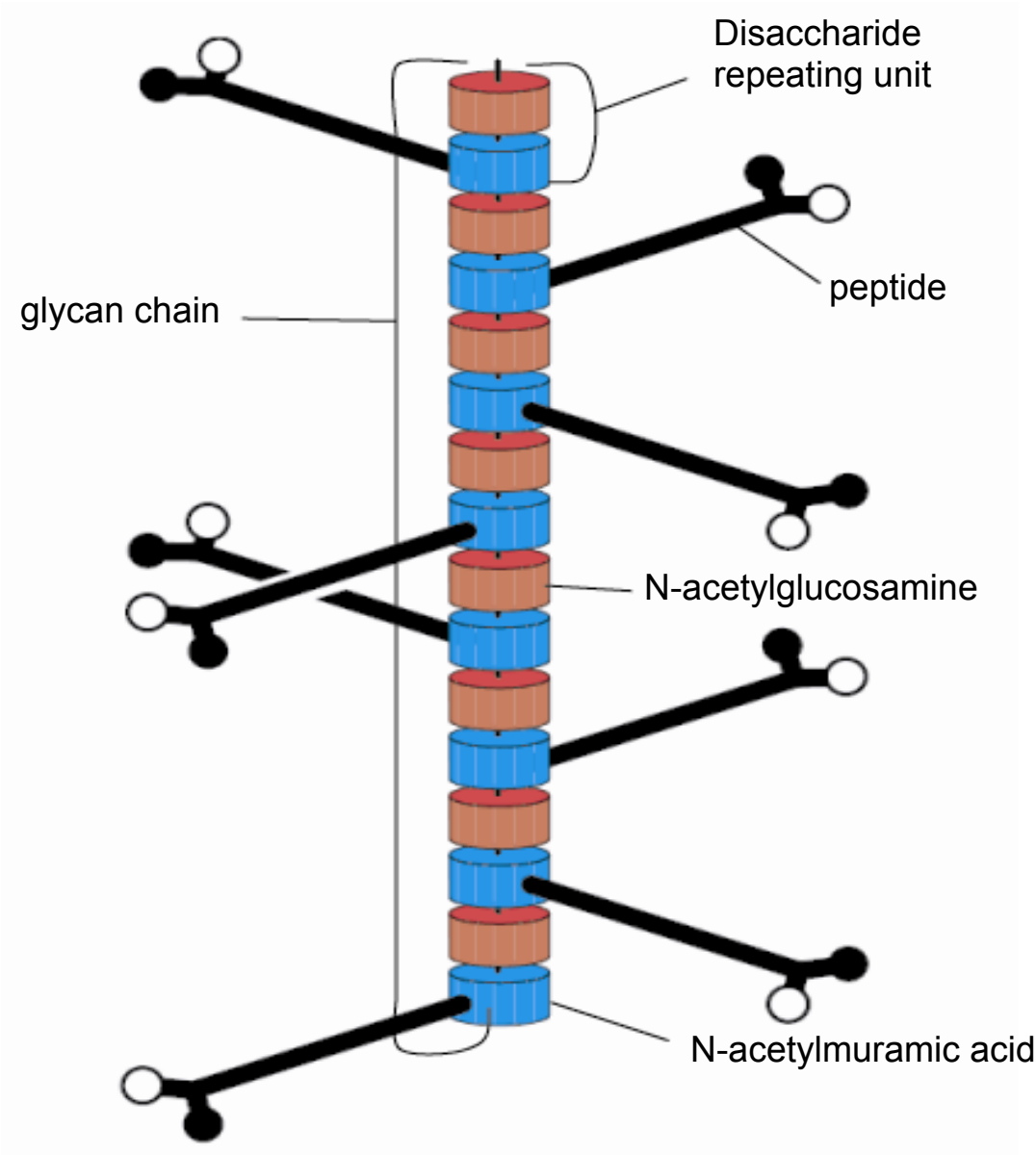

Figure 5. The peptidoglycan strand. The repeating unit of the peptidoglycan is generally made of a disaccharide of N-acetylglucosamine and N-acetylmuramic acid and a peptide containing L-alanine, D-glutamic acid, meso-diaminopimelic acid and D-alanine. The sugars alternate to form the backbone of the polymer and are connected via a 1→4 glycosidic bonds. The peptide is attached to the muramic acid and extends away from the glycan chain.(1) Figure adapted from Dmitriev, B., Toukach, F., and Ehlers, S. (2005) *Trends In Microbiology* 13(12), 569-574

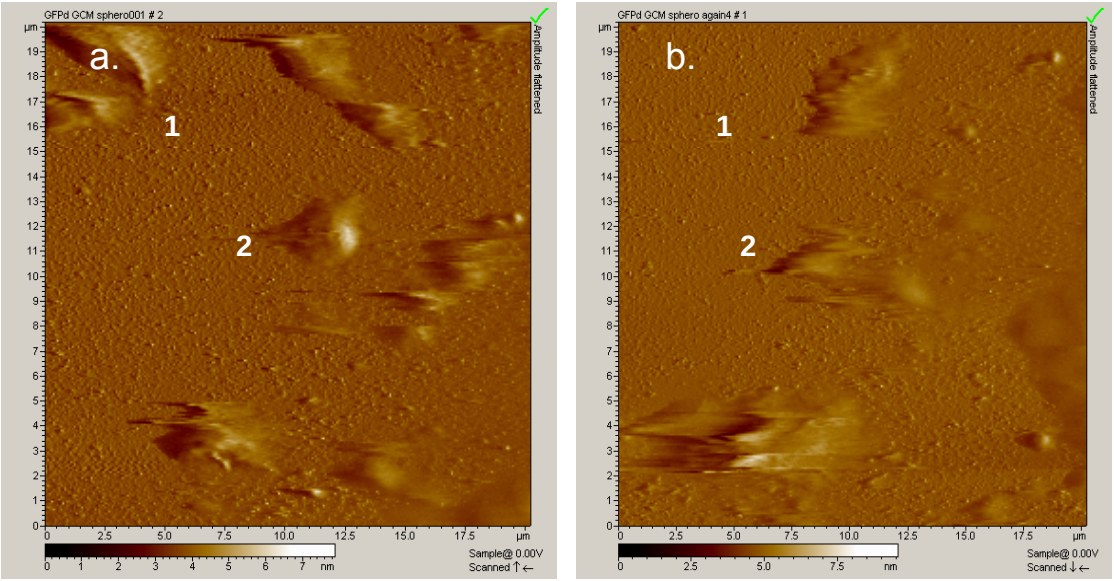

Figure 6. Spheroplasts immobilized on gelatin-coated mica. Cells were scanned at 1.5Hz and with 256 pixels per line. (a) Amplitude image after one scan, bar = 2 µm; (b) amplitude image of the same area after four scans taken within 20 min of 2a, bar = 2 µm. Note that spheroplasts are present but appear to be repositioned (1) and distorted (2) by the tip as a result of scanning.

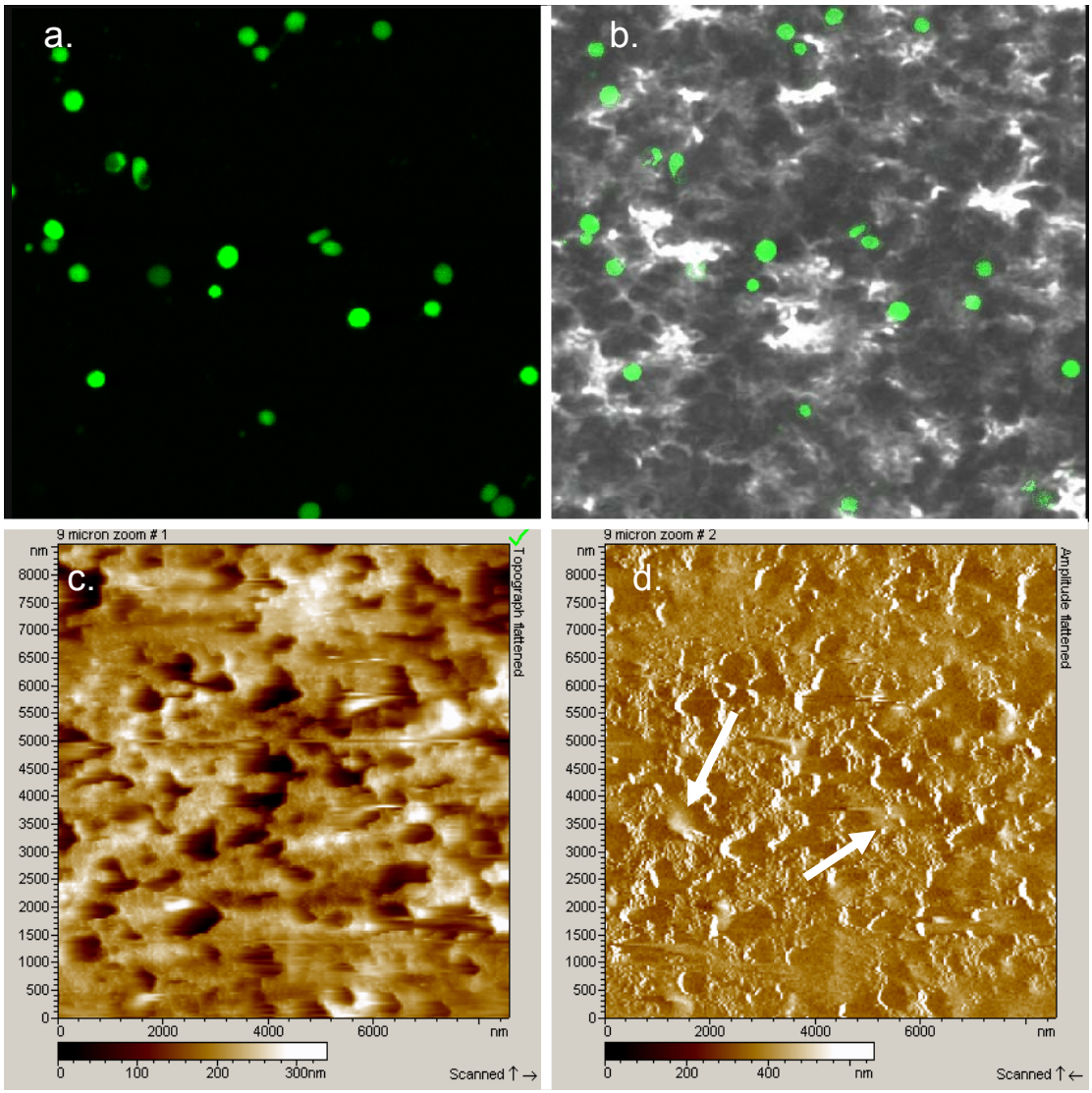

Figure 7. GFP expressing spheroplasts immobilized in isoporous filters. (a,b) Confocal images show that spheroplasts are retained in the filter membrane. (a) fluorescence image. (b) overlay of fluorescence and transmission images. (c,d) AFM images of a filter in which fluorescent spheroplasts were detected. The spheroplasts are approximately 1µm in diameter and are probably buried in the 7-22µm thick filter. (c) topograph. (d) amplitude. Note the areas with different contrast (arrows). These may be spheroplasts but the rough topography of the filter surface prevents a clear determination.

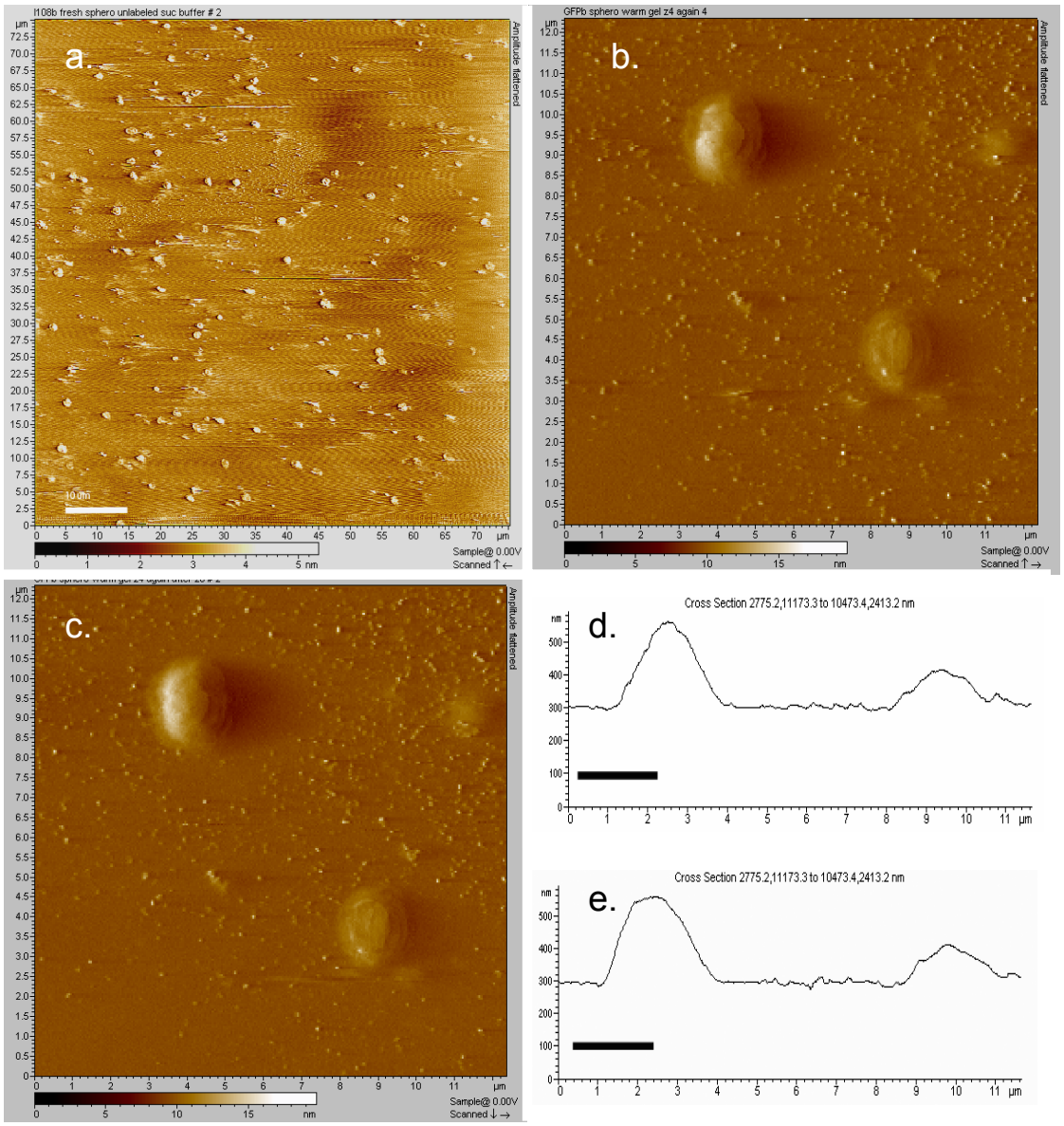

Figure 8. Spheroplasts immobilized with warm gelatin. Amplitude images are shown. (a) Representative 75 µm scan taken at 512 pixels per line and at a speed of 2 Hz, bar = 10 µm. (b) To demonstrate the stability of the preparation technique, two spheroplasts were imaged after four scans at 1.3Hz and compared with the image of the same spheroplasts, bar = 2 µm. (c) Imaged after 20 scans at 1.3Hz over a 3 h period, bar = 2 µm. (d) and (e) are cross sections from the topograph images of (b) and (c) respectively, bars = 2 µm. Note the similarity in the profiles, indicating that the spheroplasts were stably imaged without the changes noted in Figure 6.

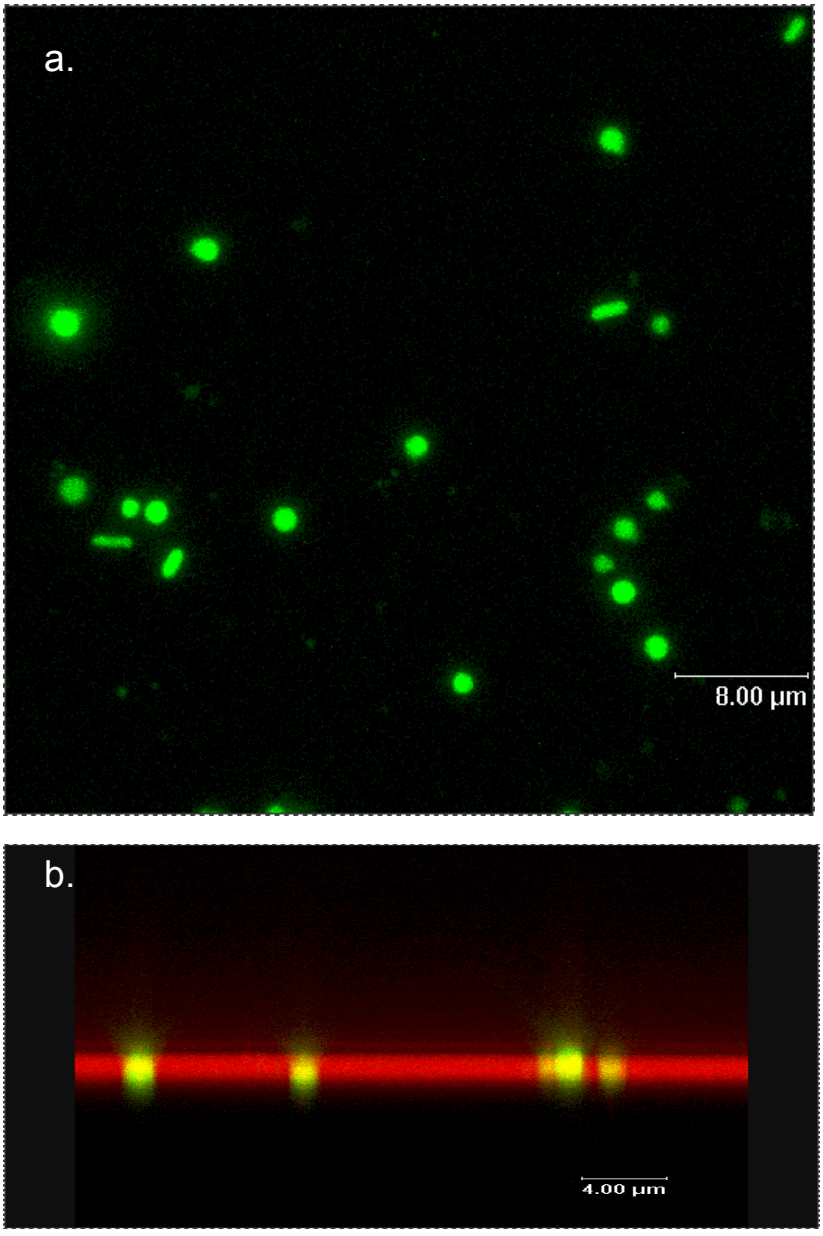

Figure 9. Spheroplasts immobilized using warm gelatin doped with rhodamine 6G. Appropriate filters for GFP and rhodamine 6G were used in each case to generate a series of confocal fluorescence images compressed into a single image. (a) GFP channel only xyz scan, bar = 8 µm. (b) Emission detected on the GFP and rhodamine 6G channels are merged to show that the spheroplasts are spherical and are in proximity of the gelatin surface. The horizontal band results from light reflection and indicates the surface of the gelatin, bar = 4 µm.

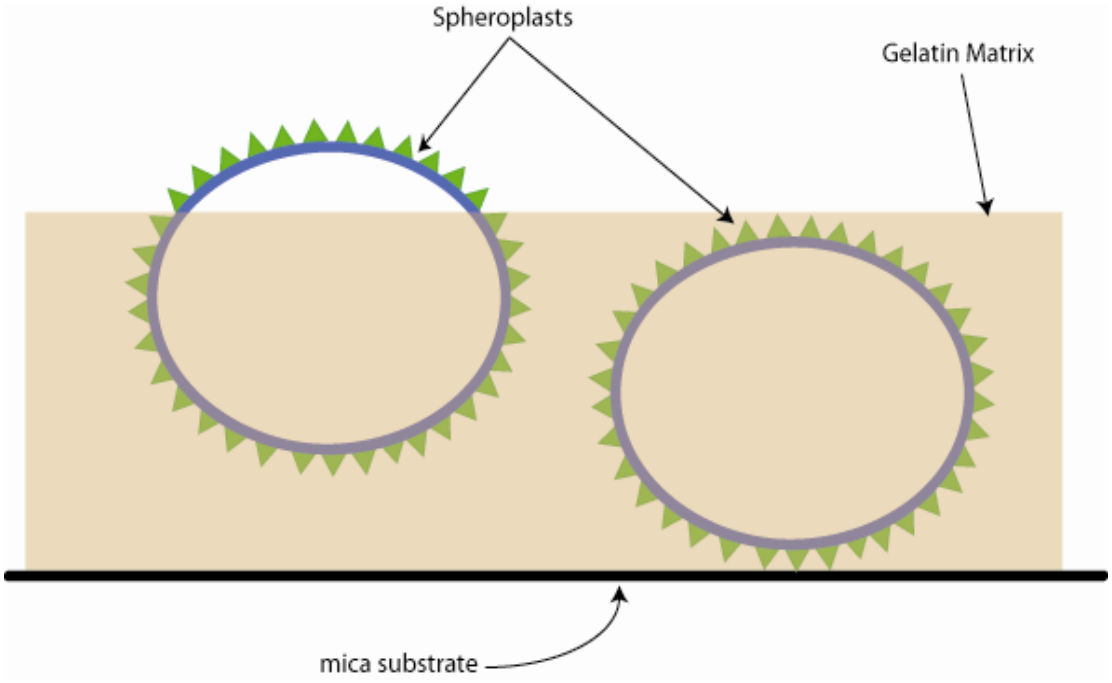

Figure 10. Cartoon of immobilization using warm gelatin mixed with spheroplasts. Cells are captured to varying degrees in the gelatin.

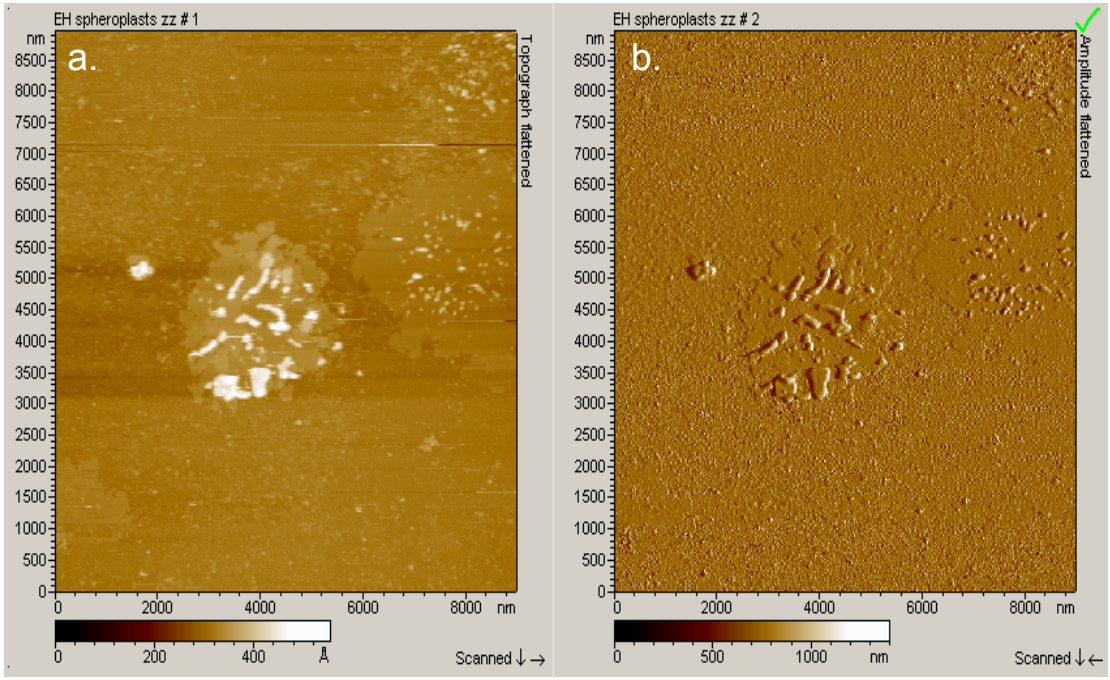

Figure 11. Spheroplasts with irregular boundaries and "lumpy" surfaces. These aberrations could be seen in samples prepared with warm gelatin. This observation raises questions about the effect the gelatin temperature might have on the cells, even those that appear to be normal. (a) topograph. (b) amplitude

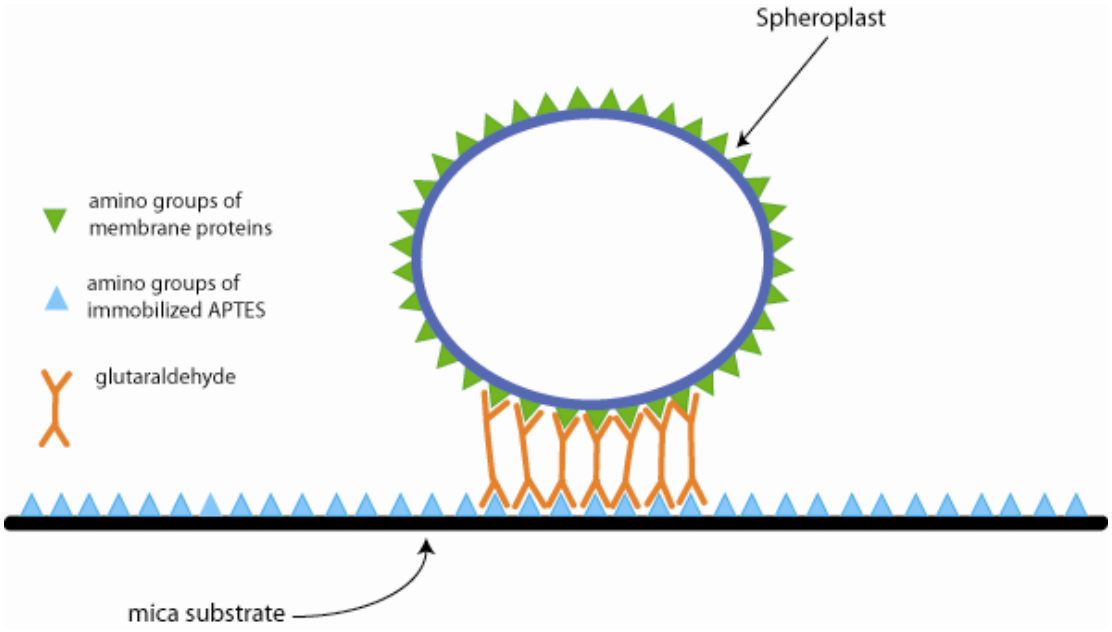

Figure 12. Schematic of APTES/glut immobilization. The drawing illustrates how glutaraldehyde crosslinks the spheroplasts to the aminopropyltriethoxysilane-treated mica via amino groups of both surfaces.

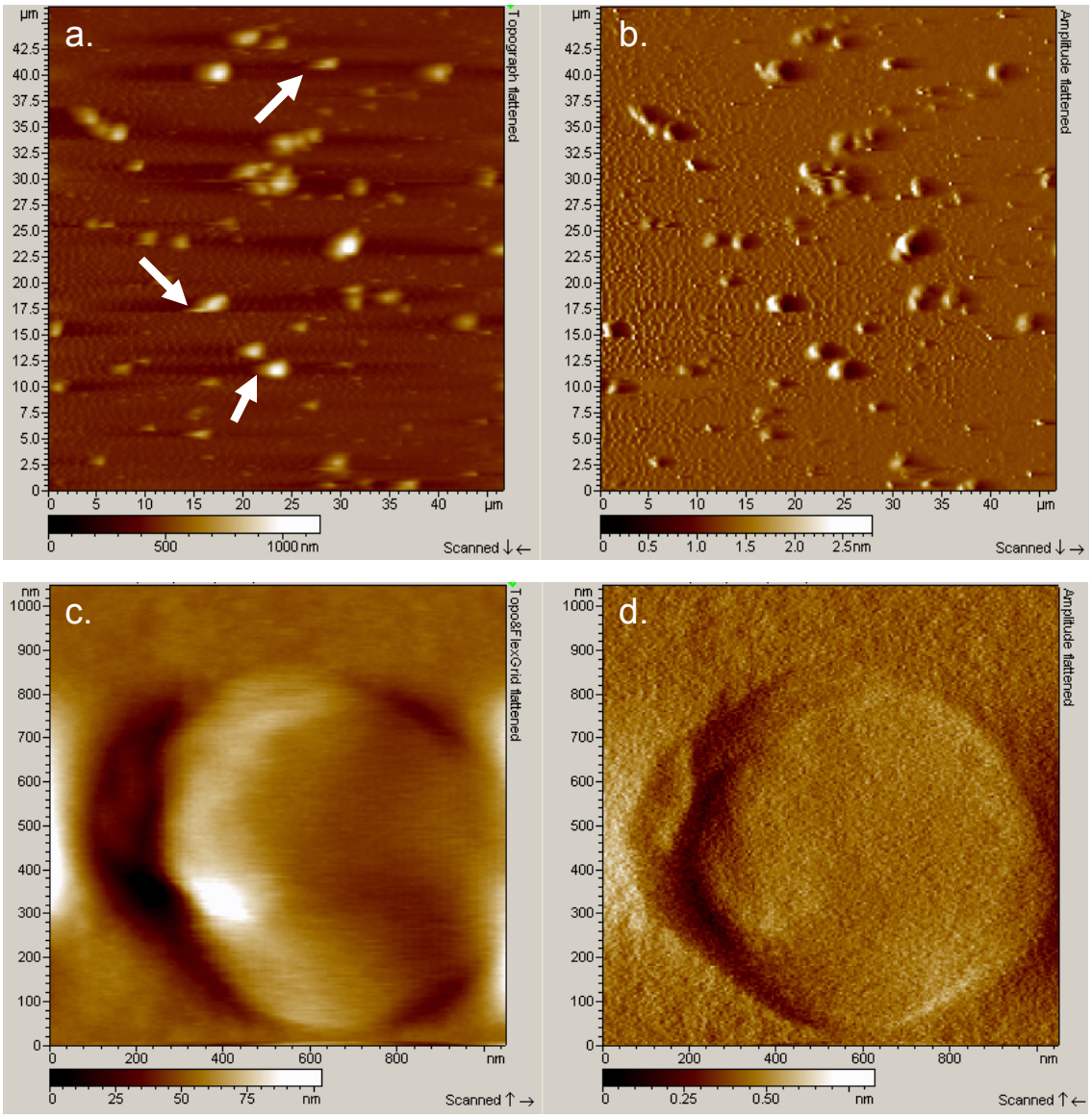

Figure 13. Images of spheroplasts immobilized on APTES/glut mica. (a,b), 45µm scan. Although the cells are clearly anchored to the substrate, the topograph image shows distortions which indicate that the spheroplasts follow the direction of the scan. (heavy arrows) The scan direction is indicated in the lower right corner of each image (thin arrows). (c,d) 1µm scan of a single cell. (a,c) topograph images. (b,d) amplitude images.

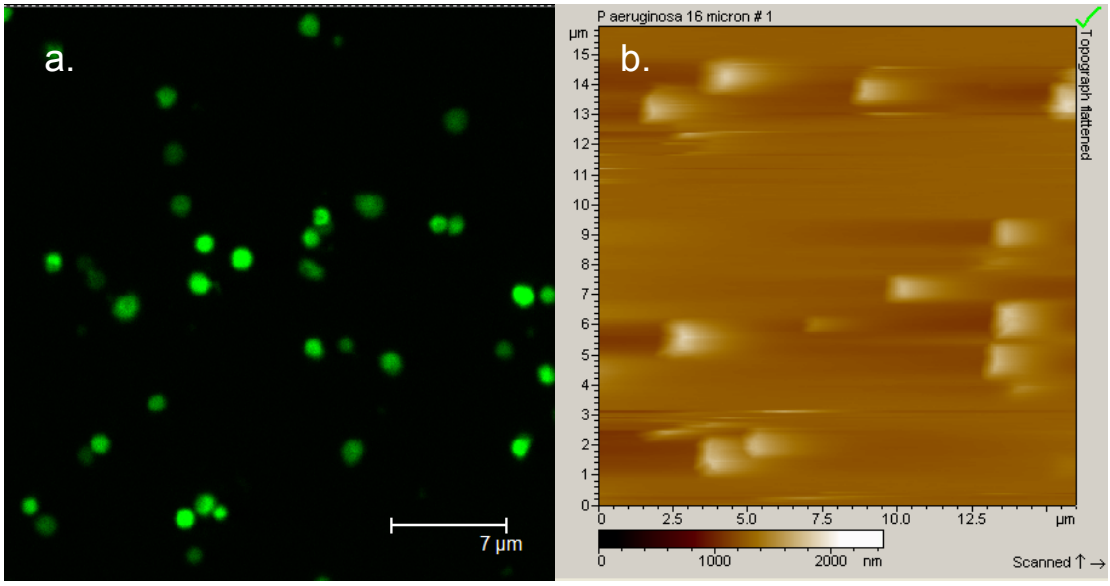

Figure 14. CC-GFP Spheroplasts immobilized on APTES/glut mica. (a) confocal image of *E. coli* spheroplasts expressing cytoplasmic GFP. (b) Topograph image of *Pseudomonas aeruginosa* spheroplasts.

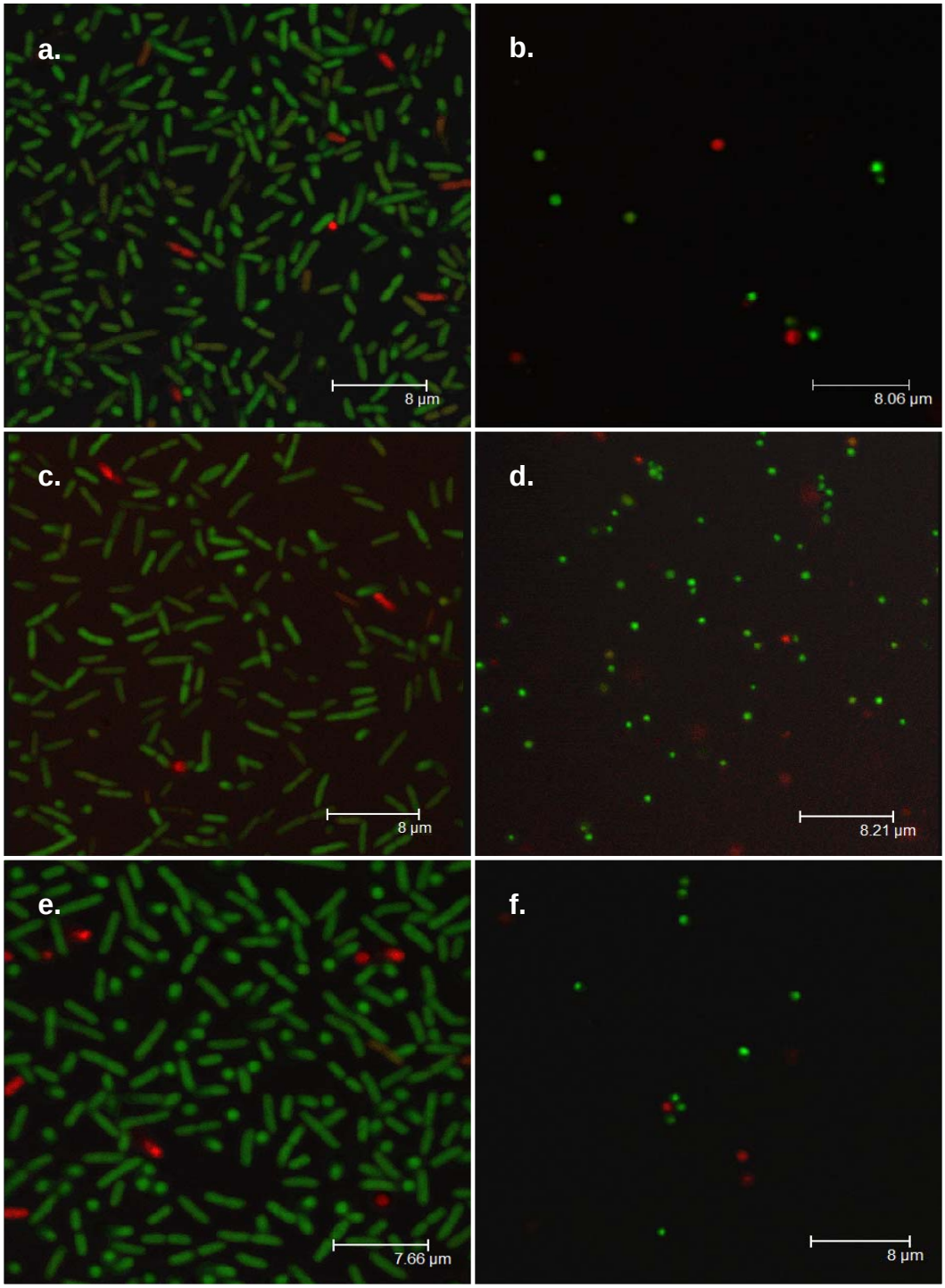

Figure 15. Live/Dead® BacLight™ assay. Immobilized cells were incubated in the manufacturer's recommended concentration of SYTO9 (component A) and propidium iodide (component B) for 10 minutes; each channel scanned sequentially. (a,b) EH, (c,d) I108, (e,f) ΔGluc

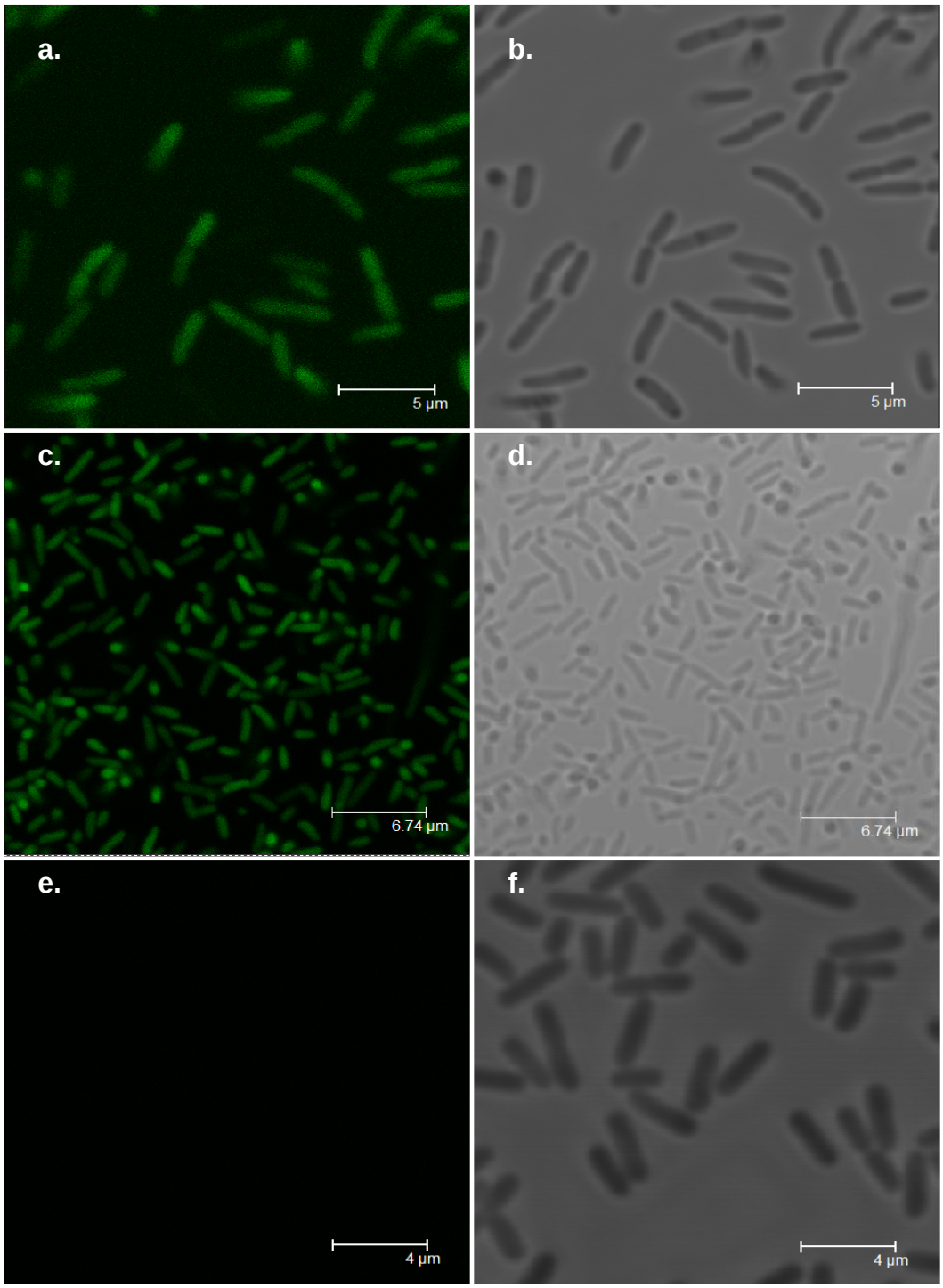

Figure 16. Fluorescent glucose assay using intact bacteria. Confocal images of intact *E. coli* mounted on a gelatin-treated substrate and treated with fluorescent glucose. Fluorescence (a,c,e) and associated transmission (b,d,f) images shown. (a,b) EH (c,d) I108 (e,f) ΔGluc (which does not take up glucose).

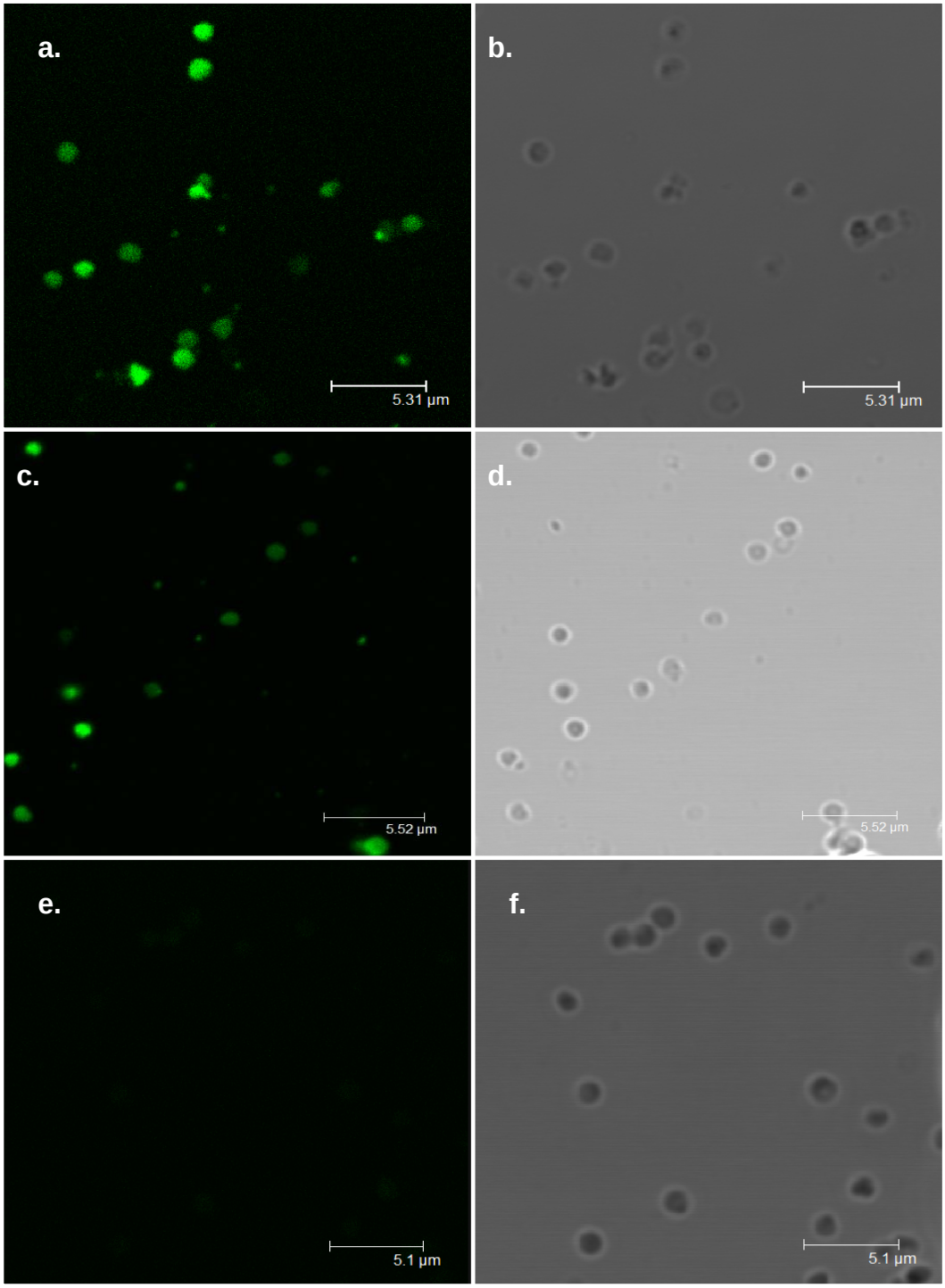

Figure 17. Fluorescent glucose assay using spheroplasts. Confocal images of spheroplasts mounted on a APTES/glut substrate and treated with fluorescent glucose. Fluorescence (a,c,e) and associated transmission (b,d,f) images shown. (a,b) EH (c,d) I108 (e,f) ΔGluc (which does not take up glucose) .

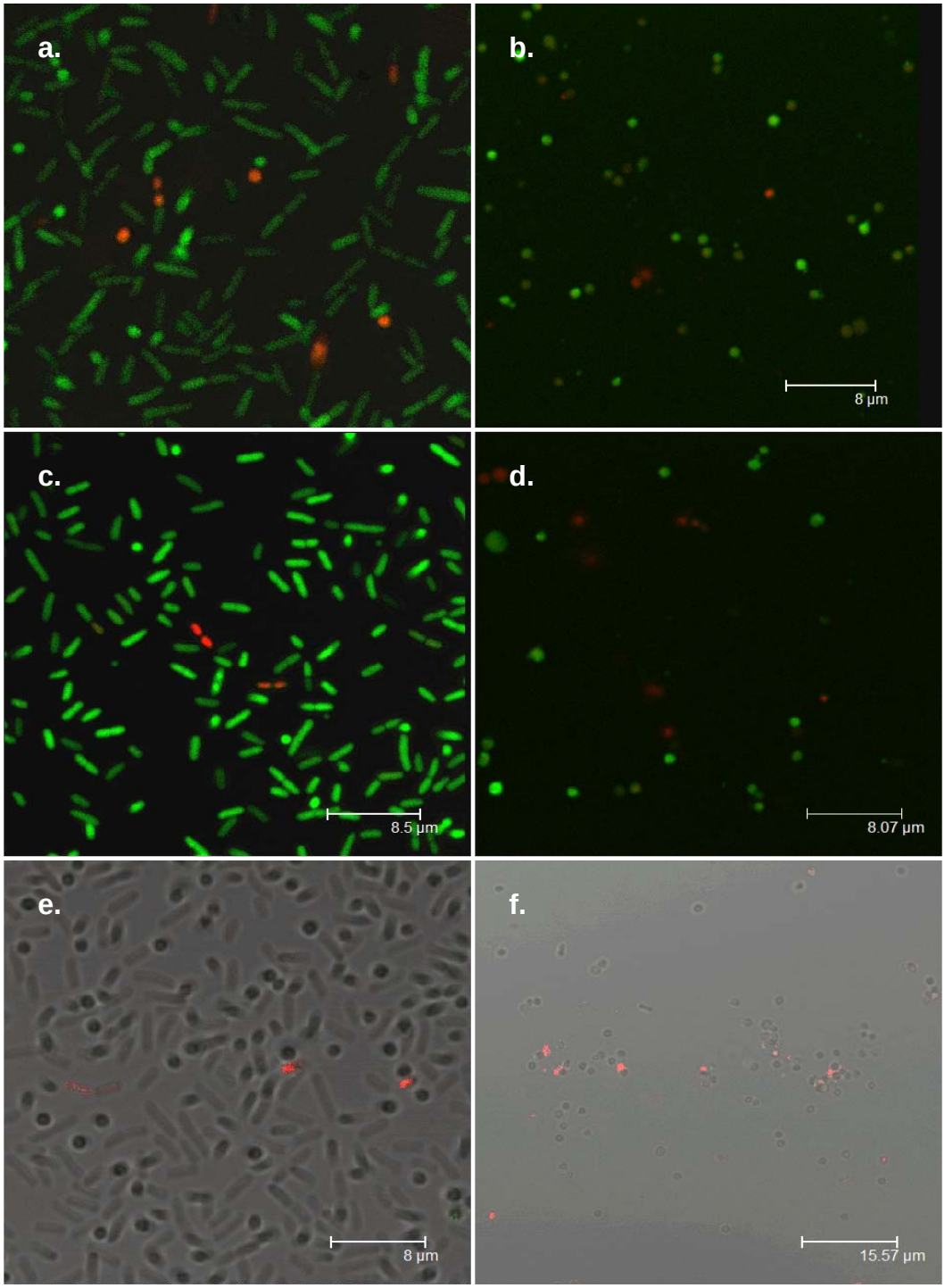

Figure 18. Glucose/Propidium Iodide assay on intact bacteria and spheroplasts. Immobilized cells were incubated with 100µM 2NBDG and the recommended concentration of Propidium Iodide from the Live/Dead® BacLight™ assay for 10 minutes; each channel scanned sequentially. (a,b) EH, (c,d) I108, (e,f) ΔGluc, overlay of transmission light and fluorescence channels

Table 2. Condition Summary Data

	Regular Baclight (Live Dead Assay)	%	Glucose Baclight (2NBDG and propidium iodide)	%	AFM	%
number of fields	7		7		11	
cells counted	291		591		2248	
green or spherical cells	220	75.60%	438	74.11%	1621	72.11%
red or flat cells	71	24.40%	153	25.89%	627	27.89%

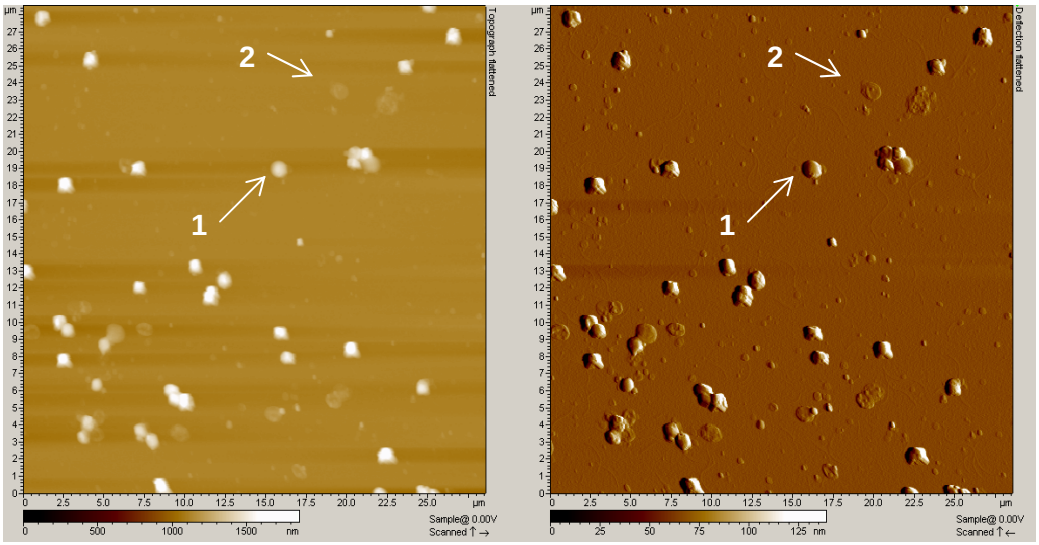

Figure 19. Contact mode AFM images of fixed spheroplasts. Images were taken in air after 0.5% glutaraldehyde fixation of the sample after immobilization. (a) topograph and (b) deflection. (1) spherical and (2) flattened cells.

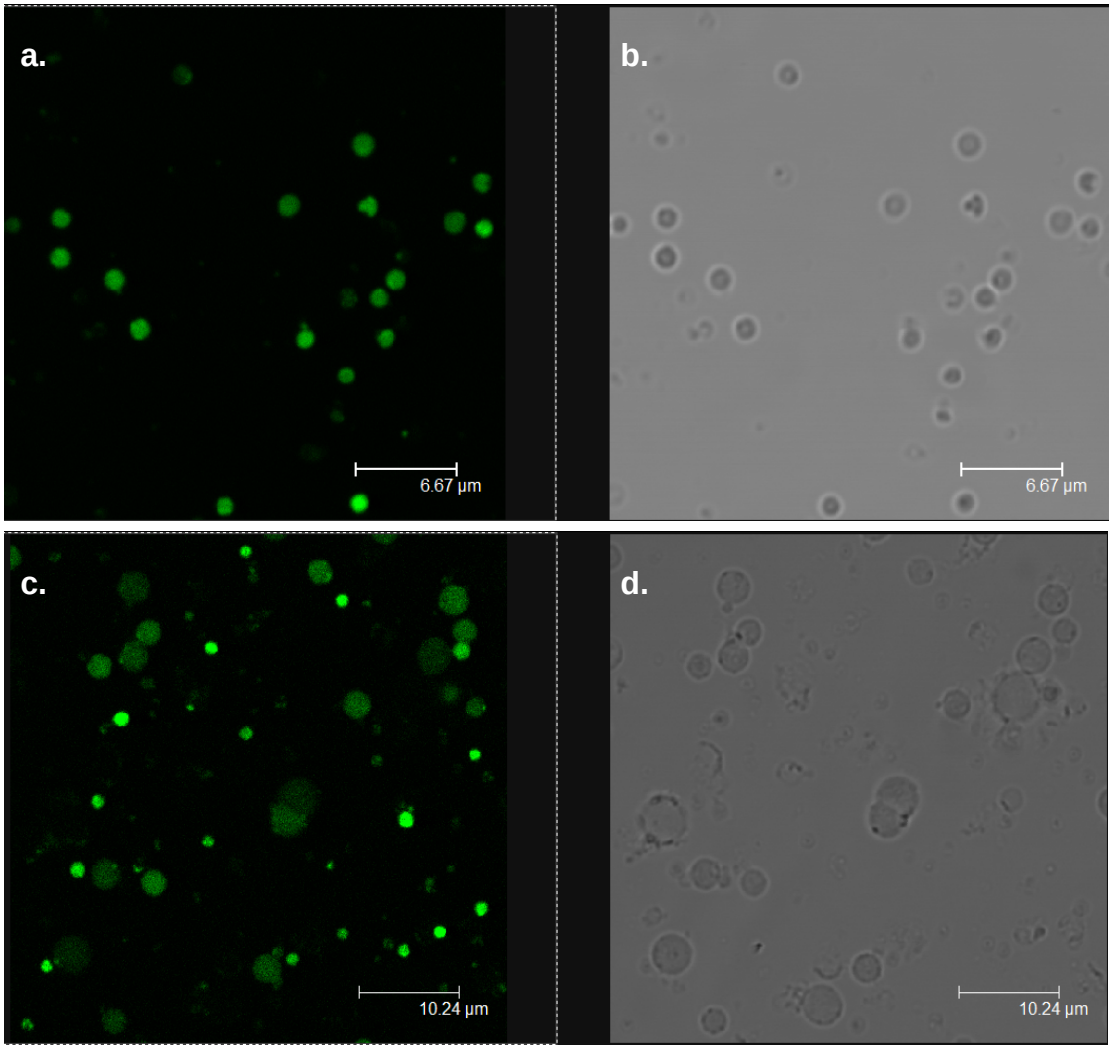

Figure 20. *E. coli* spheroplasts expressing GFP in the cytoplasm. Cells were immobilized on APTES/Glut treated mica and incubated in a recovering broth (0.25M sucrose/LB doped with 500units/ml penicillin G and selective antibiotic). (a,b) Fluorescence and transmission images of cells after 3hr incubation. (c,d) Fluorescence and transmission images of cells after overnight incubation.

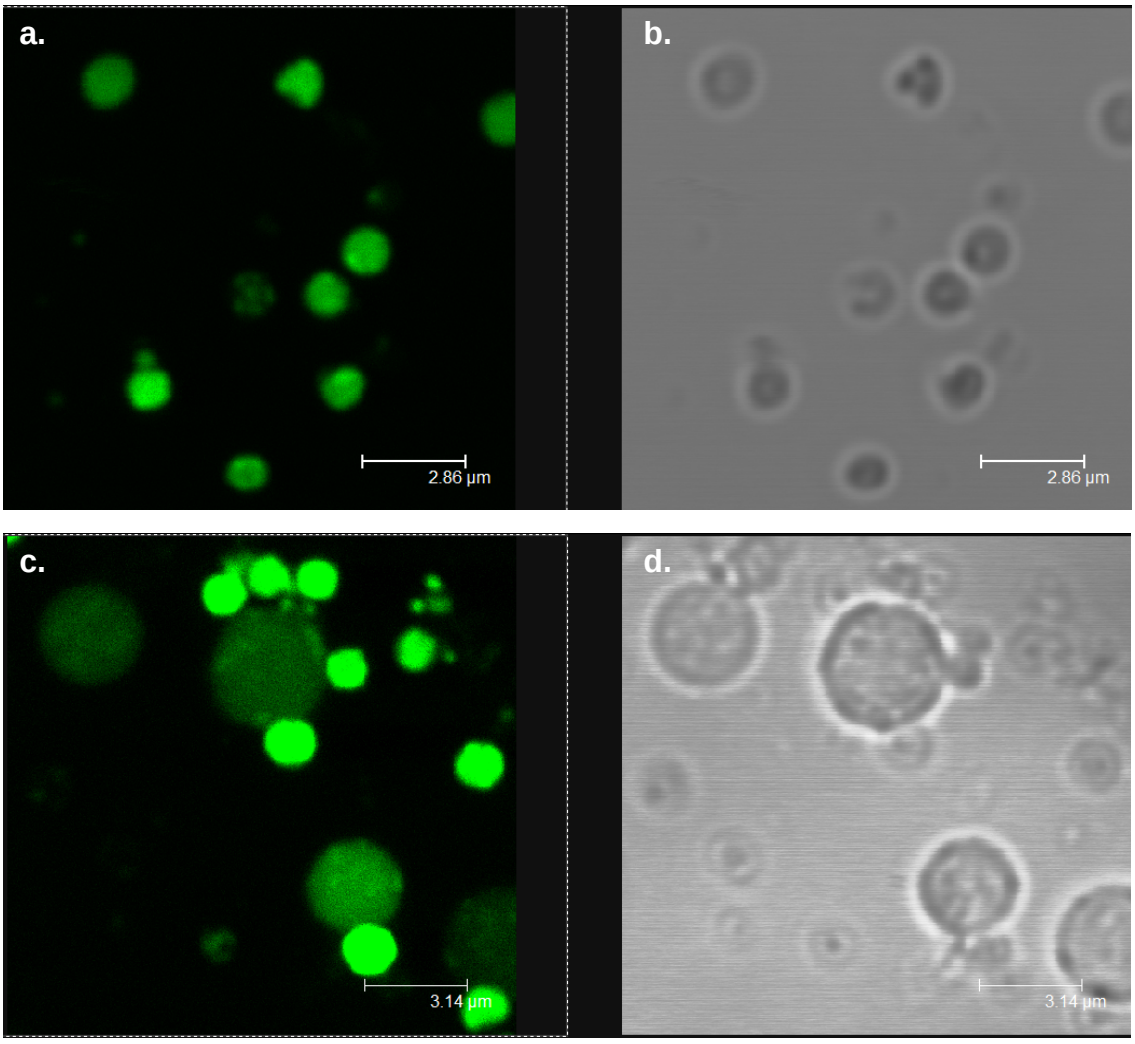

Figure 21. Zoom of *E. coli* spheroplasts expressing GFP in the cytoplasm. Magnification of regions from the samples in Figure 20. (a,b) Fluorescence and transmission images of cells after 3hr incubation. (c,d) Fluorescence and transmission images of cells after overnight incubation.

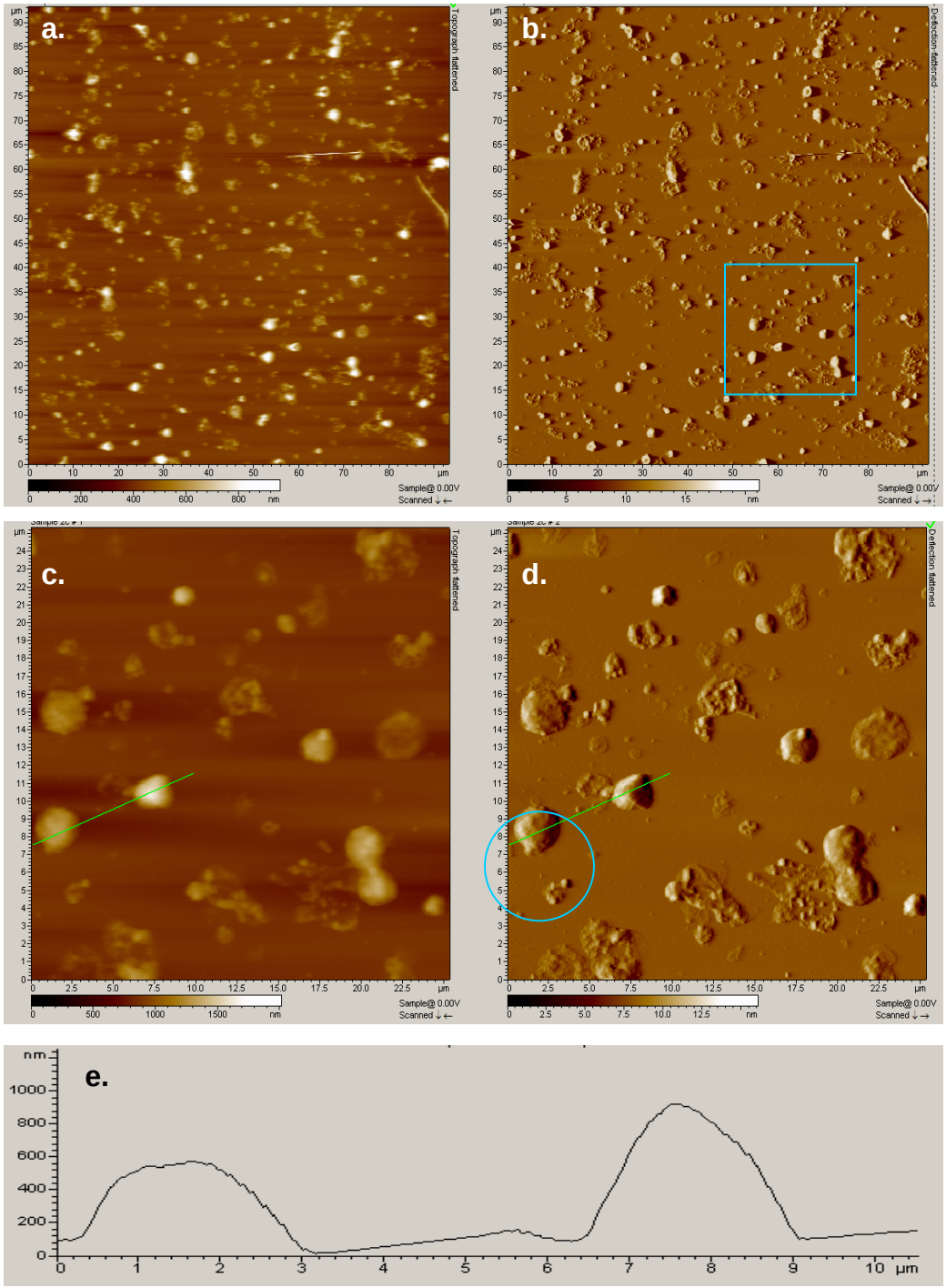

Figure 22. Contact mode AFM images of fixed overnight spheroplasts. Images of spheroplasts immobilized and incubated in recovery media overnight were taken in air after 0.5% glutaraldehyde fixation. (a, b) 95 µm topograph and deflection; (c,d) topograph and deflection image of the region in the square shown in (b). (e) cross section of the cells in (c).

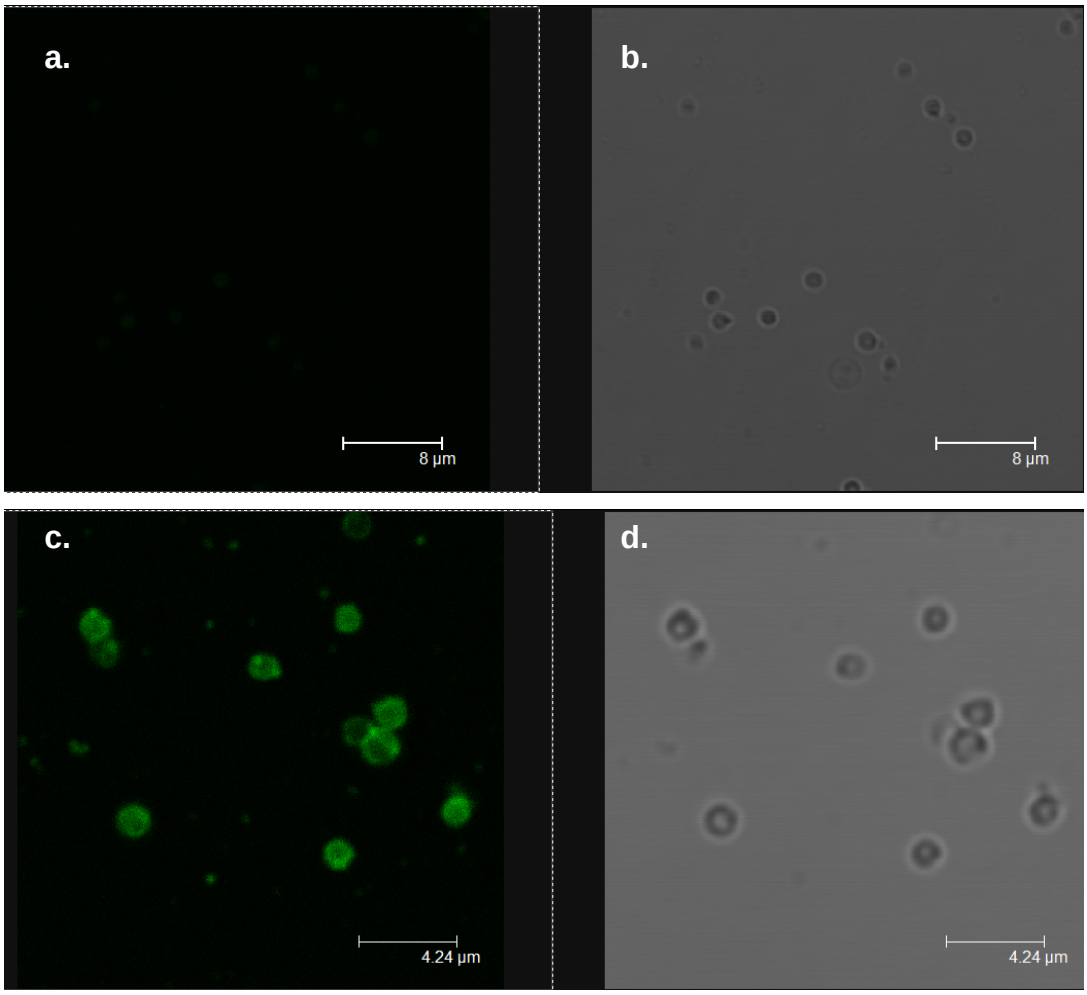

Figure 23. Spheroplasts expressing an arabinose inducible cytoplasmic GFP. Spheroplasts were generated and the cells were mounted on APTES/glut substrates. (a,b) Fluorescent and transmission images of spheroplasts before induction.

The samples were retained at 37º in recovering broth for 2 hours. Cells were subsequently incubated in fresh recovering broth which included 0.2% arabinose for 2 additional hours. (c,d) Fluorescent and transmission images of spheroplasts after induction.

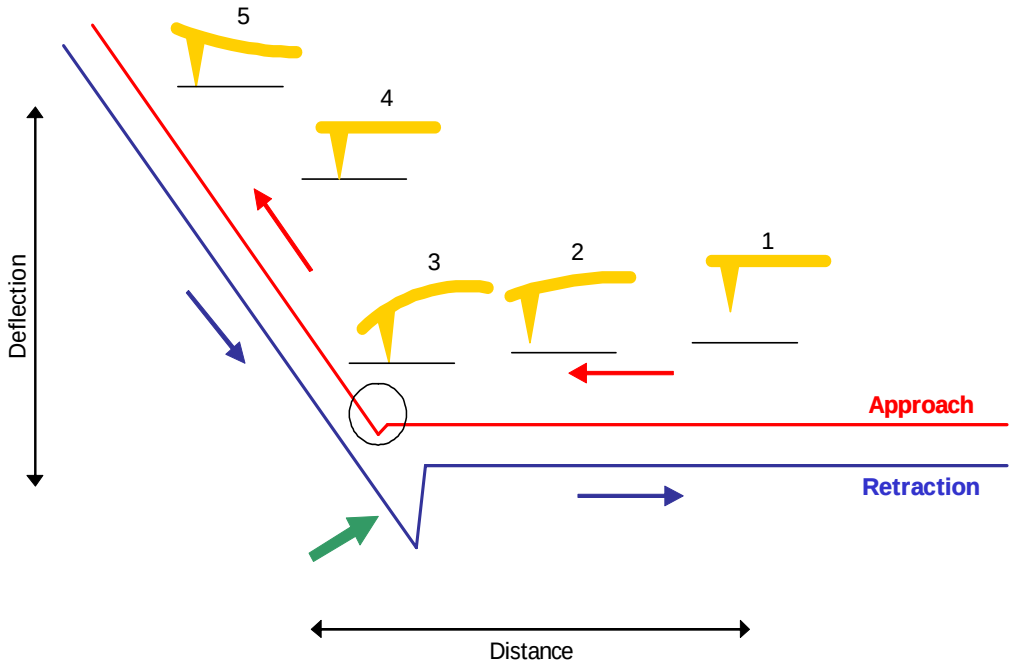

Figure 24. Stylized force-distance curves. The piezo scanner is limited to movement along the z plane. While the tip is far from the surface (1) and is not deflected, the curve is horizontal (slope = 0). In air, as the piezo moves the tip closer to the surface on the approach, attractive forces increase causing a negative deflection (3, circle). Once firm contact is made with the surface, deflection and distance increase linearly (4,5). Upon retraction, the reverse of these events occur. Larger adhesion peaks are generally seen on the retraction curve before the tip abruptly disengages from the surface (green arrow).

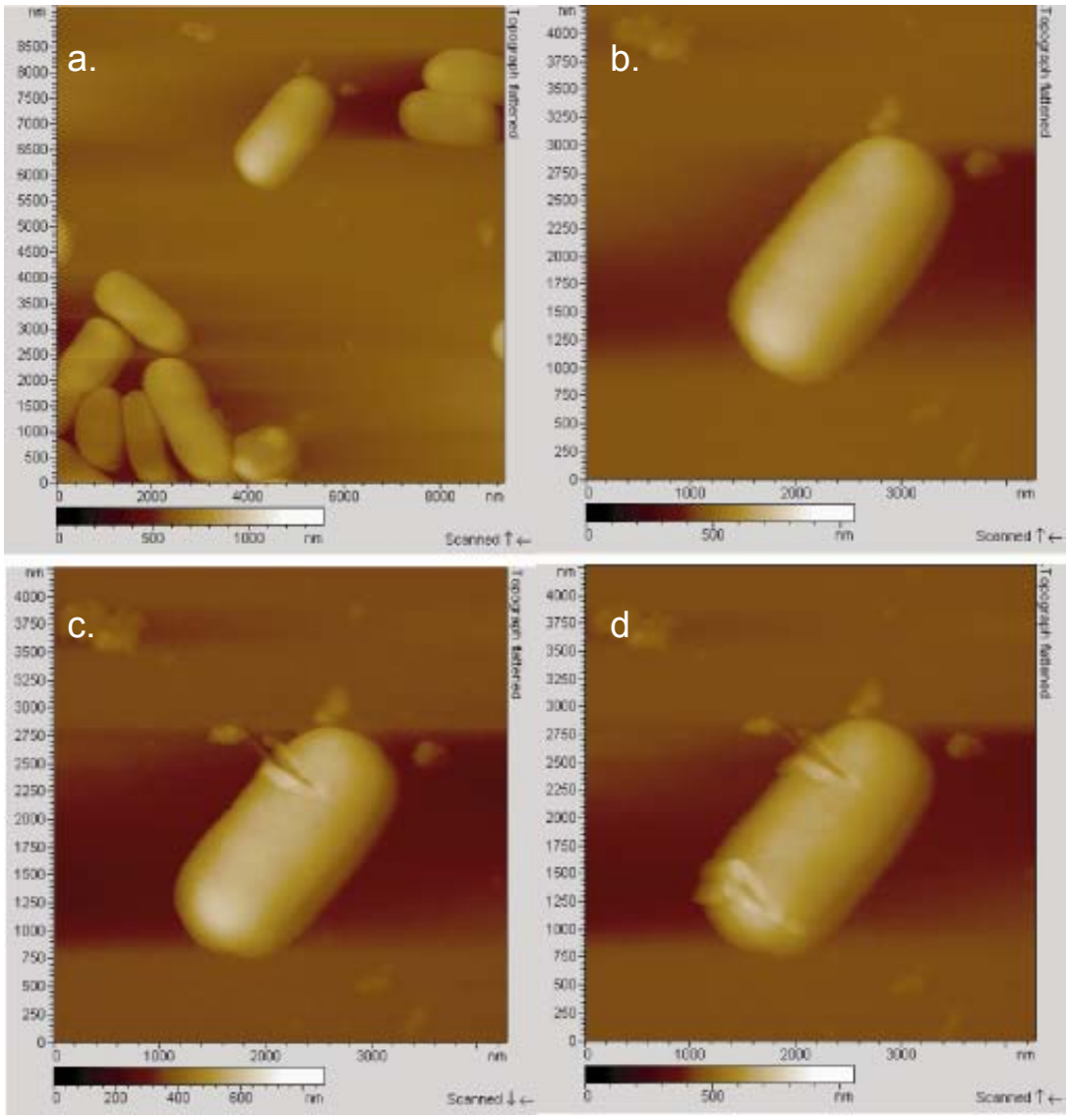

Figure 25. The importance of cantilever selection. (a, b) Bacteria were successfully imaged in MACMode using a type Ic silicon Mac Lever. (c) Force distance curves were generated on the bacteria and subsequently imaged. (d) A different location was chosen to generate force distance curves. Disruption of the bacterial surface by the stiff cantilever apparently occurred during generation of the force distance curves.

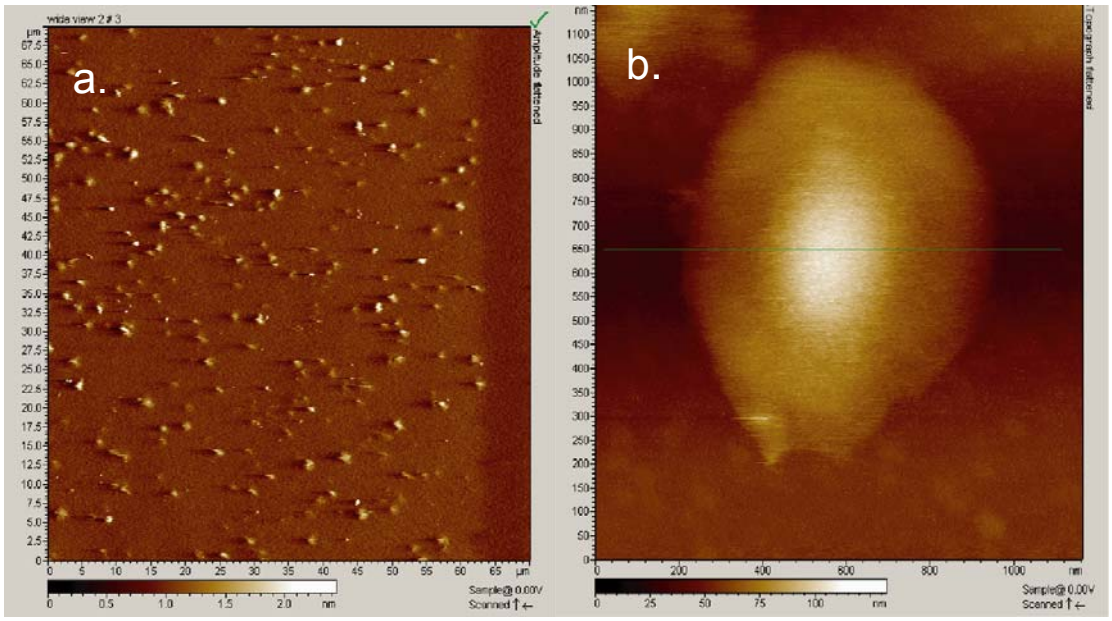

Figure 26. Spheroplasts imaged in MAC Mode® with a silicon nitride cantilever having a nominal spring constant of 0.1nN/nm. (a) 70 µm scan. (b) Individual spheroplast. (c) Cross section measurement of topograph image showing height.

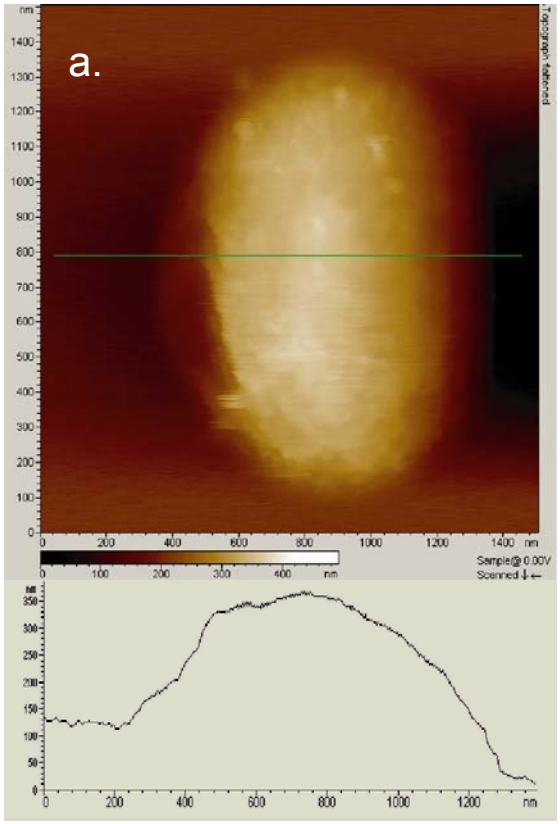

Figure 27. MAC Mode® Images of a 0.5% glutaraldehyde fixed spheroplasts. Images were acquired using a silicon nitride cantilever having a nominal spring constant of 0.1 nN/nm. (a) Topograph image. (b) Phase image. (c) Cross section measurement of topograph image.

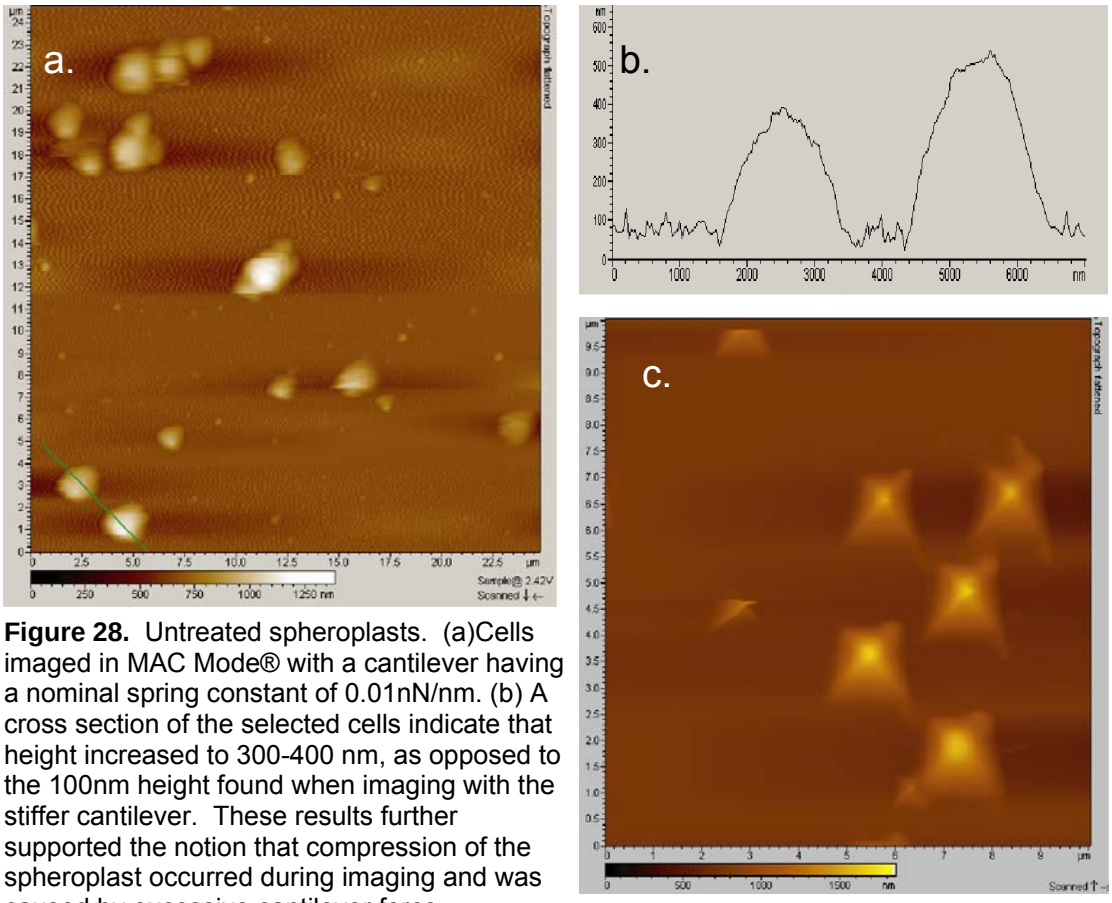

Figure 28. Untreated spheroplasts. (a)Cells imaged in MAC Mode® with a cantilever having a nominal spring constant of 0.01nN/nm. (b) A cross section of the selected cells indicate that height increased to 300-400 nm, as opposed to the 100nm height found when imaging with the stiffer cantilever. These results further supported the notion that compression of the spheroplast occurred during imaging and was caused by excessive cantilever force.

(c) Untreated spheroplasts were also imaged in contact mode using the softer (0.01nN/nm) cantilever. Contact mode imaging of the untreated spheroplasts results in a tip artifact due to the deformability of the spheroplasts during imaging.

Table 3. Spring Constant Determination - Type IVc

	FDC Method 1		FDC Method 2		FDC Method 3		
	Average	Std. Dev	Average	Std. Dev	Average	Std. Dev	
Cantilever 1	12.9583	1.1390	14.9723	0.1814	16.6233	1.0172	Conversion Coefficient
	0.0593	0.0124	0.0659	0.0021	0.0974	0.0100	Spring Constant (nN/nm)
Cantilever 2	13.9458	0.3921	16.9219	0.1515	16.9651	1.1085	Conversion Coefficient
	0.0374	0.0025	0.0539	0.0014	0.0464	0.0400	Spring Constant (nN/nm)
Cantilever 3			9.6254	0.2129	13.2245	1.0940	Conversion Coefficient
Cantilever 4			0.0807	0.0045	0.0933	0.0145	Spring Constant (nN/nm)

* Silicon nitride with nominal spring constant of 0.01nN/nm

Table 4. Spring Constant Determination (Averages) – Type IVc

	FDC Method 1		FDC Method 2		FDC Method 3	
	Average	Std. Dev	Average	Std. Dev	Average	Std. Dev
Conversion Coefficient	13.4521	0.7655	13.8398	0.1819	15.6043	1.0732
Spring Constant (nN/nm)	0.0484	0.0074	0.0668	0.0027	0.0790	0.0215

* Silicon nitride with nominal spring constant of 0.01nN/nm

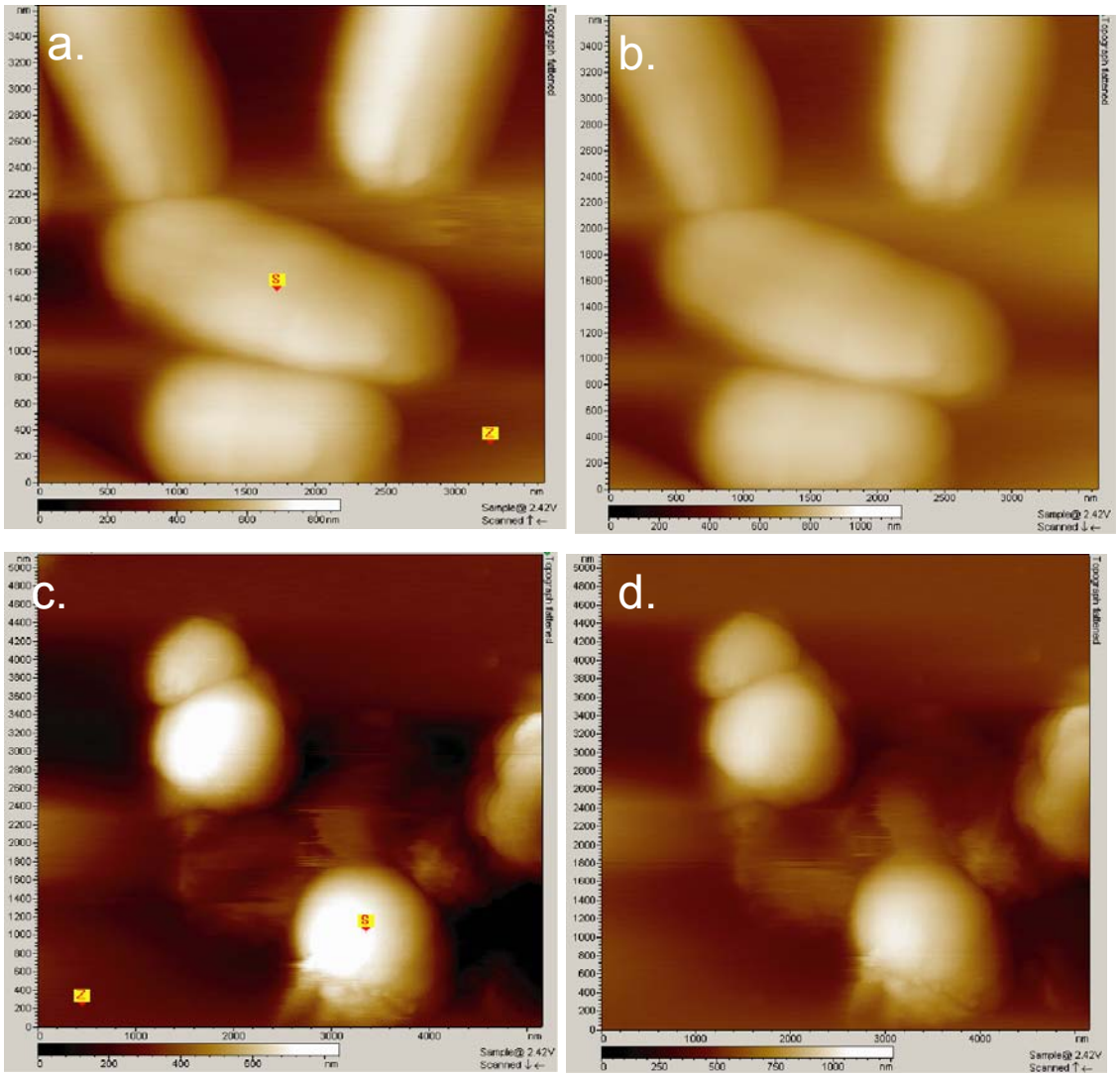

Figure 29. Force distance curves generated on intact bacteria and spheroplasts. (a-d) Topograph images taken in MAC Mode®. (a, b) Intact bacteria. (c, d) Fixed spheroplasts. (a, c) Locations where force distance curves were generated within the perimeter of the bacteria and on the substrate are represented by s and z, respectively. (b, d) Subsequent images were generated after force distance curve to verify the condition and location of the measured bacteria.

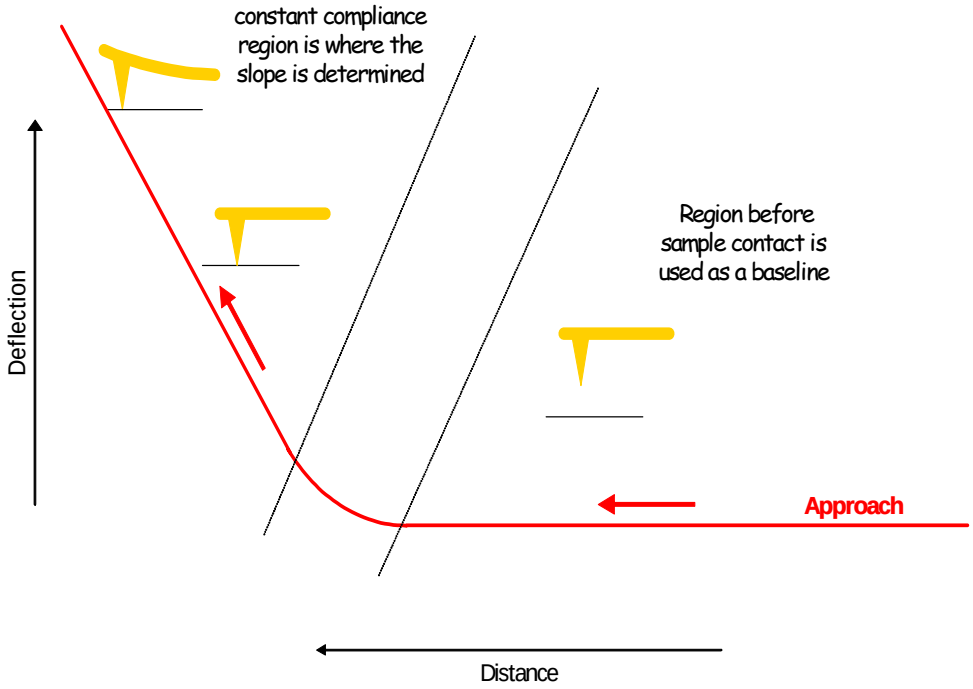

Li, X. and Logan, B. E. (2004) Langmuir 20, 8817-8822

Figure 30. Regions of force distance approach curves relevant for approach curve analysis.

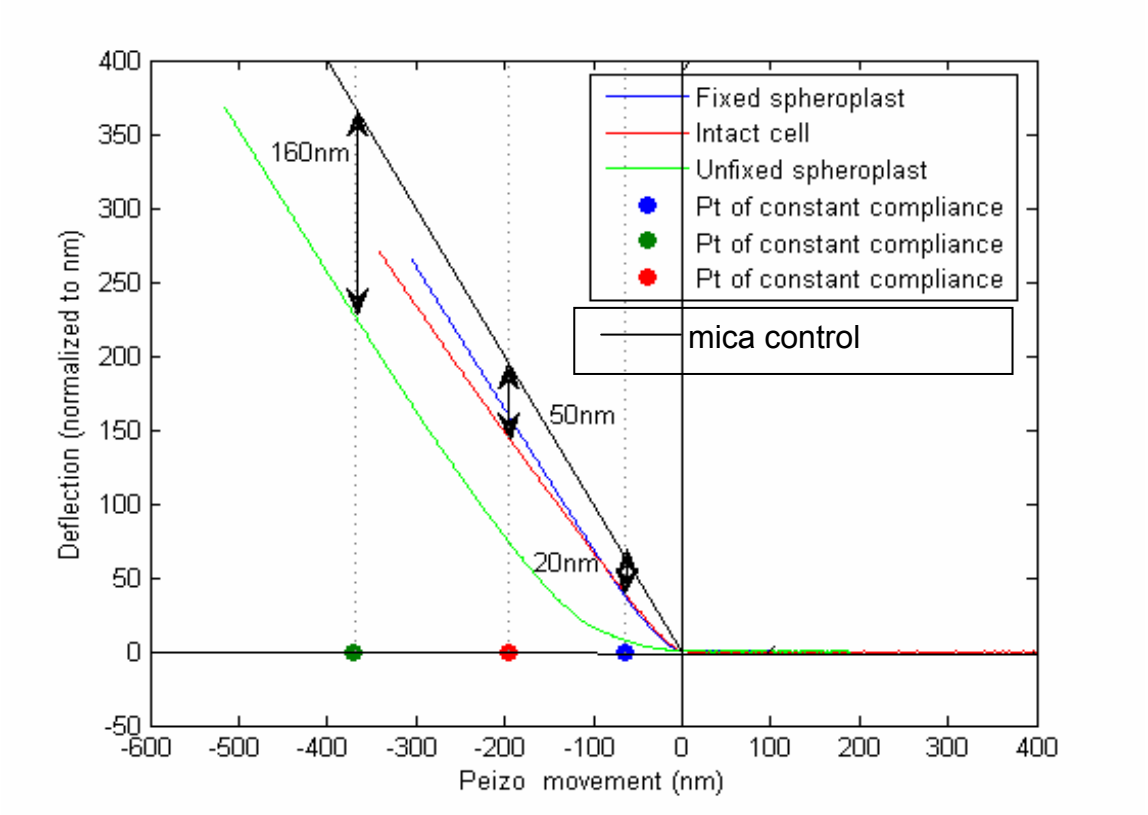

Figure 31. Graph of composite force distance curves for an intact cell, a spheroplast and a fixed spheroplast. The dotted vertical lines indicate the start of the constant compliance regions for the three cell types. The indentation values for the three cell types are indicated.

Table 5. Spring Constants and Indentation

Sample	Cantilever spring constant (k_c)	Slope	Indentation	Spring constant of bacteria (k_b)
Intact	0.0343 nN/nm (+/- 0.002)	0.85 (+/- 0.02)	50nm (+/- 11.5)	0.194nN/nm
Fixed spheroplasts	0.036425 nN/nm (+/- 0.003)	0.94 (+/- 0.06)	20nm (+/- 5)	0.571nN/nm
Untreated spheroplasts	0.0519 nN/nm (+/- 0.016)	0.97 (+/- 0.05)	160nm (+/- 21)	---

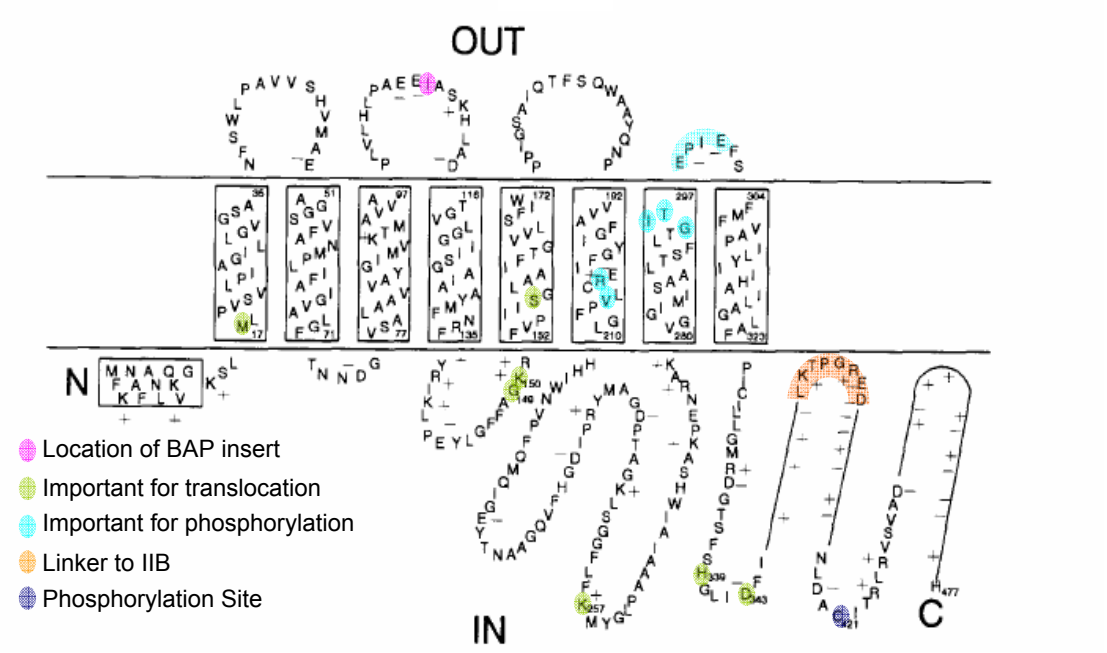

Buhr and Erni JBC 1993; 288; (16) 11599-11603

Figure 32. Topology of IICB^{Glc}. The protein has eight transmembrane helices and four periplasmic loops. Beginning at the N-terminal, the third loop between transmembrane helices 6 and 7 is the largest of the three cytoplasmic loops. Both the termini face the cytoplasm. A linker separated the IIC domain from the IIB domain. Residues important to the function of the transporter have been identified.

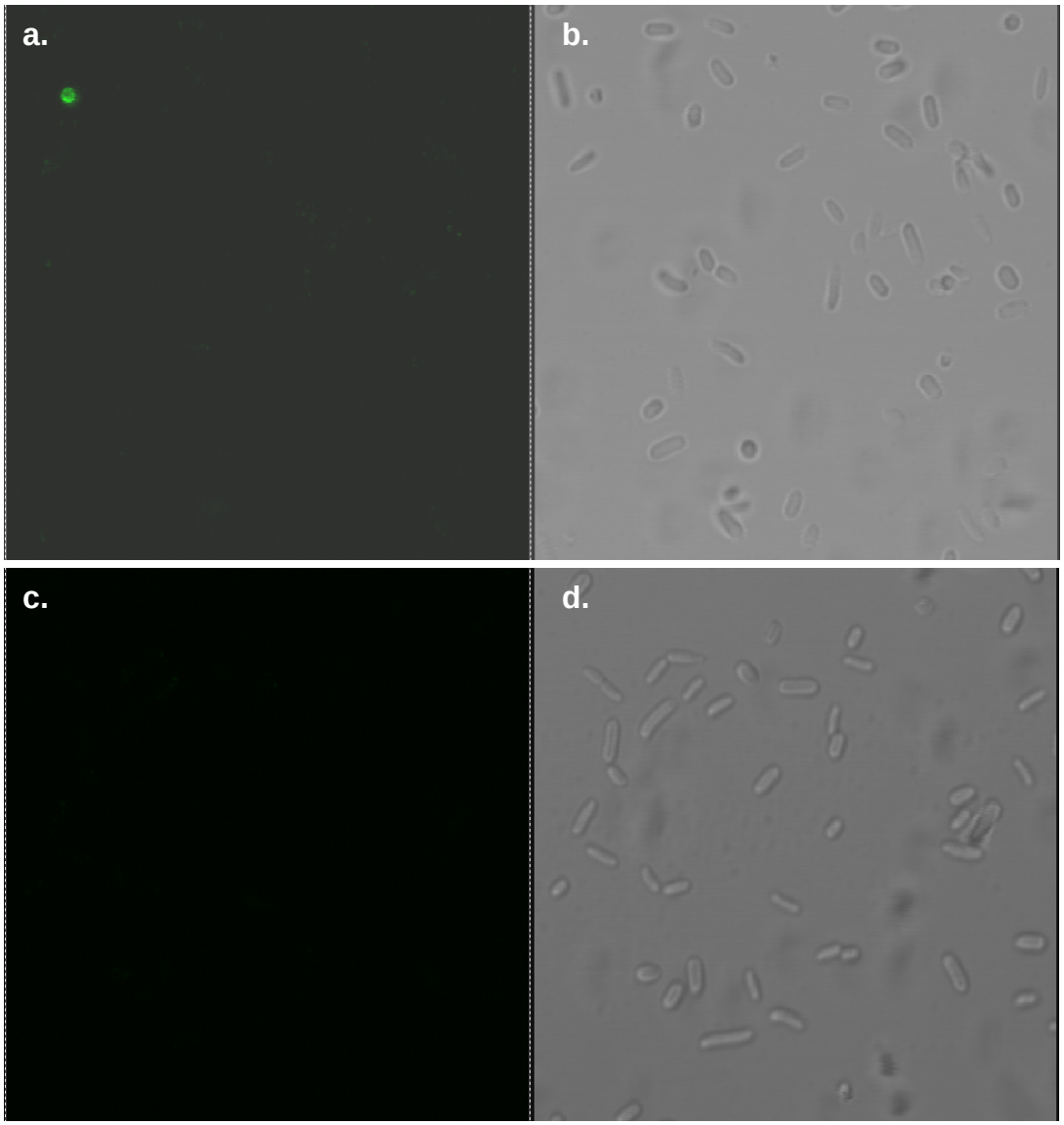

Figure 33. Confocal images of immunolabeled intact *E. coli.* Cells were labeled with a purified rabbit 1° antibody to bacterial alkaline phosphatase (PhoA) and an anti-rabbit 2° conjugated to Alexa 488. (a,b) I108 cells expressing the glucose transporter fused with PhoA in the cytoplasmic membrane; (c,d) EH cells which expresses neither the fused protein nor the endogenous glucose transporter or PhoA. (a,c) fluorescence images. (b,d) transmitted light images. Fluorescence labeling does not occur in the intact bacteria because the 1° antibody does not have access to the fused protein in the cytoplasmic membrane.

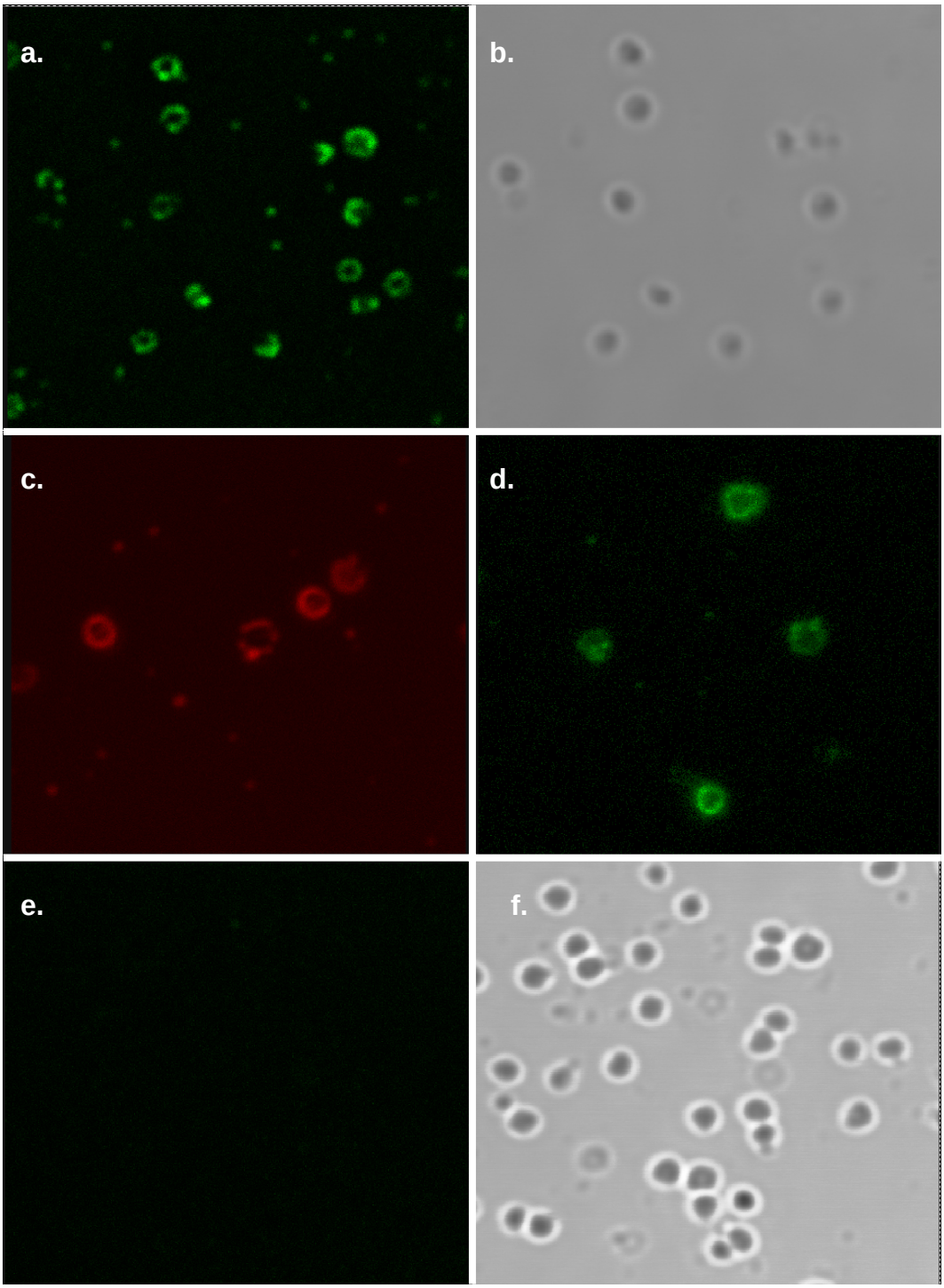

Figure 34. Confocal images of immunolabeled spheroplasts. (a,b,c,d) I108 spheroplasts labeled with antibodies to the alkaline phosphatase-tagged glucose transporter. (a,b) purified 1°antibody, Alexa 488 2°. (c) purified 1°antibody, Alexa 568 2°. (d) biotinylated 1°antibody, streptavidin Qdots 2° . (e,f) EH control spheroplasts labeled with purified 1°antibody, Alexa 488 2° . (a,c,d,e) fluorescence images. (b,f) transmission images.

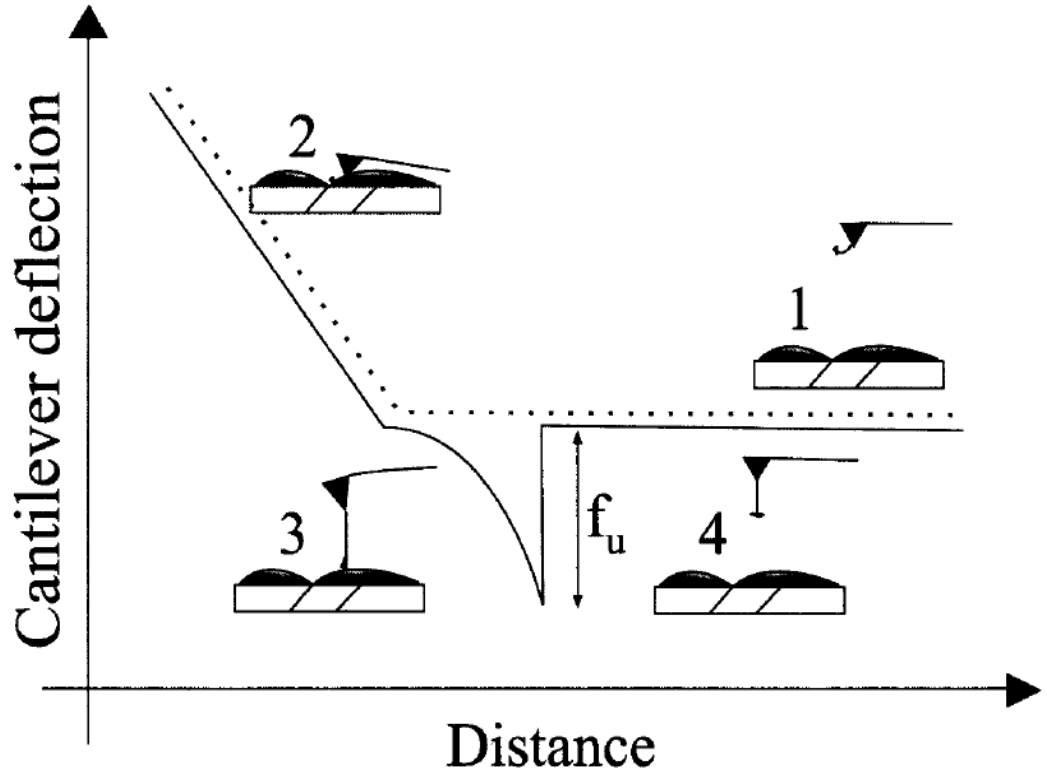

Figure 35. Identifying specific interactions using force distance curves. Idealized approach (dotted line) and retraction (solid line) force-distance curves indicating specific interaction between a cell surface molecule and a tethered ligand. (1) Far from the surface, cantilever deflection is constant and the tethered ligand is not in contact with the surface. (2) Upon contact with the surface, the cantilever bends and the ligand is in contact with the surface. As the tip is pulled away from the surface, the cantilever and cell surface relax until the original point of contact. If there is no interaction between neither the tethered molecule and the sample nor the tip and the sample, the horizontal portion of the approach curve will be retraced. (3) Interaction between the tethered molecule and the surface bound complement, however, will cause a nonlinear region to develop in the force-distance curve as the lax linker becomes stretched. Linearity returns (albeit in a region farther from the surface) when the linker is taut. (4) Further separation causes the interaction between the tethered molecule and its complement to be disrupted and the cantilever returns to its baseline position. (Ebner, A., et al (2007) *Current Nanoscience* 3(1), 49-56)

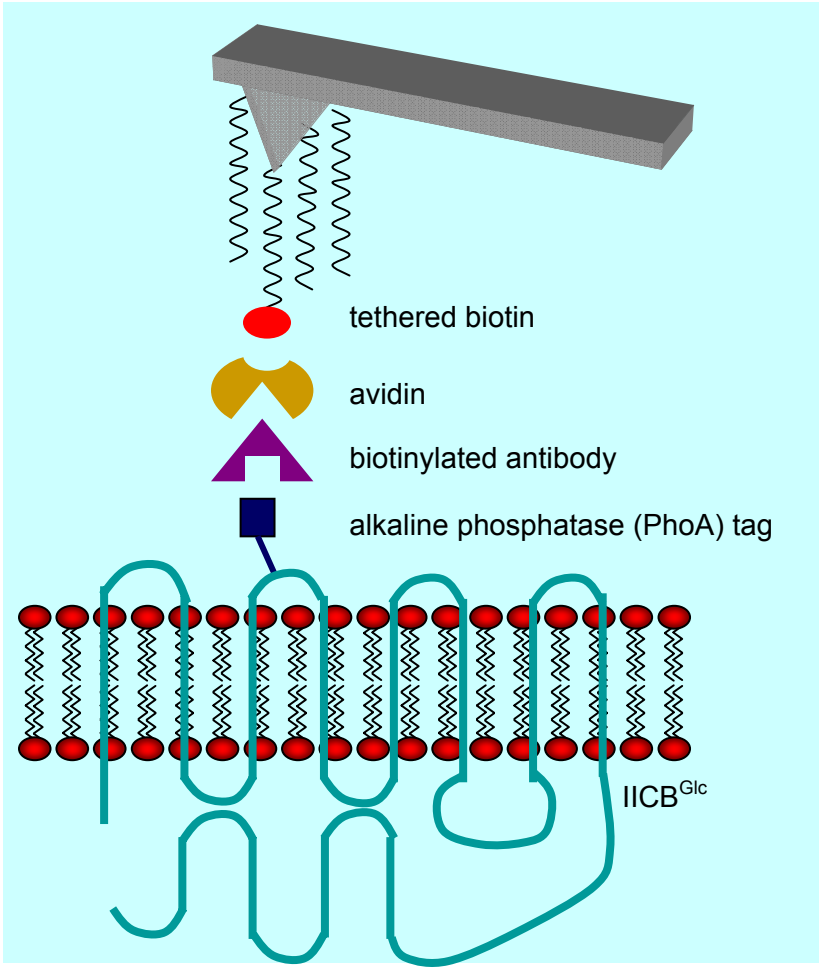

Figure 36. Schematic of AFM molecular recognition experiments. Spheroplasts expressing the PhoA-tagged glucose transporter are immunolabeled with a biotinylated antibody and treated with avidin. A cantilever functionalized with tethered biotin is used to probe this surface.

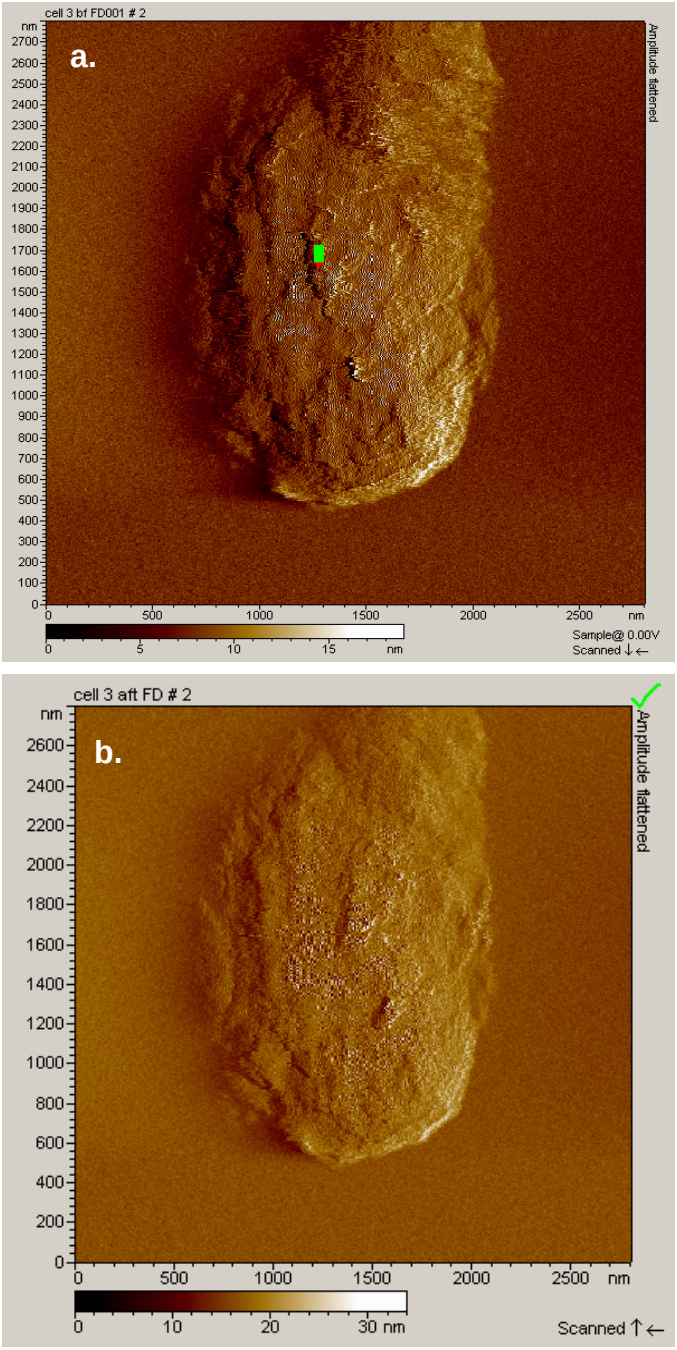

Figure 37. Immunolabeled spheroplasts used for molecular recognition by AFM. Amplitude images of a spheroplast treated with a biotinylated antibody to the PhoA-tagged glucose transporter and avidin. (a) Single spheroplasts were imaged using a small scan area. The green pointer is the location in the center of the cell where force distance curves were generated with a tip to which biotin was tethered. (b.) An image of the same cell after the force distance curves to ensure that damage did not occur and the cell remained in the same location.

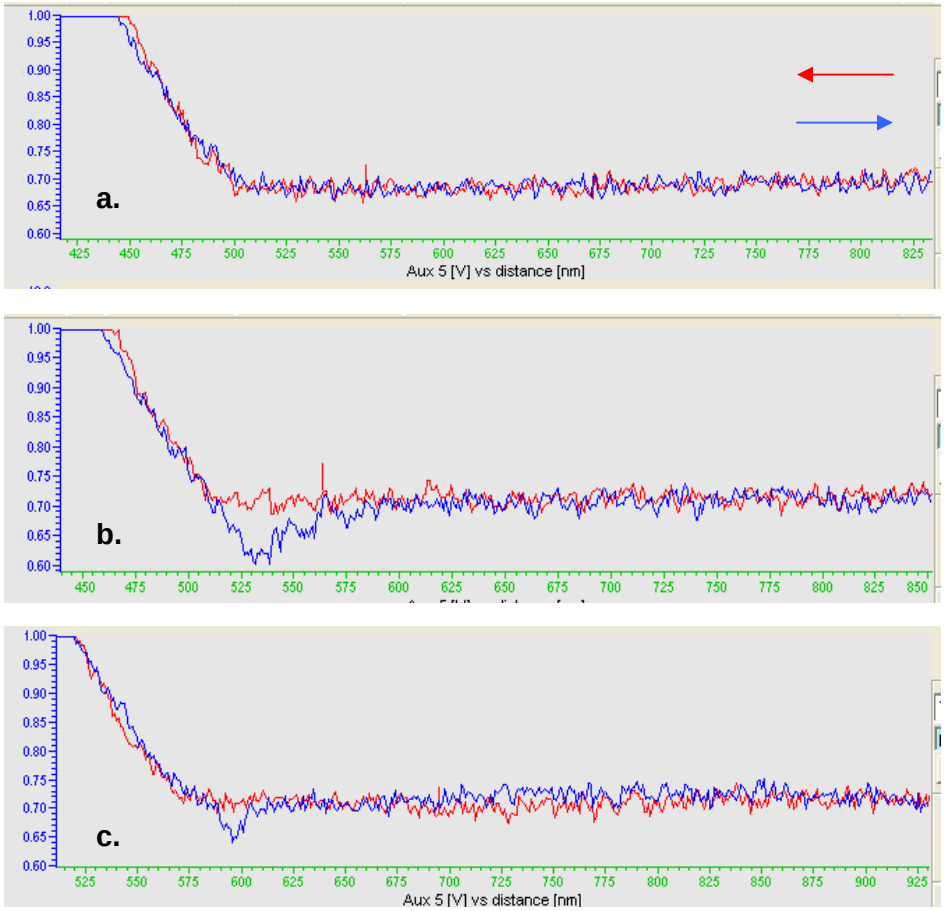

Figure 38. Actual force distance curves. The red trace is the approach curve and the blue trace is the retraction curve. (a) no adhesive interaction between the tip and sample (b) nonspecific adhesive interaction (c) a binding event.

Table 6. I108 AFM Molecular Recognition Data

		Cell 1	Cell 2	Cell 3	Cell 4	Cell 5	Cell 6	Totals
I108	Binding Events	120	58	84	51	114	81	508
	Remaining Curves	430	492	466	499	436	469	2792
	Number of Curves	550	550	550	550	550	550	3300
	Binding Probability	21.82%	10.55%	15.27%	9.27%	20.73%	14.73%	15.39%

Table 7. EH AFM Molecular Recognition Data

		Cell 1	Cell 2	Cell 3	Cell 4	Cell 5	Totals
EH	Binding Events	18	56	23	12	55	164
	Remaining Curves	532	494	527	538	495	2586
	Number of Curves	550	550	550	550	550	2750
	Binding Probability	3.27%	10.18%	4.18%	2.18%	10.00%	5.96%

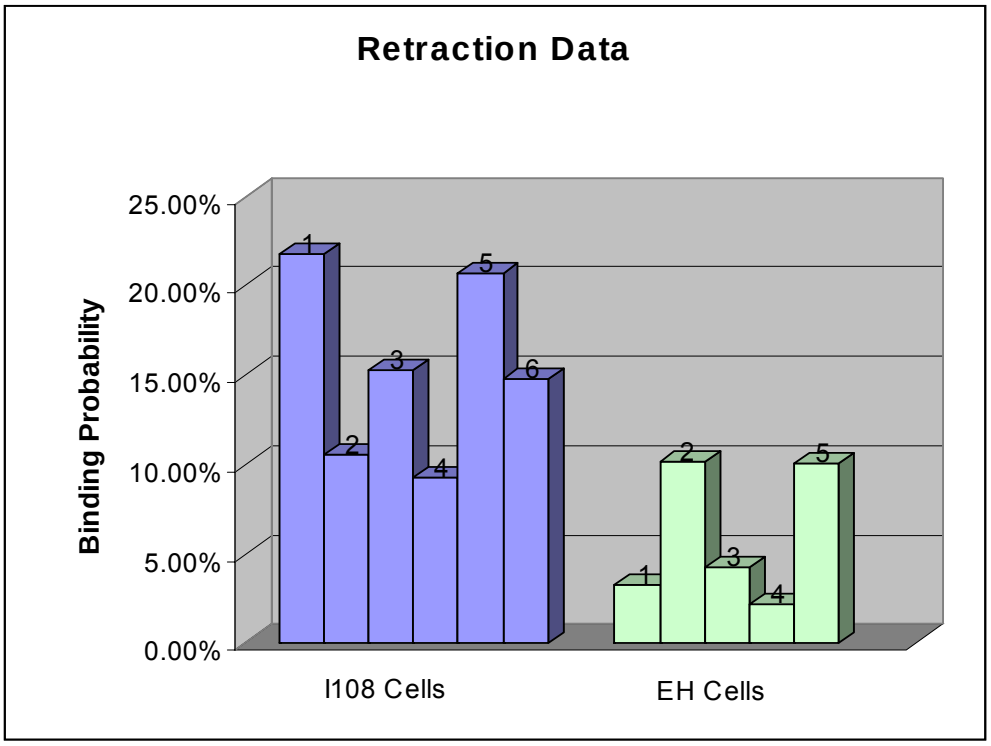

Figure 39. Graphical representation of the data in Table 6 and Table **7**.

Appendix B – Abstracts

Abstracts of Manuscripts Associated with this Thesis Work

Doktycz, M. J., C. J. Sullivan, et al. (2003). "AFM imaging of bacteria in liquid media immobilized on gelatin coated mica surfaces." Ultramicroscopy **97**(1-4): 209-216.

Immobilization of particulates, especially biomolecules and cells, onto surfaces is critical for imaging with the atomic force microscope (AFM). In this paper, gelatin coated mica surfaces are shown to be suitable for immobilizing and imaging both gram positive, Staphylococcus aureus, and gram negative, Escherichia coli, bacteria in both air and liquid environments. Gelatin coated surfaces are shown to be superior to poly-L-lysine coated surfaces that are commonly used for the immobilization of cells. This cell immobilization technique is being developed primarily for live cell imaging of Rhodopseudomonas palustris. The genome of R. palustris has been sequenced and the organism is the target of intensive studies aimed at understanding genome function. Images of R. palustris grown both aerobically and anaerobically in liquid media are presented. Images in liquid media show the bacteria is rod shaped and smooth while images in air show marked irregularity and folding of the surface. Significant differences in the vertical dimension are also apparent with the height of the bacteria in liquid being substantially greater than images taken in air. In air immobilized bacterial flagella are clearly seen while in liquid this structure is not visible. Additionally, significant morphological differences are observed that depend on the method of bacterial growth.

Sullivan, C. J., J. L. Morrell, et al. (2005). "Mounting of Escherichia coli spheroplasts for AFM imaging." Ultramicroscopy **105**(1-4): 96-102.

The cytoplasmic membrane of Escherichia coli (E coli) is the location of numerous, chemically specific transporters and recognition elements. Investigation of this membrane in vivo by atomic force microscopy (AFM) requires removal of the cell wall and stable immobilization of the spheroplast. AFM images demonstrate that spheroplasts can be secured with warm gelatin applied to the mica substrate just before the addition of a spheroplast suspension. The resulting preparation can be repeatedly imaged by AFM over the course of several hours. Confocal fluorescence imaging confirms the association of the spheroplasts with the gelatin layer. Gelatin molecules are known to reorder into a network after heating. Entrapment within this gelatin network is believed to be responsible for the immobilization of spheroplasts on mica.

Beckmann, M. A., S. Venkataraman, et al. (2006). "Measuring cell surface elasticity on enteroaggregative Escherichia coli wild type and dispersin mutant by AFM." Ultramicroscopy **106**(8-9): 695-702.

Enteroaggregative Escherichia coli (EAEC) is pathogenic and produces severe diarrhea in humans. A mutant of EAEC that does not produce dispersin, a cell surface protein, is not pathogenic. It has been proposed that dispersin imparts a positive charge to the bacterial cell surface allowing the bacteria to colonize on the negatively charged intestinal mucosa. However, physical properties of the

bacterial cell surface, such as rigidity, may be influenced by the presence of dispersin and may contribute to pathogenicity. Using the system developed in our laboratory for mounting and imaging bacterial cells by atomic force microscopy (AFM), in liquid, on gelatin coated mica surfaces, studies were initiated to measure cell surface elasticity. This was carried out in both wild type EAEC, that produces dispersin, and the mutant that does not produce dispersin. This was accomplished using AFM force-distance (FD) spectroscopy on the wild type and mutant grown in liquid or on solid medium. Images in liquid and in air of both the wild-type and mutant grown in liquid and on solid media are presented. This work represents an initial step in efforts to understand the pathogenic role of the dispersin protein in the wild-type bacteria.

Sullivan, C. J., S. Venkataraman, et al. (2007). "Comparison of the indentation and elasticity of *E. coli* and its spheroplasts by AFM." Ultramicroscopy **107**(10-11): 934-942.

Atomic force microscopy (AFM) provides a unique opportunity to study live individual bacteria at the nanometer scale. In addition to providing accurate morphological information, AFM can be exploited to investigate membrane protein localization and molecular interactions on the surface of living cells. A prerequisite for these studies is the development of robust procedures for sample preparation. While such procedures are established for intact bacteria, they are only beginning to emerge for bacterial spheroplasts. Spheroplasts are useful research models for studying mechanosensitive ion channels, membrane transport, lipopolysaccharide translocation, solute uptake, and the effects of antimicrobial agents on membranes. Furthermore, given the similarities between spheroplasts and cell wall-deficient (CWD) forms of pathogenic bacteria, spheroplast research could be relevant in biomedical research. In this paper, a new technique for immobilizing spheroplasts on mica pretreated with aminopropyltriethoxysilane (APTES) and glutaraldehyde is described. Using this mounting technique, the indentation and cell elasticity of glutaraldehyde-fixed and untreated spheroplasts of *E. coli* in liquid were measured. These values are compared to those of intact *E. coli*. Untreated spheroplasts were found to be much softer than the intact cells and the silicon nitride cantilevers used in this study.

Vita

Claretta Jackson Sullivan was born in Indianola, Mississippi in 1965. She attended public schools there and ultimately graduated from Gentry High School in 1983. She began her post secondary education in the fall of the same year at Tougaloo College near Jackson, Mississippi. In May of 1987, she graduated with honors and a bachelor's degree in mathematics/computer science. At that time she started working as a computer programmer for the Hartford Insurance Group in Hartford, Connecticut. In the summer of 1988, she moved to Atlanta, Georgia to train to become a public high school mathematics teacher. After certification, she taught for three years in the DeKalb County School System in metro-Atlanta.

After moving to Knoxville, Tennessee in the spring of 1991, Claretta worked in various training capacities for contractors at Department of Energy facilities in Oak Ridge, Tennessee. In the latest of these positions, she was the K-12 Science and Math Education Coordinator at Oak Ridge National Laboratory (ORNL). She was exposed to the research of scientists at ORNL through the responsibilities associated with this role. Inspired by what she saw, the decision was made to pursue graduate school. She spent a year working as a laboratory technician and completing undergraduate science courses in preparation. In January of 2002, she was accepted into the Genome Science and Technology graduate program at the University of Tennessee – Knoxville. She earned a Ph.D. in Life Sciences in the fall of 2007. Shortly thereafter, the circuitous route of training led to a research faculty position at Eastern Virginia Medical School.